Self-association of [Pt^{II}(1,10-Phenanthroline)(*N*-pyrrolidyl-*N*-(2,2-dimethyl-propanoyl)thiourea)]$^{+}$ and non-covalent outer-sphere complex formation with fluoranthene through cation-π interactions: A high resolution ^{1}H and DOSY NMR study

By

Izak Aldert Kotzé

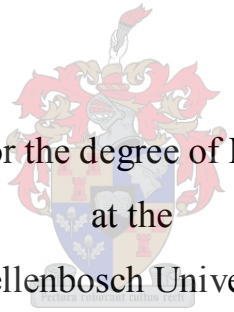

Thesis presented for the degree of Masters in Chemistry

at the

Stellenbosch University

Promoter: Professor Klaus R. Koch

December 2009

Declaration

By submitting this thesis electronically, I declare that the entirety of the work contained herein is my own, original work, that I am the owner of the copyright thereof (unless to the extent explicitly otherwise stated) and that I have not previously in its entirety or in part submitted it for obtaining any qualification.

Date: November 2009

“Die lewe gaan oor twee dinge: wins en verlies. En as jy aan die verlies kant is, moet jy dit maar met ‘n knippie sout vat...” -Terblanchie-

Acknowledgements

I would sincerely like to thank:

- My supervisor, Prof. Klaus Koch, for his motivation, enthusiasm and guidance through my studies.

- Dr. Wilhelmus Gerber for his time and editing of my thesis.

- Anglo Platinum, National Research Foundation and the University of Stellenbosch for funding.

- The staff from the NMR lab. Elsa Malherbe, Trevor Wright, Jaco Brand and Jean McKenzie.

- Mr. Mohammed Jaffer from UCT for the TEM analysis.

- The technical staff at the Analytical Chemistry department, Shafiek Mohammed, Deidre Williams, Lisinda Bailey and Roger Lawrence.

- The PGM group for their friendship and support.

- Friends and family for their love and support throughout my studies.

- God for the life he gave me.

List of Abbreviations

Fe(III)PPIX	ferriprotoporphyrin
DNA	deoxyribonucleic acid
COSY	correlated spectroscopy
NOESY	nuclear overhauser enhancement spectroscopy
NOE	nuclear overhauser effect
DOSY	diffusion ordered spectroscopy
HMBC	heteronuclear multiple bond correlation
ppm	parts per million
v/v	volume/volume
m.p.	melting point
DMSO-d_6	deuterated dimethylsulphoxide
Acetonitrile-d_3	deuterated acetonitrile
ESI(+)	positive electron spray ionization
IR	infrared
UV-VIS	ultra violet visible

Conference Proceedings

COS (Cape Organometallic Symposium).....Attended.....2008
SACI (South-African Chemical Society).....Poster Presented.....2008
South-African PhD-Project Conference.....Invited Delegate.....2009
RSC SACI-Inorganic Conference.....Poster Presented.....2009
RSC SACI-Inorganic Conference.....This Work Presented by Dr. Gerber.....2009

Publications

Izak A. Kotzé, Wilhelmus J. Gerber, Jean M. Mckenzie, and Klaus R. Koch, *European Journal of Inorganic Chemistry*, 2009, **12**, 1626–1633. (From this work-Appendix C)

Abstract

A series of mixed-ligand [Pt^{II}(phen)(L^n-*S,O*)]Cl complexes have been synthesised and characterized (where phen is 1,10-phenanthroline and HL-*S,O* represents various chelating *N*-acyl-*N,N'*-dialkylthioureas). The Pt^{II}(1,10-phenanthroline)(*N*-pyrrolidyl-*N*-(2,2-dimethyl-propanoyl)thiourea)]Cl ([Pt^{II}(phen)(L^1-*S,O*)]Cl) complex has been used for the development of a viable system for the studying of the weak intermolecular interactions leading to aggregation of these complexes in solution, using ^{1}H NMR spectroscopy.

Competing outer-sphere self-association of [Pt^{II}(phen)(L^1-*S,O*)]$^+$ (M) to form dimer aggregates and the hetero-association of M with fluoranthene (F) have been investigated by means of the significant concentration dependence of ^{1}H NMR chemical shifts as well as by diffusion coefficients obtained from DOSY NMR spectroscopy. The NMR spectroscopic data of [Pt^{II}(phen)(L^1-*S,O*)]Cl in acetonitrile solution is only consistent with the formation of a "dimer" M···M aggregate according to $2M \rightleftharpoons M_2$ at several temperatures, resulting in calculated K_D of ca. 46±7 M^{-1} at 273.5 K and $\Delta_r H°$ and $\Delta_r S°$ of -25129±3112 and -61±11 J.mol^{-1} respectively. The effect of D_2O on the extent of self-association of [Pt^{II}(phen)(L^1-*S,O*)]$^+$ was also investigated. The dimer model accounted for the experimental data exceptionally well in 0 - 30% (v/v) D_2O:CD_3CN with the dimerization constants, K_D, calculated at 299.2K increasing from 17 M^{-1} to 71 M^{-1}. However, at higher percentages D_2O:CD_3CN (50 - 100%) the dimerization model does not fit the data, suggesting that higher order aggregation takes place; models which invoke trimers, tetramers etc. and combinations thereof were attempted without success. Possible micelle or super-sized aggregate formation in these solutions is suggested by the transmission electron microscopy images obtained for these solutions.

$[Pt^{II}(phen)(L^1\text{-}S,O)]Cl$ forms non-covalent hetero-association complexes with aromatic molecules such as fluoranthene (F), presumably through cation-π-type interactions between M and F according to M + F⇌MF in acetonitrile. This process studied by ^1H NMR shows that relatively strong cation-π complexes form (K_B≈67±7 M^{-1} at 273.5 K) with $\Delta_r H°$ and $\Delta_r S°$ calculated for M···M (-25129±3112 and -61±11 $J.mol^{-1}$) and M···F (-13560±3180 and -17±11 $J.mol^{-1}$). Interestingly any potential F···F aggregation interactions are negligible for the fluoranthene under the same conditions for the concentration range up to 0.1 M, indicating that non-covalent π–π interactions between fluoranthene molecules 2F⇌F_2 are negligible under these conditions in solution.

Opsomming

Die suksesvolle sintese van 'n reeks [Pt^{II}(phen)(L^n-*S,O*)]Cl word beskryf (waar phen is 1,10-phenantrolien en HL-*S,O* verteenwoordig verskeie *N*-asiel-*N,N'*-dialkieltiourea ligande). Die Pt^{II}(1,10-phenantrolien)(*N*-pirrolediel-*N*-(2,2-dimetiel-propanoïel)tiourea)] Cl ([Pt^{II}(phen)(L^1-*S,O*)]Cl) is gebruik vir die ontwikkeling vir 'n betroubare sisteem om die swak intermolekulêre interaksies, wat lei tot die aggregasie van hierdie komplekse in oplossing, te studeer met behulp van ^{1}H NMR spektroskopie.

Kompeterende buitenste-sfeer self-aggregasie van [Pt^{II}(phen)(L^1-*S,O*)]$^+$ (M) om dimeer aggregate te vorm en die hetero-aggregasie van M met fluoranteen (F) is bestudeer met behulp van merkwaardige konsentrasie afhanklikheid van die ^{1}H NMR chemiese verskuiwings asook die difusie koefisiënte verkry van DOSY NMR spektroskopie. Die NMR spektroskopie data van [Pt^{II}(phen)(L^1-*S,O*)]Cl in asetonitriel is konsistent met die

vorming van slegs dimeer M···M aggregate volgens $2M \rightleftharpoons M_2$ by verskeie temperature,

wat lei tot K_D waardes van 46±7 M^{-1} by 273.5 K en $\Delta_r H°$ en $\Delta_r S°$ waardes van -25129±3112 en -61±11 J.mol^{-1} respektiewelik. Die effek van D_2O op die mate van self-aggregasie van [Pt^{II}(phen)(L^1-*S,O*)]$^+$ was ook ondersoek. Die dimeer model beskryf die eksperimentele data goed vir die 0 - 30% (v/v) D_2O:CD_3CN oplossings met berekende dimerisasie konstantes, K_D, vermeerder van 17 M^{-1} tot 71 M^{-1} by 299.2K. Die dimerisasie model kon nie die eksperimentele data beskryf by hoër persentasies D_2O:CD_3CN (50 - 100%) nie wat beteken dat hoër orde aggregasie teenwoordig moet wees. Moonlike super-groot aggregaat vorming in hierdie oplossings is voorgestel deur die transmisie elektron mikroskopie foto's verkry.

Daar is gevind dat [Pt^{II}(phen)(L^1-*S,O*)]Cl nie-kovalente hetero-aggregaat komplekse vorm met aromatiese molekules soos fluoranteen (F), deur katioon-π tipe interaksies

tussen M en F volgens M + F⇌MF in asetonitriel. Hierdie proses is bestudeer met ^{1}H

NMR en is gevind dat relatiewe sterk katioon-π komplekse vorm (K_B≈67±7 M^{-1} by 273.5 K) waarvan die $\Delta_r H°$ en $\Delta_r S°$ bereken is vir M···M (-25129±3112 en -61±11 J.mol^{-1}) en M···F (-13560±3180 en -17±11 J.mol^{-1}) respektiewelik. Potensiële F···F aggregasie is weglaatbaar klein by dieselfde kondisies vir ‘n konsentrasie tot by 0.1 M, wat beteken dat die nie-kovalente π-π interaksies tussen die fluoranteen molekules

$2F \rightleftharpoons F_2$ weglaatbaar is by hierdie kondisies in oplossing.

Table of Content

Declaration....ii
Acknowledgements....iii
Abbreviations....iv
List of Conferences....v
Abstract....vi
Opsomming....viii
Table of Contents....x
List of Figures....xiii
List of Tables....xviii
List of Schemes and Diagrams....xix

Chapter 1 – General Introduction and Background

1.1 Bioactivity of Platinum(II) Complexes....1
1.2 Anti-malarial Drug Design....2
1.3 Non-Covalent Intermolecular Interactions....4
1.3.1 Hydrogen bonding Interactions....4
1.3.2 Ion pairing....5
1.3.3 Cation-π Interactions....6
1.3.4 π -π Interactions....7
1.4 Objectives of this Study....8

Chapter 2 – Ligand and Complex Synthesis, Characterization and Experimental

2.1 Introduction....11
2.2. Synthesis of [Pt^{II}(1,10-phenanthroline)(*N,N*-di(alkyl)-*N'*-acylthiourea)]Cl complexes....12
2.2.1 Synthesis of [$Pt^{II}Cl_2$(1,10-phenanthroline)]....15
2.2.2 Synthesis of the *N,N*-di(alkyl)-*N'*-acylthiourea ligands....16
2.2.3 Synthesis of the [Pt^{II}(1,10-phenanthroline)(*N,N*-di(alkyl)-*N'*-acylthiourea)]Cl

Complexes.....17
2.3. Aqueous Solubility and Stability Tests.....19
2.4 Detailed analysis of the ^{1}H, COSY, HMBC, NOESY and DOSY NMR spectra for the assignment of the [Pt^{II}(phen)(L^{1}-*O,S*)]Cl complex.....19
2.5. DOSY Spectroscopy and Computational Methodology.....30
2.5.1 DOSY Spectroscopy.....30
2.5.2 Computational Details of the Models for Aggregation.....33
2.6 Experimental.....36
2.6.1 Instrumentation.....36
2.6.2 Sample preparation for ^{1}H NMR Spectroscopy.....36
2.6.3 Reagents.....37
2.6.4 Characterization.....37

Chapter 3 – Self-association of [Pt^{II}(phen)(L^{1}-S,O)]$^{+}$ in acetonitrile and aceto-nitrile/water mixtures

3.1 Introduction.....57
3.2 Results and discussion.....59
3.2.1 Self-association of [Pt^{II}(phen)(L^{n}-*S,O*)]$^{+}$: A High Resolution ^{1}H NMR Study...59
3.2.2 ^{1}H Diffusion Ordered Spectroscopy (DOSY) Study of the Self-association of [Pt^{II}(phen)(L^{n}-*S,O*)]$^{+}$.....65
3.2.3 Self-association Mass Spectroscopy in vacuo.....69
3.2.5 Proposed Dimer Structure.....70
3.2.4 Self-association Study using UV-*VIS* Spectroscopy.....70
3.3 Effect of Solvent Composition on the Extent of Association.....71
3.3.1 Water/acetonitrile mixtures up to 30% (v/v) D_2O.....73
3.3.2 Water/acetonitrile mixtures > 30% (v/v) D_2O.....79

Chapter 4 – Non-covalent hetero-association of [Pt^{II}(phen)(L^{1}-S,O)]$^{+}$ and fluoranthene

4.1 Introduction.....82

4.2 Results and Discussion.....83
4.2.1 ^{1}H NMR Concentration Dependence Study.....83
4.2.1 Proposed Non-covalent Hetero-dimer Structure in Solution.....89
4.2.3 Comparison of the Self- and Hetero-association of $[Pt^{II}(phen)(L\text{-}S,O)]^{+}$ and Fluoranthene in Acetonitrile.....94

Chapter 5 – Conclusions.....96

References.....99

Appendix A
^{1}H NMR Data and calculated dimerization constants.....104

Appendix B
Infrared Spectra.....113

Appendix C
Publication (From this work).....117

List of Figures

Figure 1.1: *The life cycle of the malaria parasite Plasmodium*

Figure 1.2: *Representation from Egan et al. of the mode of action of chloroquine (CQ) in the malaria parasite in the human red blood cell.*

Figure 1.3: *Different types of hydrogen bonding. a) Normal hydrogen bond with one acceptor. b) Bifurcated hydrogen bonding. c) Trifurcated hydrogen bonding. d) Prototype of a hydrogen bond with the water dimer as an example.*

Figure 1.4: *(a) Schematic drawing of the charge distribution of benzene showing the positively charged σ-framework and negatively charged π-electron cloud forming a quadrupole moment and (b) the cation-π interactions showing the contact of the K+ cation and benzene.*

Figure 1.5: *The limiting types of aromatic π-π interactions: (a) face-to-face (interplanar distance about 3.3-3.8 Å) and (b) edge-to-face orientations. (c) The repulsion between negatively charged π-electron clouds of facially oriented aromatic rings.*

Figure 1.6: *Representation of the coplanar stacking of the potential anti-malarial complexes with hematin.*

Figure 2.1: *Previous anti-malarial complexes synthesized by Koch and co-workers.*

Figure 2.2: *Series of $[Pt^{II}$(1,10-phenantroline)(N,N-di(alkyl)-N'-acylthiourea)]Cl complexes synthesized*

Figure 2.3: *^{1}H NMR spectrum of $[Pt^{II}Cl_2$(phen)] in DMSO-d_6*

Figure 2.4: *^{1}H NMR spectrum of HL^1 in DMSO-d_6*

Figure 2.5: *^{1}H NMR spectrum of $[Pt^{II}$(phen)(L^1-S,O)]Cl in acetonitrile-d_3 showing the 1,10-phenanthroline protons in the aromatic region and the N-pyrrolidyl-N-(2,2-dimethylpropanoyl)thiourea protons in the aliphatic region of the spectrum.*

Figure 2.6: *The ^{1}H NMR spectra of Pt^{II}(phen)(L^1-S,O)]Cl and the precursor $[Pt^{II}Cl_2$(phen)] in DMSO-d_6.*

Figure 2.7: *$^{1}H,^{1}H$ COSY spectrum of $Pt^{II}(phen)(L^{1}\text{-}S,O)]Cl$ in Acetonitrile-d_3 where (a) is the full COSY spectrum (b) the aromatic region and (c) is the aliphatic region of the spectrum*

Figure 2.8: *NOESY plot of $[Pt^{II}(phen)(L^{5}\text{-}S,O)]Cl$ where (a) is the aromatic region and (b) is the aliphatic region presenting correlations that point towards NOE correlations within the separate ligands.*

Figure 2.9: *NOE correlations for $[Pt^{II}(phen)(L^{5}\text{-}S,O)]Cl$*

Figure 2.10: *$^{1}H,^{15}N$ HMBC plot showing the ^{1}H and ^{15}N correlations in acetonitrile-d_6. Nitrogen chemical shifts are reported relative to nitromethane.*

Figure 2.11: *The ^{1}H NMR spectrum of $Pt^{II}(phen)(L^{1}\text{-}S,O)]Cl$ showing broad unresolved ^{195}Pt satellites that are more visible (a) at 400 MHz (11.74 T) than (b) at a higher magnetic field of 600 MHz (14.09 T).*

Figure 2.12: *Attenuation of the ^{1}H NMR signals of a mixture of $[Pt^{II}(phen)(L^{1}\text{-}S,O)]^{+}$, acetonitrile and water during a typical DOSY experiment with increasing gradient strength (0.0107-0.449 $G.m^{-1}$).*

Figure 2.13: *DOSY plot of a mixture of $[Pt^{II}(phen)(L^{1}\text{-}S,O)]^{+}$, acetonitrile and water showing an average diffusion coefficient for a diffusion delay of 30 ms. The gradient pulse duration was 2 ms and 20 gradients intervals between 0.0107-0.449 $G.m^{-1}$ were used.*

Figure 2.14: *^{1}H NMR spectrum and assignment of phen and $[Pt^{II}Cl_2(phen)]$*

Figure 2.15: *^{1}H NMR spectrum and assignment of HL^{1} in DMSO-d_6 at 25°C*

Figure 2.16: *^{1}H NMR spectrum and assignment of $[Pt^{II}(phen)(L^{1}\text{-}S,O)]Cl$ in CD_3CN*

Figure 2.17: *^{1}H NMR spectrum and assignment of HL^{2} in DMSO-d_6*

Figure 2.18: *^{1}H NMR spectrum and assignment of $[Pt^{II}(phen)(L^{2}\text{-}S,O)]Cl$ in DMSO-d_6*

Figure 2.19: *^{1}H NMR spectrum and assignment of HL^{3} in DMSO-d_6*

Figure 2.20: *^{1}H NMR spectrum and assignment of $[Pt^{II}(phen)(L^{3}\text{-}S,O)]Cl$ in DMSO-d_6*

Figure 2.21: *^{1}H NMR spectrum and assignment of HL^{4} in DMSO-d_6*

Figure 2.22: *^{1}H NMR spectrum and assignment of $[Pt^{II}(phen)(L^{4}\text{-}S,O)]Cl$ in DMSO-d_6*

Figure 2.23: *^{1}H NMR spectrum and assignment of HL^{5} in $CDCl_3$*

Figure 2.24: *^{1}H NMR spectrum and assignment of $[Pt^{II}(phen)(L^{5}\text{-}S,O)]Cl$ in $CDCl_3$*

Figure 2.25: *^{1}H NMR spectrum and assignment of fluoranthene in CD_3CN at 25°C*

Figure 3.1: *^{1}H NMR spectra (599.99 MHz) of $[Pt^{II}(phen)(L^{1}\text{-}S,O)]^{+}$ in CD_3CN at 273.4 K with increasing complex concentration. Only a partial spectrum is shown as several nuclei (N-pyrrolidyl-N-(2,2-dimethylpropanoyl)-thiourea protons) exhibit no or little chemical shift concentration dependence*

Figure 3.2: *Concentration dependence of the protons of $[Pt^{II}(phen)(L^{1}\text{-}S,O)]^{+}$ in CD_3CN at 299 K with increasing complex concentration, where* ***(a)*** *is the phenanthroline protons in the aromatic region and (b) the thiourea protons in the aliphatic region.*

Figure 3.3: *Excellent agreement was obtained between the dimer model least-squares fits and the experimental (symbols) chemical shift dependence of the 1,10-phenanthroline H^{2} proton on the concentration of $[Pt^{II}(phen)(L^{1}\text{-}S,O)]^{+}$.*

Figure 3.4: *^{1}H NMR spectra (599.99 MHz) of $[Pt^{II}(phen)(L^{1}\text{-}S,O)]^{+}$ in CD_3CN (1.026×10^{-2} M) as a function of temperature. Only a partial spectrum is shown as several nuclei (N-pyrrolidyl-N-(2,2-dimethylpropanoyl)-thiourea protons) exhibit no or little chemical shift temperature dependence.*

Figure 3.5: *The good linear fit obtained with the Van't Hoff equation is further validation for the self-association of $[Pt^{II}(phen)(L^{1}\text{-}S,O)]^{+}$ in CD_3CN. The 95% confidence interval of the slope and intercept for the $[Pt^{II}(phen)(L^{1}\text{-}S,O)]^{+}$ dimer equal 3087.1 ($\pm$ 374.2)x -7.5 ($\pm$1.3)*

Figure 3.6: *Good agreement was obtained between the dimer model least-squares fit and the experimental (symbols) diffusion coefficient dependence on the concentration of $[Pt^{II}(phen)(L^{1}\text{-}S,O)]^{+}$ at 299.2 K.*

Figure 3.7: *ESI(+) Mass Spectrum of $[Pt^{II}(phen)(L^{1}\text{-}S,O)]Cl$ in acetonitrile.*

Figure 3.8: *Broadening of the ^{1}H NMR resonance signals of $[Pt^{II}(phen)(L^{1}\text{-}S,O)]^{+}$ due to the increased dimerisation as a result from (a) an increase in D_2O content, (b) an increase in concentration and (c) a decrease in temperature.*

Figure 3.9: *Chemical shift concentration dependence of the 1,10-phenanthroline H^2 proton on the concentration of $[Pt^{II}(phen)(L^1\text{-}S,O)]^+$ in CD_3CN:D_2O mixtures (299K).*

Figure 3.10: *Excellent agreement was obtained between the dimer model least-squares fits and the experimental (symbols) chemical shift dependence of the 1,10-phenanthroline H^2 proton on the concentration of $[Pt^{II}(phen)(L^1\text{-}S,O)]^+$ in (a) 10:90, (b) 20:80 and (c) 30:70 v/v D_2O:CD_3CN mixtures.*

Figure 3.11: *Van't Hoff Plots of solutions 0% - 30% D_2O. The good linear fit obtained with the Van't Hoff equation is further validation for the self-association of $[Pt^{II}(phen)(L^1\text{-}S,O)]^+$ in CD_3CN.*

Figure 3.12: *Chemical shift dependence of the 1,10-phenanthroline H^2 proton on the concentration of $[Pt^{II}(phen)(L^1\text{-}S,O)]^+$ in solutions containing only D_2O.*

Figure 3.13: *Proton spectrum of $[Pt^{II}(phen)(L^1\text{-}S,O)]^+$ in D_2O showing the phenanthroline protons in the aromatic region of the spectrum.*

Figure 3.14: *TEM image of $[Pt^{II}(phen)(L^1\text{-}S,O)]Cl$ in H_2O stained with uranyl acetate.*

Figure 4.1: *^1H NMR spectra of $[Pt^{II}(phen)(L\text{-}S,O)]^+$ (colour red) and fluoranthene in CD_3CN at 299.2K as a function of fluoranthene concentration.*

Figure 4.2: *Excellent agreement was obtained between the experimental (symbols) chemical shift dependence of (a) the 1,10-phenanthroline H^2 proton and (b) the fluoranthene H^{2*} proton as a function of fluoranthene concentration and the self- and hereto association dimer model least-squares fits.*

Figure 4.3: *Species distribution diagram when increasing amounts of fluoranthene is added to a Pt^{II} solution, with determined constants K_D and K_B of 56 (±13) M^{-1} and 72 (±7) M^{-1} respectively at 267.1 K. Fluoranthene π-π stacking is negligible in the concentration range below 0.1 M.*

Figure 4.4: *The good linear fit obtained with the Van't Hoff equation is further validation for the other-sphere dimer formation of $[Pt^{II}(phen)(L\text{-}O,S)]^+$ and fluoranthene in CD_3CN*

Figure 4.5: *Concentration dependence of the protons of $[Pt^{II}(phen)(L\text{-}S,O)]^{+}$ in CD_3CN at 299 K with increasing fluoranthene concentration, where (a) is the phenanthroline protons in the aromatic region and (b) the acylthiourea protons in the aliphatic region.*

Figure 4.6: *Literature structures of two complexes with fluoranthene where (a) fluoranthene / benzene dimer and (b) most stable $Cr(fluoranthene)_2$ isomer.*

Figure 4.7: *^1H NMR spectrum and assignment of fluoranthene in CD_3CN at 25°C*

List of Tables

Table 2.1: *Ligands and complexes synthesised with full and abbreviated names*

Table 2.2: *Summary of the ^{15}N and ^{1}H chemical shifts obtained from the $^{1}H,^{15}N$ HMBC experiments.*

Table 2.3: *^{1}H NMR data of phen and $[Pt^{II}Cl_2(phen)]$ in DMSO-d_6 at 25ºC*

Table 2.4: *^{1}H NMR data of HL^1 and $[Pt^{II}(phen)(L^1\text{-}S,O)]Cl$ in DMSO-d_6 at 25ºC*

Table 2.5: *^{1}H NMR data of HL^2 and $[Pt^{II}(phen)(L^2\text{-}S,O)]Cl$ in DMSO-d_6 at 25ºC*

Table 2.6: *^{1}H NMR data of HL^3 and $[Pt^{II}(phen)(L^3\text{-}S,O)]Cl$ in DMSO-d_6 at 25ºC*

Table 2.7: *^{1}H NMR data of HL^4 and $[Pt^{II}(phen)(L^4\text{-}S,O)]Cl$ in DMSO-d_6 at 25ºC*

Table 2.8: *^{1}H NMR data of HL^5 and $[Pt^{II}(phen)(L^5\text{-}S,O)]Cl$ in $CDCl_3$ at 25ºC*

Table 2.9: *^{1}H NMR data of fluoranthene in CD_3CN at 25ºC*

Table 3.1: *Calculated dimerization constants, K_D for $[Pt^{II}(phen)(L^1\text{-}S,O)]^+$ in CD_3CN and thermodynamic data.*

Table 3.2: *Diffusion coefficients D ($\times 10^{-10}$ m^2s^{-1}) hydrodynamic radii r_H (Å) and hydrodynamic volumes V_H ($Å^3$) for $[Pt^{II}(phen)(L^1\text{-}S,O)]^+$ in CD_3CN at different complex concentrations (mM).*

Table 3.3: *Calculated dimerisation constants, K_D for $[Pt^{II}(phen)(L^1\text{-}S,O)]^+$ in different D_2O:CD_3CN mixtures.*

Table 3.4: *Thermodynamic data for the self-association of $[Pt^{II}(phen)(L^1\text{-}S,O)]^+$ in D_2O:CD_3CN mixed solutions at 299.3K.*

List of Schemes and Diagrams

Scheme 2.1: *Reaction scheme for the synthesis of $[Pt^{II}Cl_2(phen)]$*

Diagram 2.1: *Deshielding of N^1 and H^2 due to the electron withdrawing effect the strong Pt-S bond in the trans position that is enhanced by the inductive effect of the pyrrolidyl nitrogen.*

Diagram 2.2: *Calculated chemical shift difference between $N^1 - N^{10}$ and $H^2 - H^9$.*

Scheme 2.2: *Reaction scheme for the synthesis of the N,N-di(alkyl)-N'-acylthiourea ligands*

Scheme 2.3: *Reaction scheme for the synthesis of the $[Pt^{II}(phen)(L^n\text{-}S,O)]Cl$ complexes*

Scheme 2.4: *Resonance stabilization of the deprotonated N,N-di(alkyl)-N'-acylthiourea ligands*

Scheme 2.5: *Structure and numbering scheme for $[Pt^{II}(phen)(L^1\text{-}O,S)]Cl$*

Scheme 2.6: *Representation of molecular diffusion in an PFG experiment.*

Scheme 3.1: *Structure and numbering scheme for $[Pt^{II}(phen)(L^1\text{-}S,O)]Cl$*

Diagram 3.1: *Estimation of the r_H of $[Pt^{II}(phen)(L^1\text{-}S,O)]^+$ from two closely related crystal structures*

Scheme 3.2: *Proposed average $[Pt^{II}(phen)(L^1\text{-}S,O)]^+$ dimer aggregate structures in solution.*

Scheme 4.1: *Proposed possible average $[Pt^{II}(phen)(L\text{-}S,O)]^+$/fluoranthene dimer aggregate structures in solution. The highlighted structure is used as the average structure the $[Pt^{II}(phen)(L\text{-}S,O)]^+$/fluoranthene dimer aggregate.*

Chapter 1

General Introduction and Background

Chapter 1

General Introduction and Background

1.1 Bioactivity of Platinum(II) Complexes

The proven bioactivity of platinum(II) complexes continue to stimulate fundamental research for medicinal applications.[1-5] The interest in platinum(II) complexes escalated with the discovery of the now famous *cis*-diaminedichloroplatinum(II) complex ("cisplatin") by Barnett and Rosenberg[6] used for the treatment of ovarian cancer.[3] Due to the success of cisplatin, the coordinated ligands have been extensively tailored in order to develop new anti-cancer drugs.[7-10] In this context Aldrich-Wright and co-workers studied the potential bioactivity of platinum(II)diimine complexes.[11-15] Their research focuses on DNA intercalating compounds and methods to transport the drug molecule via encapsulation within two calix[4]arene molecules to target cancer cells.[14,15] Barton and co-workers found that platinum(II)diimine complexes upon intercalation into the DNA stack, promote photo-reductive and oxidative damage within the DNA duplex due to its excited-state oxidation and reduction potentials.[16] Interestingly when the diimine ligand is 1,10-phenanthroline, Cusumano and Pietro found that these platinum(II)phenanthroline complexes intercalate with DNA as well as aggregate in solution.[17] Several years ago Egan and Koch showed that cationic $[Pt^{II}$(diimine)(*N*,*N*-di(alkyl)-*N'*-acylthiourea)$]^{+}X^{-}$ complexes display significant anti-malarial activity in chloroquine resistant strains of *Plasmodium Falciparum*.[18] Moreover similar complexes also showed antimicrobial activity thought to arise from interesting DNA intercalation with demonstrable *in vivo* activity toward bacterial *E. coli* AB1886 *(uvr A)* cultures.[19]

The persistent use of platinum(II) complexes for medicinal applications stems from the unique chemistry associated with the platinum(II) metal centre. In particular, the relatively slow ligand exchange kinetics ensure that the drug molecule reaches the intended target sites intact. The square planar geometry of platinum(II) complexes allows

for possible non-covalent interactions with the metal centre as well as the coordinated ligands.[20,21] Moreover the ligands can be tailored with specific functional groups for covalent interactions.

1.2 Anti-malarial Drug Design

The high death toll in Africa due to the malaria parasite *Plasmodium Falciparum* accompanied by drug resistance necessitates the discovery of new drugs. Anti-malarial drug design focuses on identifying stages in the parasite life-cycle (Figure 1.1) for possible drug targets.

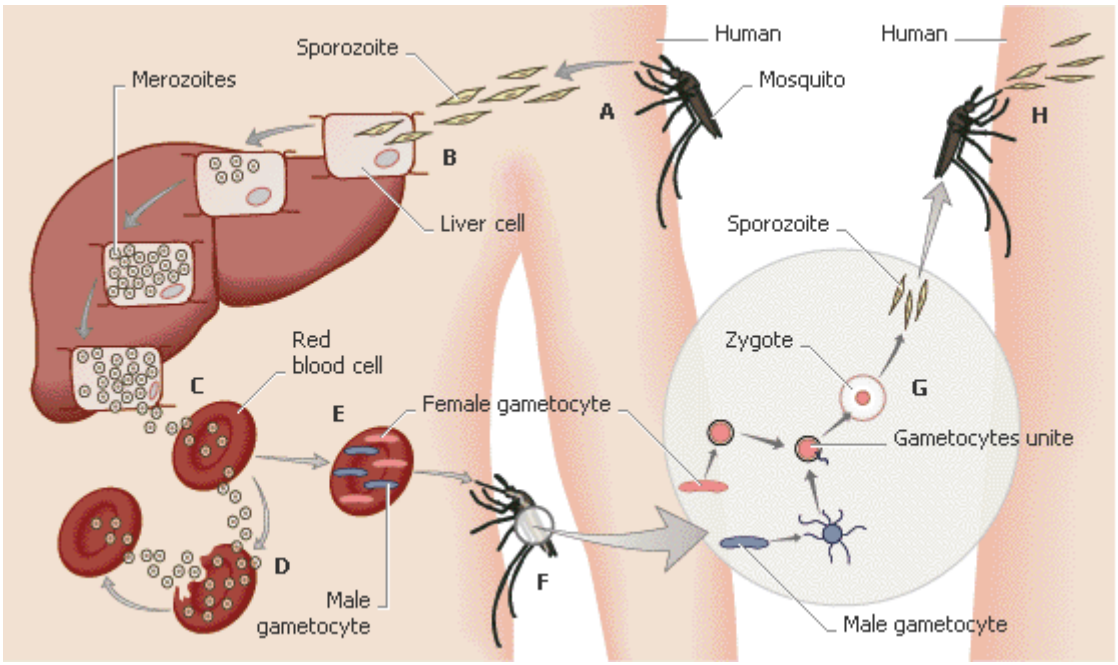

Figure 1.1: *The life cycle of the malaria parasite Plasmodium (picture reproduced from MSN Encarta)*[22]

The life cycle of the malaria parasite consist of three major stages in which it resides in two hosts, the female mosquito and humans. Current anti-malarials are designed to target the parasite when present in human red blood cells (Figure 1.1). The postulated mechanism of anti-malarial activity in the red blood cells is thought to be due to the following processes.[23]

Haemoglobin (Hb) from the human red blood (Figure 1.2) cell enters the cytoplasm (cyt; blue) of the parasite and migrates to the food vacuole (FV; white) for digestion. Haemoglobin consists of indigestible haematin (h) and proteins that are digested to polypeptides (pp) and finally amino acids (aa). However, the indigestible hematin is a toxin for the malaria parasite and at high enough concentration causes the death of the parasite.

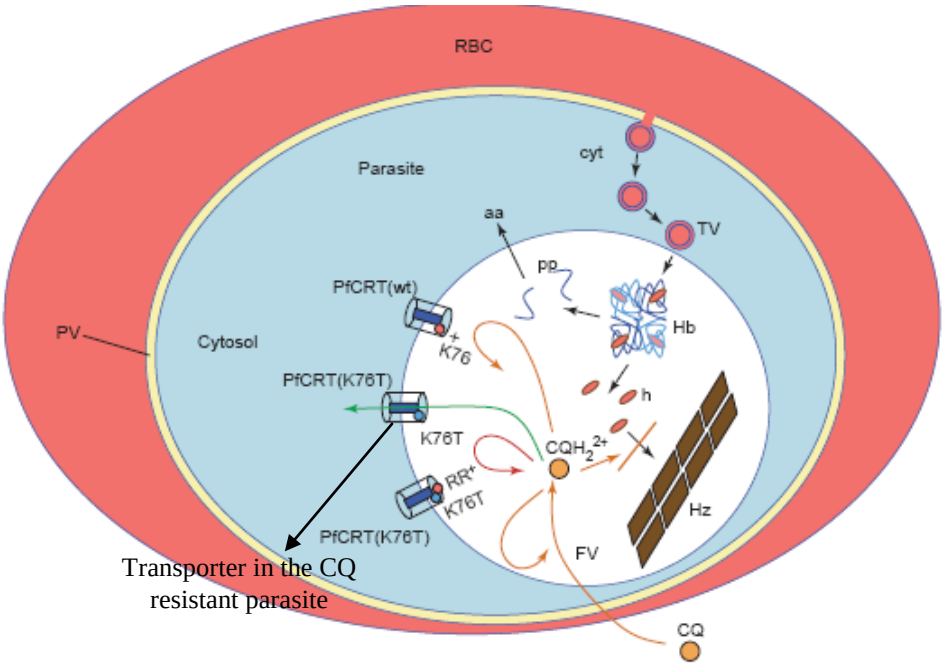

Figure 1.2: *Representation from Egan et al. of the mode of action of chloroquine (CQ) in the malaria parasite in the human red blood cell.*[23]

To prevent the build-up of haematin, the parasite converts haematin to insoluble polymeric malaria pigments called haemazoin (Hz) that appears as black spots under a microscope.[24] Chloroquine (CQ) is a known effective anti-malarial drug. It accumulates in the food vacuole of the parasite in the protonated form (CQH_2^{2+}) through pH trapping and is known to inhibit haemazoin formation leading to the self-poisoning of the malaria parasite. The accumulation of chloroquine and the association with haemazoin has been directly observed by electron microscopic autoradiography.[25] However, due to a mutation of the PfCRT transporter (K76T) in the membrane of the food vacuole the protonated chloroquine concentration is decreased leading to ineffective haemazoin inhibition.[26,27] Koch and Egan hypothesized four essential properties for potential drug compounds to inhibit haemazoin formation.[18]

These are:

1. Accumulation in the food vacuole of the parasite through pH trapping
2. Association (complexation) with Fe(III)PPIX (haematin) via coplanar stacking
3. Inhibition of haemazoin formation due to the potential coplanar stacking between the drug and haemazoin
4. Death of the parasite because of a build-up of toxic hematin

The coplanar stacking or intermolecular association of the drug molecule with haematin could be due to several non-covalent interactions.

1.3 Non-Covalent Intermolecular Interactions

The weak nature of non-covalent intermolecular interactions as well as the complexity of these interactions makes it difficult to identify the type and the energies involved in these interactions. The Gibbs energy of formation associated with non-covalent interactions is relatively small compared to covalent bonding. Meuller-Dethlefs and Hobza have published a review on intermolecular interactions and emphasized the difficulty of experimental and theoretical studies on these weak interactions.[28]
The most common non-covalent intermolecular interactions known are hydrogen bonding, cation-π interactions, hydrophobic forces, van der Waals forces, π-π interactions and electrostatic effects. In some cases non-covalent interactions arise from a combination of several interactions mentioned e.g. ion-pairing, hydrogen bonding, cation-π and π-π interactions.[28]

1.3.1 Hydrogen bonding Interactions

Hydrogen bonding is the most common non-covalent intermolecular interaction. It dictates molecular conformation and aggregation in chemical systems ranging from inorganic[29] to biological systems[14-17]. Hydrogen bonding is difficult to define explicitly and several types of hydrogen bonds are known.[30] The most common hydrogen bond, X–H···A, is formed between a hydrogen attached to an electronegative donor atom (X) and a neighbouring acceptor atom (A). Other types of hydrogen

bonding that are mainly inferred from solid state crystallographic data are illustrated in Figure 1.3.

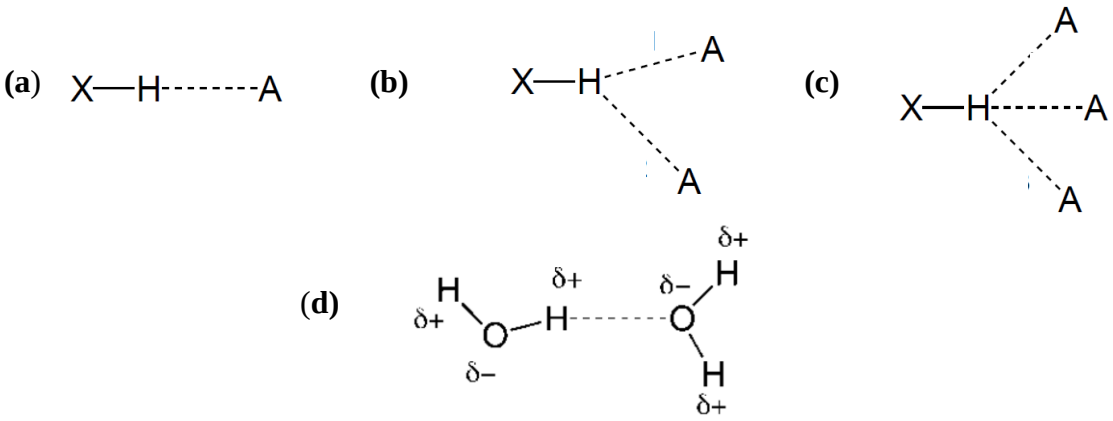

Figure 1.3: *Different types of hydrogen bonding.* ***(a)*** *Normal hydrogen bond with one acceptor.* ***(b)*** *Bifurcated hydrogen bonding.* ***(c)*** *Trifurcated hydrogen bonding.* ***(d)*** *Prototype of a hydrogen bond with the water dimer as an example.*[30]

All hydrogen bonds can be considered as developing proton transfer reactions and in strong hydrogen bonding interactions the proton transfer can be in a highly developed state.[30]

1.3.2 Ion pairing

When oppositely charged ions are held together by electrostatic interaction, without the formation of a covalent bond, an ion pair is formed.[31] Ion pairs are classified in two groups, contact ion pairs and loose ion pairs.[32] Contact ion pairs are formed when ions are directly in contact with no solvent between them. Bakker and co-workers reported contact ion pairs only in their most concentrated samples in their study of ion pairing in metal based polymer electrolytes.[33] Loose ion pairs are defined when the two constituent ions are separated by one or more solvent molecules and can be further subdivided into two groups of solvent-sharing and solvent-separated ion pairs. Solvent separated ion pairs are difficult to detect and are normally identified by indirect spectroscopic and conductivity measurements.[34]

1.3.3 Cation-π Interactions

Cation-π interactions are generally the result of the attractive forces between a simple cation, such as K^+ and the π-face of an aromatic molecule.[20,21,28,35-37] The aromatic molecule consists of delocalized π-electrons above/below the plane and a slightly positive σ-framework in the plane of the molecule forming a quadrupole moment (Figure 1.4a). The attraction between an aromatic molecule and a simple cation is graphically represented in Figure 1.4b where the slight negative charge above/below the plane of the aromatic molecule attracts positively charged cations.

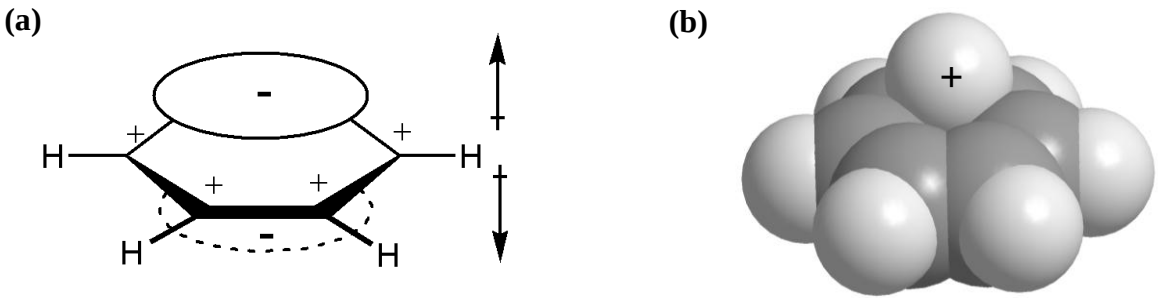

Figure 1.4: (a) *Schematic drawing of the charge distribution of benzene showing the positively charged σ-framework and negatively charged π-electron cloud forming a quadrupole moment and* ***(b)*** *the cation-π interactions showing the contact of the K^+ cation and benzene.*[35]

The cation associates with the face of the aromatic molecule through electrostatic attraction. These interactions can be relatively strong (-19.0 kcal.mol^{-1} for K^+···benzene in the gas phase) and can be the driving force of non-covalent association reactions.[36] Dougherty and co-workers have carried out extensive theoretical as well as experimental studies on the energetically favoured cation-π interactions in protein structures.[37] The cation-π interactions in proteins are agued to significantly contribute to the stability of the protein structure and the amino acids have a preference for the amino acids it binds to through cation-π interactions.[37] Hydrogen bonding to the π-system of aromatic moieties are similar to cation-π interactions where the slightly positive hydrogen atom interacts with the slightly negative π-electron cloud, a common interaction in supramolecular chemistry. There is also a phenomenon called anion-π

interaction where the anion associates with the positively charged σ-framework of the aromatic moiety.[38,39] This interaction is however weaker and less common than the cation-π interaction discussed.

1.3.4 π -π Interactions

Hunter and Sanders have developed a model for non-covalent intermolecular reactions between two π-systems commonly referred to as "π-π interactions" from their study on porphyrin aggregation.[40] They developed a simple electrostatic model which suggests that the mode of interaction is dominated by residual electrostatic interactions and the overall energy of the interaction between the two π-systems is a combination of electrostatic, dispersion, induction and repulsion contributions:

$$E_{Total} = E_{Electrostatic} + E_{Dispersion} + E_{Induction} + E_{Repulsion}$$

This model of "π-π interactions" between uncharged aromatic and quasi-aromatic planar molecules is supported by the predicted offset interaction widely found in the solid state of such systems, arising from the face to face "π-π stacking" shown in Figure 1.5a. The π-π stacking interaction is also explained by the quadrupolar moment of the aromatic moiety (Figure 1.4a) and in this sense is similar to the formal cation-π interaction due to the quadrupole of benzene. The related π–π stacking is associated with different geometrical configurations (Figure 1.5).[35]

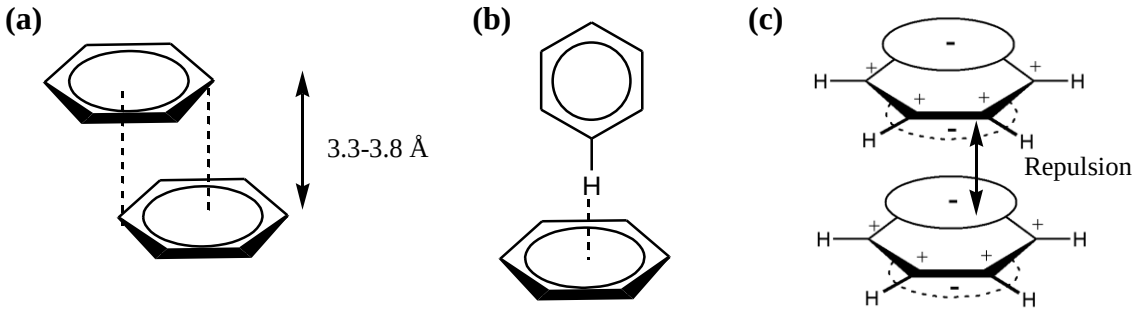

Figure 1.5: *The limiting types of aromatic π-π interactions:* ***(a)*** *face-to-face (interplanar distance approximately 3.3-3.8 Å) and* ***(b)*** *edge-to-face orientations.* ***(c)*** *The repulsion between negatively charged π-electron clouds of facially oriented aromatic rings.*[35]

The face-to-face π-π interaction (Figure 1.5a) is established when the attraction between the π-electron cloud and the positive σ-framework outweighs the unfavourable π-π electron repulsion (Figure 1.5c). The face-to-face π-π interactions are key interactions for the tertiary structure of proteins[41,42] and intercalation of drug molecules into DNA.[43] The edge-to-face interaction (Figure 1.5b) is in principle similar to a cation-π interaction and occurs when the slightly positively polarised hydrogen atom and the negative π-electron cloud of the aromatic molecule attract each other. These interactions are also found in the solid state.[40]

1.4 Objectives of This Study

Active $[Pt^{II}(diimine)(N,N\text{-di(alkyl)-}N'\text{-acylthiourea})]^{+}X^{-}$ complexes (Scheme 1.1) against malaria have previously been synthesized and tested by Koch and Egan.[18]

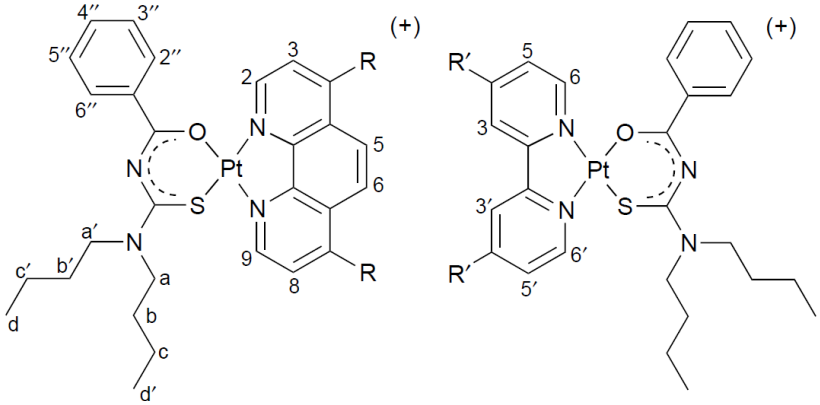

Scheme 1.1: *Structure of mixed ligand $[Pt^{II}(diimine)(L^{n}\text{-}S,O)]PF_6$ complexes.*[36]

These complexes were also found to aggregate in solution as shown by Lawrence et al, and it is reasonable to expect that these complexes interact via cation-π interactions.[36] The π-π and cation-π interactions between the platinum(II) metal centre and the diimine ligands are postulated to be the main interaction concerning the potential anti-malarial activity of these $[Pt^{II}(diimine)(N,N\text{-di(alkyl)-}N'\text{-acylthiourea})]^{+}X^{-}$ complexes. The mode of anti-malarial activity is postulated to be the coplanar stacking of the drug molecules with haematin (Figure 1.6). However, the mechanism is still contentious and methods for studying the non-covalent interactions of these complexes are essential.[23] The anti-

malarial activity of platinum(II) metal based drugs have received comparatively little attention in literature.[18,36]

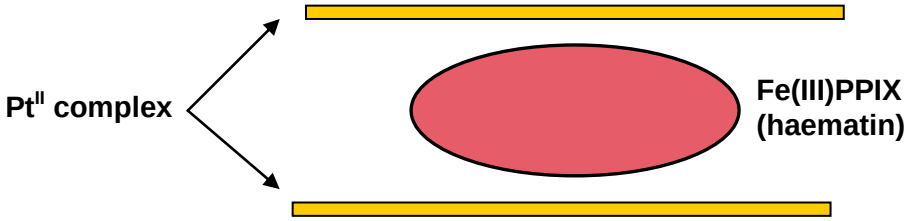

Figure 1.6: *Representation of the coplanar stacking of the potential anti-malarial complexes with hematin.*

In this context, the study involves the synthesis of novel square planar [Pt^{II}(diimine)(*N*,*N*-di(alkyl)-*N'*-acylthiourea)]$^{+}$X^{-} complexes (Scheme 1.2) from the same class of compounds that is known to be anti-malarial. The anti-malarial drug design is aimed at targeting haemazoin inhibition in the same way as current anti-malarials due to the effectiveness of this drug target.

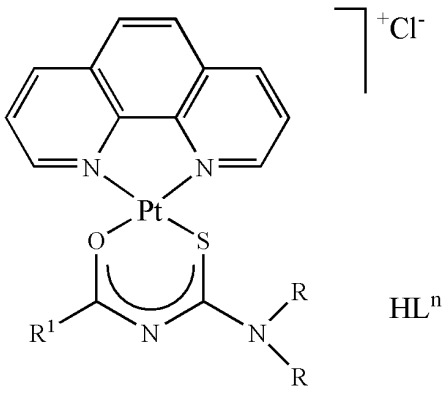

R^1 = ^{t}Bu or 

R = Various alkyl groups

HL^n = *N*,*N*-di(alkyl)-*N'*-benzoylthiourea or
N,*N*-di(alkyl)-*N'*-^{t}butylthiourea

Scheme 1.2: *Schematic representation and nomenclature of the [Pt^{II}(phen)(N,N-di(alkyl)-N'-acylthiourea)]Cl or [Pt^{II}(phen)(L^n-S,O)]Cl complexes used in this study.*

Given the cationic nature of the [Pt^{II}(phen)(L^n-*S*,*O*)]Cl the objective of this study was to

a) develop methods to study the self-association (aggregation) of such complexes in acetonitrile as well investigate the effect of deuterium oxide on the aggregation of these complexes in acetonitrile-d_6.

b) to investigate the possibility and nature of the cation-π interactions of such $[Pt^{II}(phen)(L^n\text{-}S,O)]^+$ cations with uncharged aromatic molecules such as fluoranthene and estimate the extent of the hetero-association of such systems to get insight into the mechanism of anti-malarial activity.

In this context we used ^{1}H NMR as well as Diffusion Ordered Spectroscopy (DOSY) to investigate these phenomena.

Chapter 2

Ligand and Complex Synthesis, Characterization and Experimental

Chapter 2

Ligand and Complex Synthesis, Characterization and Experimental

2.1 Introduction

In a previous study Koch and co-workers synthesized a series of potential anti-malarial platinum(II) complexes (Figure 2.1).[18,19,36] Aqueous solubility of these platinum(II) complexes is low and drastically improved when the *N',N'*-dibutyl group was replaced with the *N',N'*-di-2-hydroxyethyl and Cl^- as the counter ion (Figure 2.1b) .[18,19] Aqueous solubility is essential regarding their potential use as anti-malarial drugs.

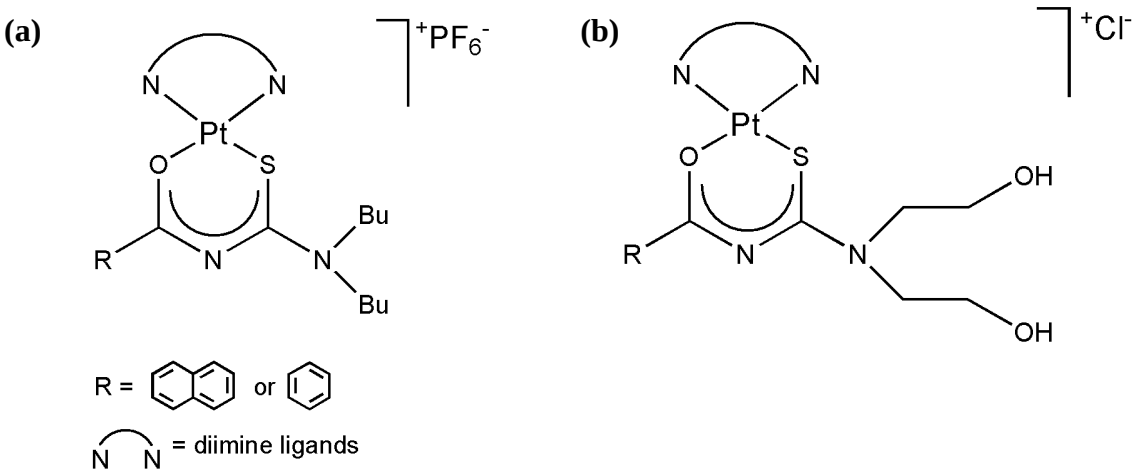

Figure 2.1: *Previous anti-malarial complexes synthesized by Koch and co-workers.*[18,19,36]

The addition of the hydroxide groups improved aqueous solubility and ensured protonatability of the complex (Figure 2.1b) for accumulation in the food vacuole of the malaria parasite. Moreover, upon variation of the diimine moiety, Koch and Egan found that the complexes with 1,10-phenanthroline exhibited the best anti-malarial activity as well as the tendency to self-associate in solution.[18,36]

The aim of this study was to synthesize platinum(II) complexes with the desired aqueous solubility properties without using ligands containing hydroxyl and benzoyl groups to avoid unwanted hydrogen bonding and additional π-π interactions. Moreover the study involves the investigation of the self- and hetero-association of these complexes by means of various techniques. A series of complexes were synthesized, characterized and tested for water solubility and stability.

2.2. Synthesis of [Pt^{II}(1,10-phenanthroline)(*N*,*N*-di(alkyl)-*N'*-acylthiourea)]Cl complexes

For clarity a simplified synthesis scheme of the [Pt^{II}(1,10-phenanthroline)(*N*,*N*-di(alkyl)-*N'*-acylthiourea)]Cl complexes is shown in Figure 2.2 with the abbreviated names of the ligands and complexes summarized in Table 2.1.

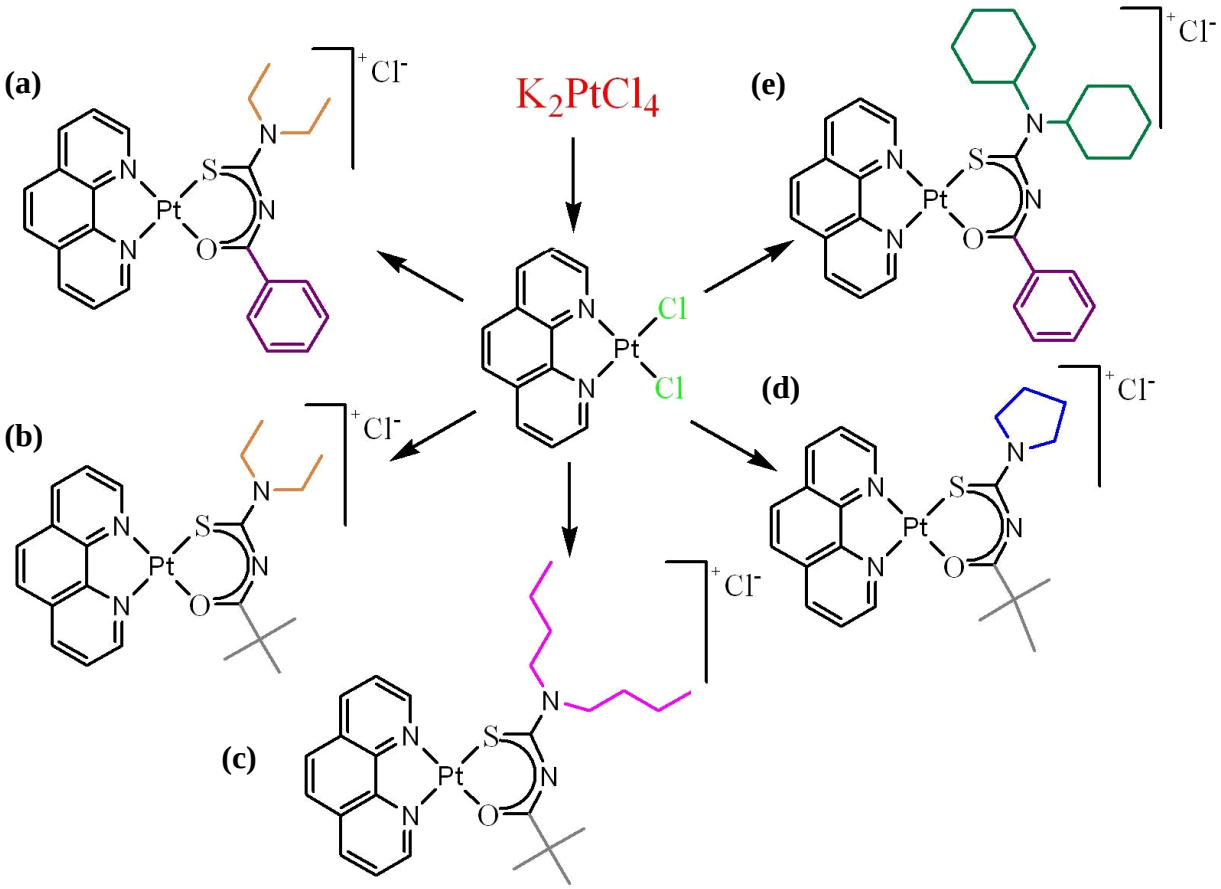

Figure 2.2: *Series of [Pt^{II}(1,10-phenantroline)(N,N-di(alkyl)-N'-acylthiourea)]Cl complexes synthesized*

Table 2.1: *Ligands and complexes synthesised with full and abbreviated names*

Ligand name	Abbreviation	Complex name	Abbreviation
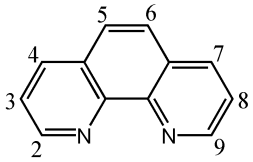 1,10-phenanthroline	phen	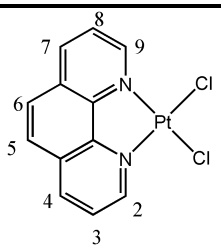 [$Pt^{II}Cl_2$(1,10-phenanthroline)]	[Pt^{II}(phen)Cl_2]
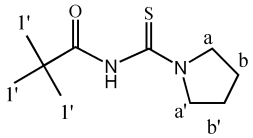 *N*,*N*-pyrolidyl-*N'*-^{t}butylthiourea	HL^1	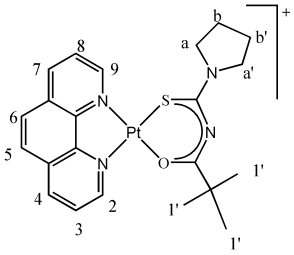 [Pt^{II}(1,10-phenanthroline)(*N*,*N*-pyrolidyl-*N'*-^{t}butylthiourea)]$^{+}$	[Pt^{II}(phen)(L^1-*S*,*O*)]$^{+}$
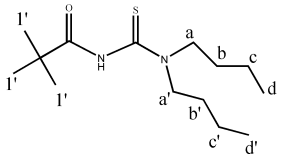 *N*,*N*-di(n-butyl)-*N'*-^{t}butylhiourea	HL^2	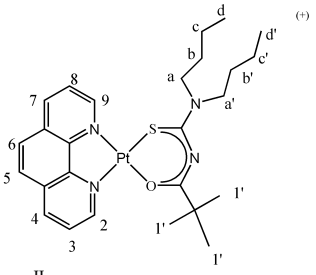 [Pt^{II}(1,10-phenanthroline)(*N*,*N*-di(n-butyl)-*N'*-^{t}butylthiourea)]$^{+}$	[Pt^{II}(phen)(L^2-*S*,*O*)]$^{+}$
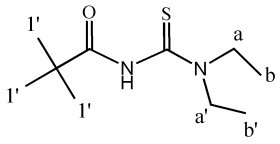 *N*,*N*-di(n-buthyl)-*N'*-^{t}butylthiourea	HL^3	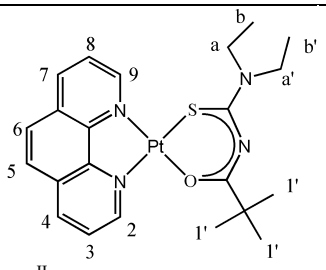 [Pt^{II}(1,10-phenanthroline)(*N*,*N*-di(ethyl)-*N'*-^{t}butylthiourea)]$^{+}$	[Pt^{II}(phen)(L^3-*S*,*O*)]$^{+}$

Table 2.1: *Ligands and complexes synthesised with full and abbreviated names*

Ligand name	Abbreviation	Complex name	Abbreviation
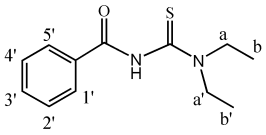 *N*,*N*-di(n-buthyl)-*N'*-benzoylthiourea	HL^4	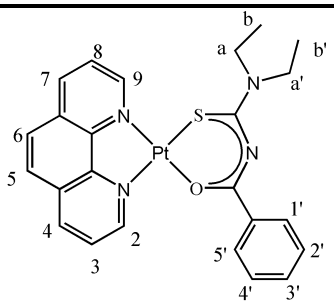 [Pt^{II}(1,10-phenanthroline)(*N*,*N*-di(ethyl)-*N'*-benzoylthiourea)]$^+$	[Pt^{II}(phen)(L^4-*S*,*O*)]$^+$
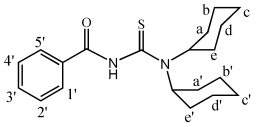 *N*,*N*-di(cyclohexyl)-*N'*-benzoyl- thiourea	HL^5	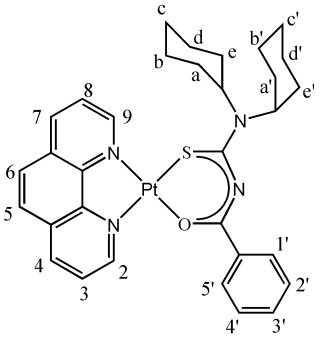 [Pt^{II}(1,10-phenanthroline)(*N*,*N*-di(cyclohexyl)-*N'*-benzoylthiourea)]$^+$	[Pt^{II}(phen)(L^5-*S*,*O*)]$^+$

The *N*,*N*-di(alkyl)-*N'*-acylthiourea ligand of the [Pt^{II}(1,10-phenanthroline)(*N*,*N*-di(alkyl)-*N'*-acylthio-urea)]Cl complexes was varied in an attempt to improve solubility in water. *N*,*N*-di(n-buthyl)-*N'*-thiourea (Figure 2.2a) was not sufficiently soluble and the benzoyl group was replaced with a ^{t}butyl group (Figure 2.2b). An improvement in the water solubility for this complex was observed and the ^{t}butyl functionality was reserved while the amine side of the *N*,*N*-di(alkyl)-*N'*-acylthiourea ligand was tailored further. Longer carbon chains on the amine side (Figure 2.2c) resulted in decreased water solubility as expected. The amine side was changed to the pyrrolidyl variation (Figure 2.2d). This made the complexe sufficiently soluble and stable to ligand substitution as stability tests in dimethylsulfoxide solutions showed (*vide infra*). The *N*,*N*-di(cyclohexyl)-*N'*-benzoylthiourea variation (Figure 2.2e) was synthesized for the NOESY experiments that will be discussed in this chapter.

The general synthesis steps discussed:

2.2.1 Synthesis of [$Pt^{II}Cl_2$(1,10-phenanthroline)]

2.2.2 Synthesis of the *N*,*N*-di(alkyl)-*N'*-acylthiourea ligands

2.2.3 Synthesis of the [Pt^{II}(1,10-phenanthroline)(*N*,*N*-di(alkyl)-*N'*-acylthiourea)]Cl complexes

The characterization of Pt^{II}(1,10-phenanthroline)(*N*-pyrrolidyl-*N*-(2,2-dimethyl-propanoyl)thiourea)]Cl or [Pt^{II}(phen)(L^1-*O*,*S*)]Cl (Figure 2.2d) and its precursors is included in the general synthesis discussion below. The characterization of the remaining complexes synthesized can be found in section 2.6. The numbering scheme (assignments) of these complexes will be discussed in detail later in this chapter.

2.2.1 Synthesis of [$Pt^{II}Cl_2$(1,10-phenanthroline)]

[$Pt^{II}Cl_2$(1,10-phenanthroline)] was synthesized according to the method described by Morgan and Bustall (Scheme 2.1).[44] The bidentate 1,10-phenanthroline displaces two of the chlorides to form the square planar [$Pt^{II}Cl_2$(phen)] complex. HCl (2ml 4.0M) was added to the reaction mixture to prevent the aquation of the $PtCl_4^{2-}$ species. A bright yellow product was obtained in high yield (85-93%). ^{195}Pt-^{1}H satellites are barely visible at the base of the ^{1}H resonance signal assigned to H^{2+9} due to chemical shift anisotropy (CSA) effects which will be discussed in the next chapter.

The neutral [$Pt^{II}Cl_2$(phen)] complex is stable in dimethylsulphoxide solutions for longer than 6 weeks and is sparingly soluble in a range of solvents including DMSO. This complex was characterized by means of ^{1}H NMR, IR spectroscopy and Elemental analysis (see section 2.6).

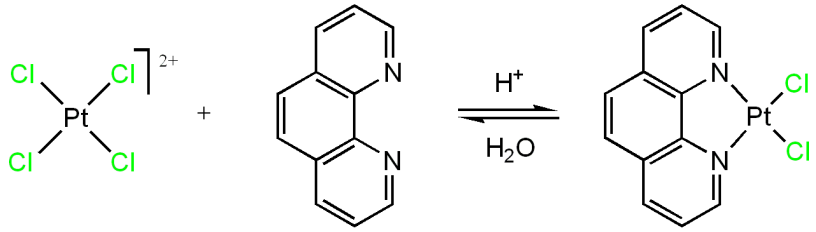

Scheme 2.1

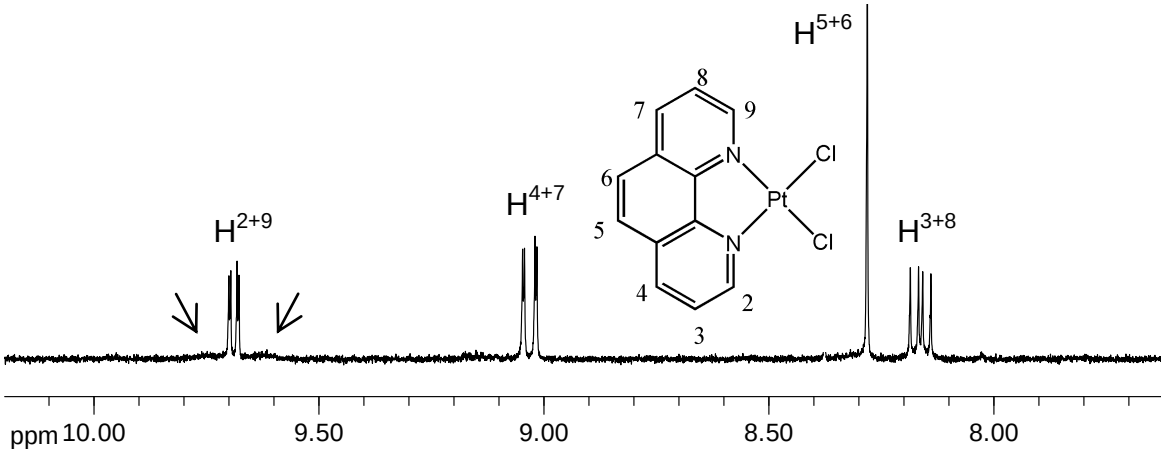

Figure 2.3: *^{1}H NMR spectrum of $[Pt^{II}Cl_2(phen)]$ in DMSO-d_6*

2.2.2 Synthesis of the *N,N*-di(alkyl)-*N'*-acylthiourea ligands

The general methodology of Douglass and Dains was used to prepare the *N,N*-di(alkyl)-*N'*-acylthiourea (Scheme 2.2).[45] The synthesis involves reaction of potassium thiocyanate in anhydrous acetone with benzoyl / ^{t}butyl chloride to form benzoyl isothyanate that reacts with the appropriate amine to form a crude product which is purified by recrystallization from acetone/water mixtures. The ^{1}H NMR spectrum of HL^1 in DMSO-d_6 is shown in Figure 2.4.

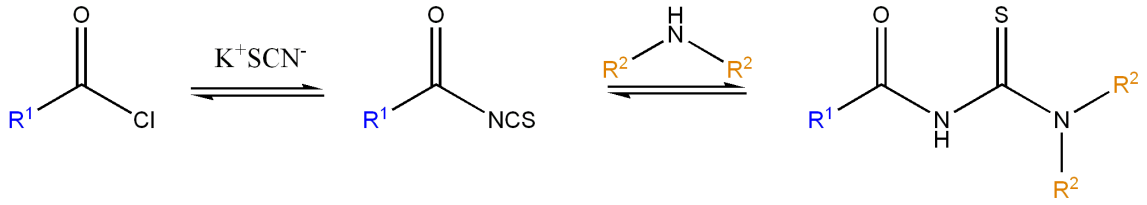

Scheme 2.2

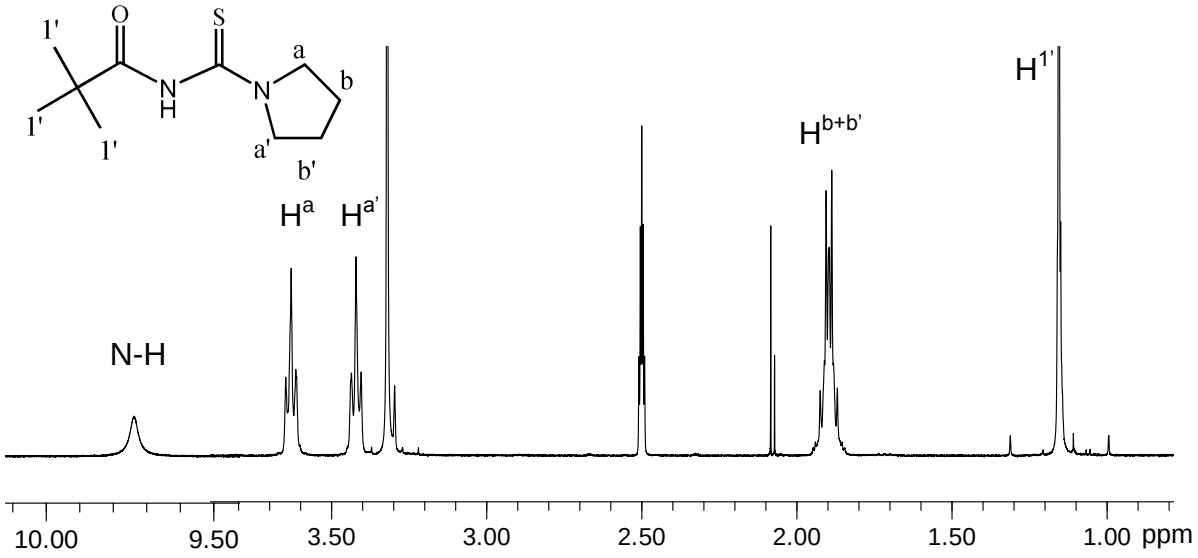

Figure 2.4: *^{1}H NMR spectrum of HL^1 in DMSO-d_6*

2.2.3 Synthesis of the [Pt^{II}(1,10-phenanthroline)(*N*,*N*-di(alkyl)-*N'*-acylthiourea)]Cl complexes

The general method for the synthesis of mixed-ligand [Pt(diimine)(L^n-*S*,*O*)]PF_6 described by Koch *et al*,[36] was used for the preparation of the [Pt^{II}(phen)(L^n-*S*,*O*)]Cl complexes (Scheme 2.3).

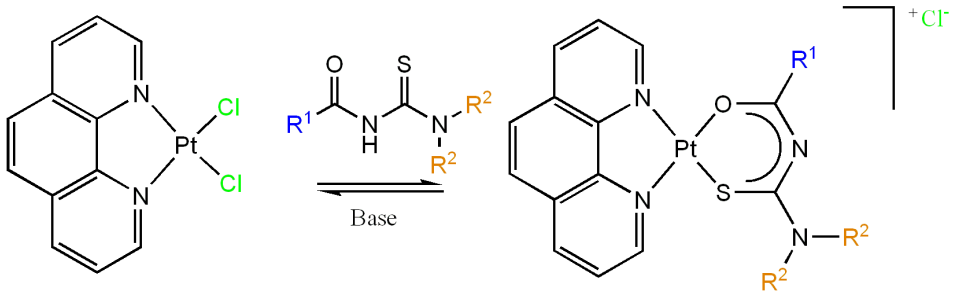

Scheme 2.3

To the relative insoluble [Pt^{II}Cl$_2$(phen)] complex the appropriate *N*,*N*-di(alkyl)-*N'*-acylthiourea ligand was added as well as a weak base (sodium acetate) to deprotonate the ligand. The deprotonated ligand can be thought to be resonance stabilized as shown in Scheme 2.4 which results in the ligand being more nucleophillic in order to coordinate to the metal centre.

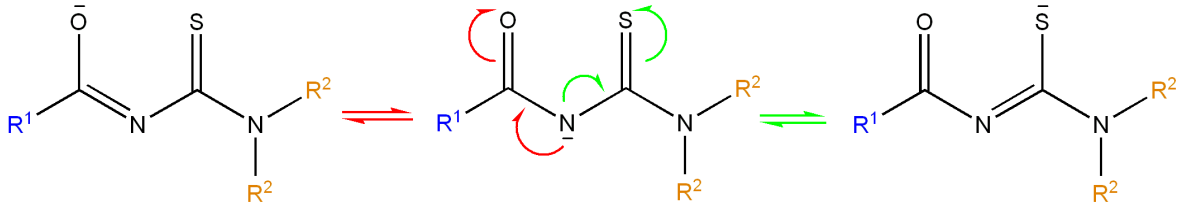

Scheme 2.4

Quantitative yields (>90%) could be obtained by heating the reaction in acetonitrile under reflux overnight. The ^{1}H NMR spectrum of [Pt^{II}(phen)(L^{1}-*S*,*O*)]Cl in acetonitrile-d_6 is shown in Figure 2.5.

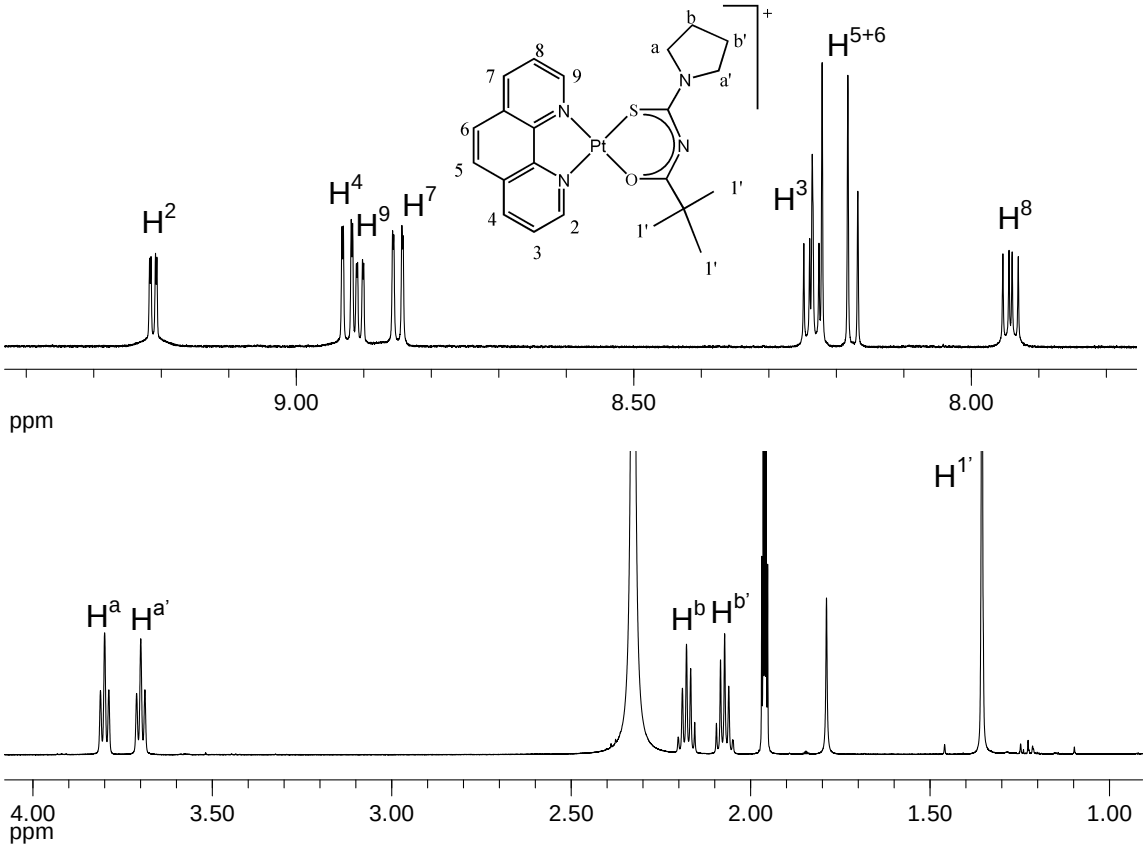

Figure 2.5: *^{1}H NMR spectrum of [Pt^{II}(phen)(L^{1}-S,O)]Cl in acetonitrile-d_3 showing the 1,10-phenanthroline protons in the aromatic region and the N-pyrrolidyl-N-(2,2-dimethylpropanoyl)thiourea protons in the aliphatic region of the spectrum.*

2.3. Aqueous Solubility and Stability Tests

For the solubility and stability studies dimethylsulfoxide (DMSO) and water were used. DMSO was chosen in addition to water as it is a relatively polar solvent and is known to coordinate to platinum(II).[46] The series of complexes synthesized (Figure 2.2) were dissolved in deuterated DMSO and ^{1}H NMR spectroscopy was used to monitor whether coordination of DMSO to the platinum(II) complexes occurs. Additional peaks appeared in the ^{1}H NMR spectra of all the complexes and imply DMSO coordination. However, [Pt^{II}(phen)(L^1-*S,O*)]Cl (Scheme 2.5) was found to be stable in DMSO solutions for more than two weeks. This result illustrates that [Pt^{II}(phen)(L^1-*S,O*)]Cl is kinetically inert compared to the other complexes in the series (Figure 2.2). Moreover, [Pt^{II}(phen)(L^1-*S,O*)]Cl was the most soluble in water (±0.025M) and was consequently used onwards in studying the interactions and association properties of these [Pt^{II}(phen)(*N,N*-di(alkyl)-*N'*-acylthiourea)]Cl complexes.

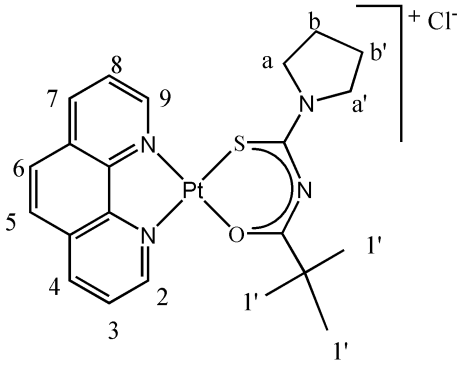

Scheme 2.5: *Structure and numbering scheme for [Pt^{II}(phen)(L^1-O,S)]Cl*

2.4 Detailed analysis of the ^{1}H, COSY, HMBC, NOESY and DOSY NMR spectra for the assignment of the [Pt^{II}(phen)(L^1-*O,S*)]Cl complex

The ^{1}H NMR assignments of platinum(II)(diimine)(*N,N*-di(alkyl)-*N'*-acylthiourea) complexes is still a point of contention.[17] Several two-dimensional NMR experiments were conducted to unambiguously assign the proton spectra of these complexes. The ^{1}H NMR spectrum (Figure 2.5) of [Pt^{II}(phen)(L^1-*S,O*)]Cl is relatively straightforward

compared to the spectra of the other [Pt^{II}(phen)(L^{2-5}-*S,O*)]Cl complexes (see experimental section 2.6). In Figure 2.6 the ^{1}H NMR spectrum of the precursor, [$Pt^{II}Cl_2$(phen)], and the [Pt^{II}(phen)(L^{1}-*S,O*)]Cl complex are shown. The neutral [$Pt^{II}Cl_2$(phen)] complex has a plane of symmetry indicated with a dashed line in Figure 2.6. The symmetry results in a ^{1}H NMR spectrum with four sets of resonance signals. The singlet at 8.29ppm can be allocated to protons H^5 and H^6 while the doublet of doublets at 8.17ppm showed two coupling constants typically in the range of three-bond coupling (J^3) and were consequently allocated to H^3 and H^8. The most deshielded resonance signal (9.70ppm) was allocated to H^2 and H^9 due to the nitrogen atoms in the phenanthroline ligand withdrawing electron density. The remaining resonance signal was allocated to H^4 and H^7.

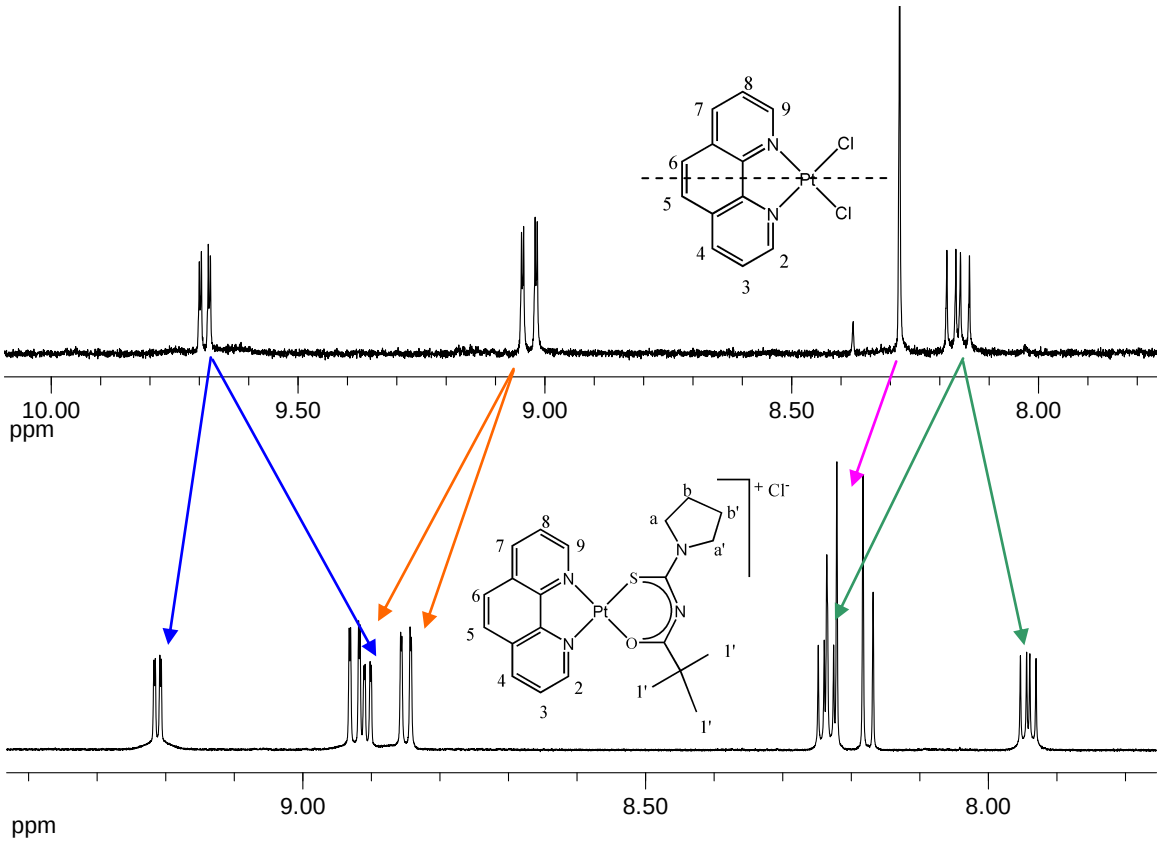

Figure 2.6: *The ^{1}H NMR spectra of Pt^{II}(phen)(L^{1}-S,O)]Cl and the precursor [$Pt^{II}Cl_2$(phen)] in DMSO-d_6.*

The assignment of the phenanthroline protons of [Pt^{II}(phen)(L^{1}-*S,O*)]Cl was not trivial due to the coupling constants being more or less of the same magnitude. To attain the

complete assignment of the ^{1}H NMR spectrum of [Pt^{II}(phen)(L^{1}-*S,O*)]Cl two-dimensional methods were required. The complete COSY (*Correlated spectroscopy*) spectrum obtained for [Pt^{II}(phen)(L^{1}-*S,O*)]Cl is shown in Figure 2.7a. For clarity the aromatic and aliphatic region were enlarged in Figure 2.7b&c.

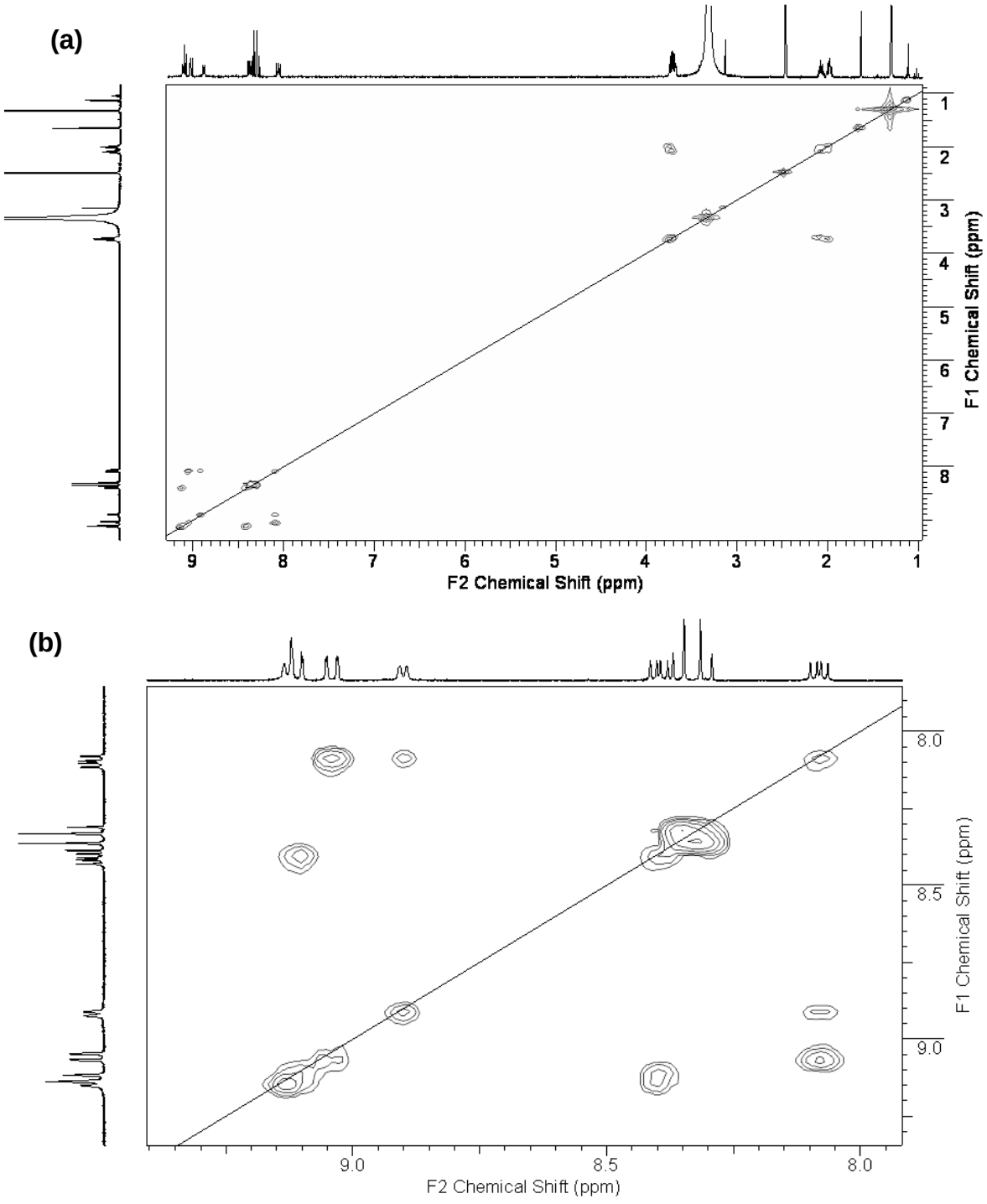

Figure 2.7: *^{1}H,^{1}H COSY spectrum of Pt^{II}(phen)(L^{1}-S,O)]Cl in acetonitrile-d_3 where* ***(a)*** *is the full COSY spectrum and* ***(b)*** *is the aromatic region.*

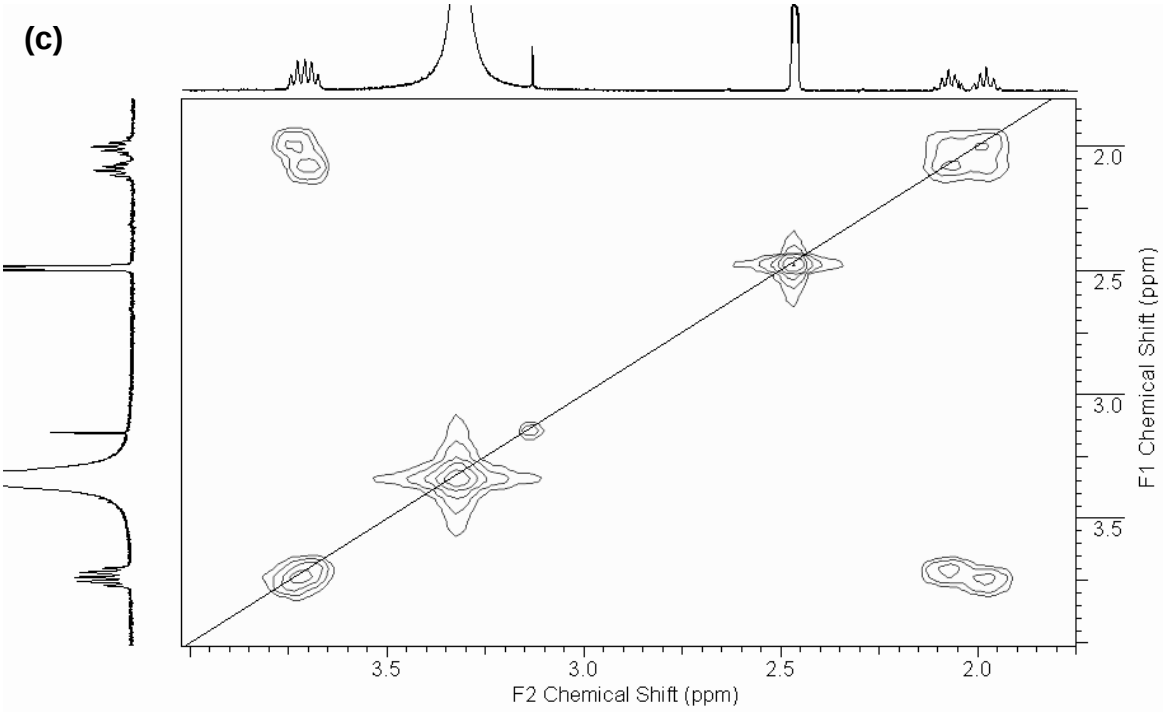

Figure 2.7: *$^{1}H,^{1}H$ COSY spectrum of [Pt^{II}(phen)(L^{1}-S,O)]Cl in acetonitrile-d_3 where* ***(c)*** *is the aliphatic region of the spectrum.*

The correlation diagram (Figure 2.7) clearly shows all the expected J^3 proton couplings. However, unambiguous assignment is not possible because an initial assignment is required to completely assign the spectrum. For now we assume that the nitrogen trans to the sulphur atom is N^1 and the most deshielded proton resonance signal is allocated to H^2. Preliminary assignment (Scheme 2.5) of all the protons of Pt^{II}(phen)(L^1-*S,O*)]Cl can now be made using the assumption made above and the correlations obtained from the COSY spectrum (Figure 2.7). There are no overlapping peaks for the phenanthroline protons except for protons H^5 and H^6 which are indistinguishable and consequently labelled H^{5+6}.

The unambiguous assignment of the proton spectrum of [Pt^{II}(phen)(L^1-*S,O*)]Cl requires more spectroscopic evidence. In particular NOE (*Nuclear Overhauser Effect*) experiments are frequently used to provide structural information.[47] NOE experiments will yield the through-space correlation between nuclei in close proximity, i.e. due to cross-relaxation between the nuclei. Even though it is known which protons are *J* coupled to each other it is not known which proton (H^2 or H^9) will have through space correlations with the protons of the *N,N*-di(alkyl)-*N'*-acylthiourea ligand. Before

attempting NOE experiments on [Pt^{II}(phen)(L^1-*S,O*)]Cl, we conducted the experiment using [Pt^{II}(phen)(L^5-*S,O*]Cl (Figure 2.1e). It was thought that the bulky cyclohexyl groups would have a better chance of interacting with the corresponding H^2/H^9. The NOESY (*Nuclear Overhauser Enhancement Spectroscopy*) experiment was used to establish the NOE interactions in the form of a two-dimensional plot with all correlations as positive signals (Figure 2.8).

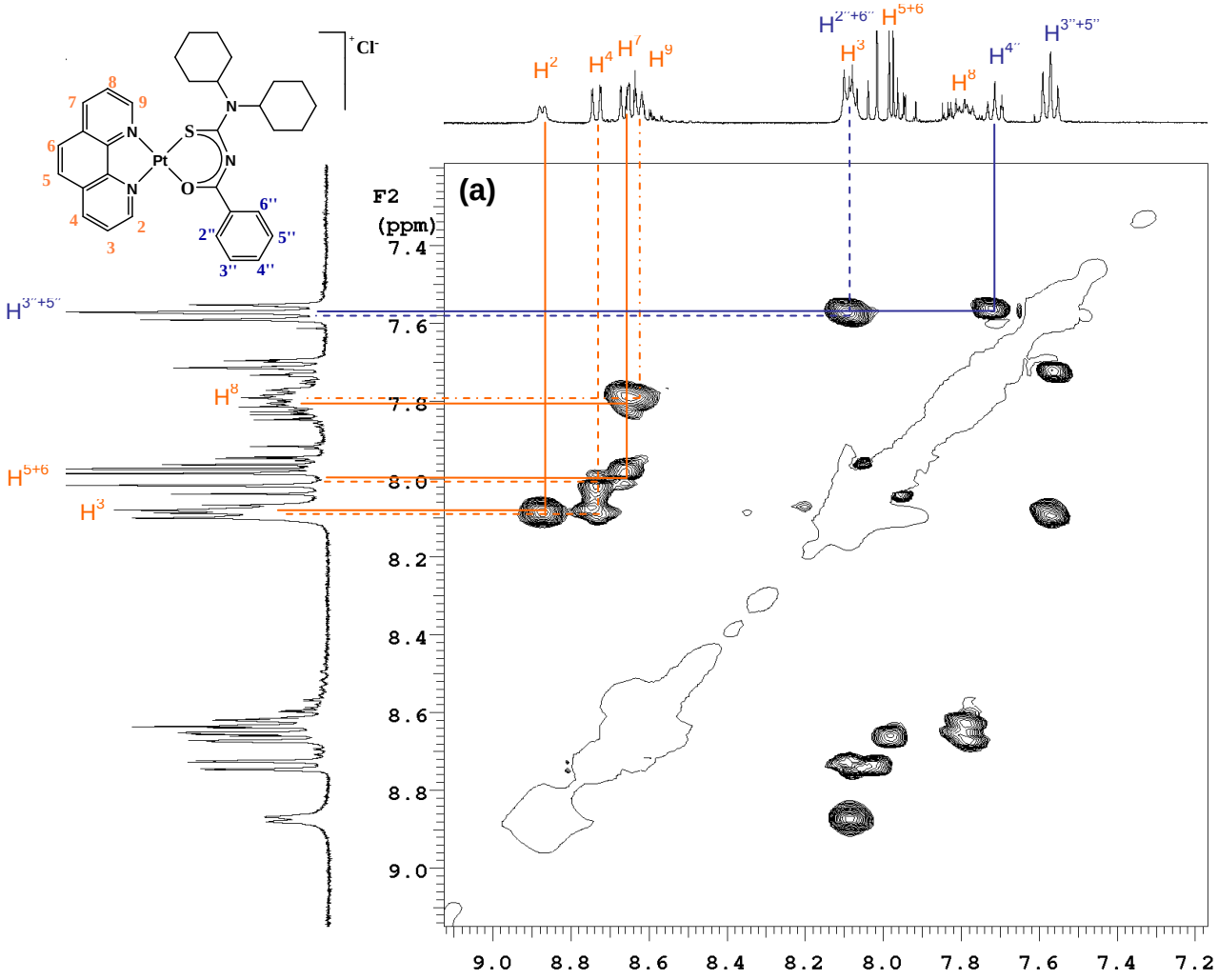

Figure 2.8: *NOESY plot of [Pt^{II}(phen)(L^5-S,O)]Cl where* ***(a)*** *is the aromatic region.*

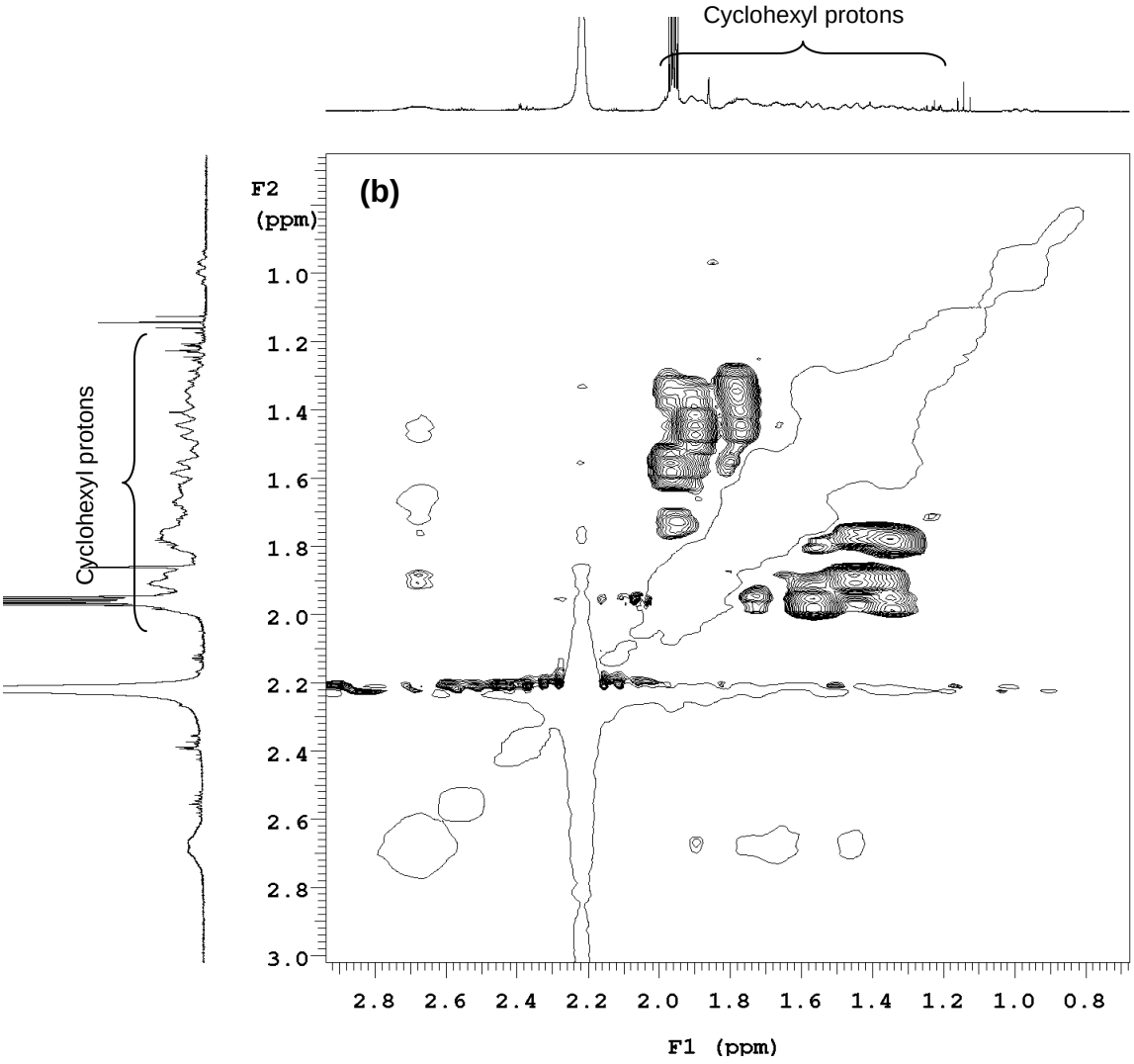

Figure 2.8: *NOESY plot of [Pt^{II}(phen)(L^5-S,O)]Cl where* ***(b)*** *is the aliphatic region presenting correlations that point towards NOE correlations within the separate ligands.*

The NOESY correlation diagram (Figure 2.8) does not show the desired inter-ligand through-space correlations between the phenanthroline ligand and the *N,N*-di(cycohexyl)-*N*'-benzoylthiourea ligand. However, through space correlations between neighbouring protons in the aromatic region, Figure 2.8a, ($H^{2–9}$ and $H^{2''–6''}$) and the aliphatic region (Figure 2.8b) are observed. The proton resonance signals of the cyclohexyl groups are overlapping multiplets (see experimental section 2.6) compared to the aromatic protons that are resolved. The correlations regarding the aromatic protons are summarized in Figure 2.9.

$H^2 \Leftrightarrow H^3$

$H^3 \Leftrightarrow H^2$ and H^4

$H^4 \Leftrightarrow H^3$ and H^{5+6}

$H^{5+6} \Leftrightarrow H^4$ and H^7

$H^7 \Leftrightarrow H^8$ and H^{5+6}

$H^8 \Leftrightarrow H^7$ and H^9

$H^{2''+6''} \Leftrightarrow H^{3''+5''}$

$H^{3''+5''} \Leftrightarrow H^{2''+6''} \Leftrightarrow H^{4''}$

$H^{4''} \Leftrightarrow H^{3''+5'}$

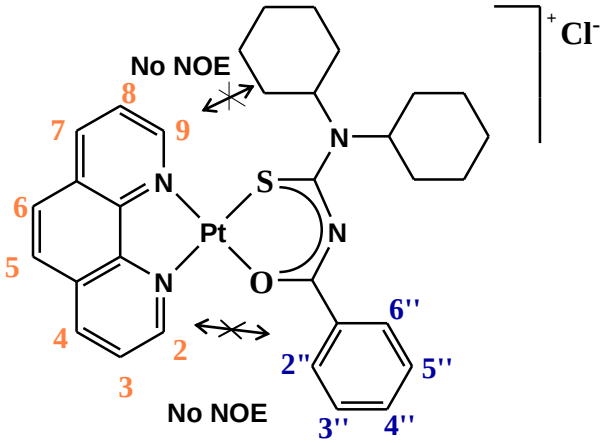

Figure 2.9: *NOE correlations for [Pt^{II}(phen)(L^5-S,O)]Cl*

The NOESY experiment confirmed the correlations obtained previously from the COSY experiments without the desired inter-ligand correlations. The absence of the desired correlation peaks can be attributed to the relatively large inter-nuclear distance between the protons of the phenanthroline ligand and the cyclohexyl protons. This can be understood when considering that the sterically less hindered structure of the complex is most likely when the cyclohexyl groups are perpendicular to the plane of the phenanthroline ligand rather than in the xy-plane as represented. The degree of rotation around the C-N bond is also restricted due to the partial double bond character and would essentially lock the cyclohexyl groups in the sterically less hindered position. It was doubtful that the NOESY experiment would work for the [Pt^{II}(phen)(L^1-*S,O*)]Cl complex in the light of the above result and was therefore not attempted. Alternative experiments need to be considered for a reliable assignment of the ^{1}H NMR spectrum of [Pt^{II}(phen)(L^1-*S,O*)]Cl.

^{1}H,^{15}N HMBC (*Heteronuclear Multiple Bond Correlation*) experiments were conducted to obtain more information on the nitrogen atoms with the intention that the assignment of H^2 and H^9 (Scheme 2.5) could be made with more confidence. In this experiment we used [Pt^{II}(phen)(L^1-*O,S*)]Cl (Scheme 2.5) since the proton spectrum has no overlapping peaks and the complex has a relatively high solubility. The HMQC method is the preferred technique for obtaining ^{15}N chemical shifts due to NOE of the coupled protons which makes it more sensitive than conventional ^{15}N NMR. In Figure 2.10 the cross-

peak correlation to all nitrogens is observed accept the imine nitrogen which are too far from any protons.

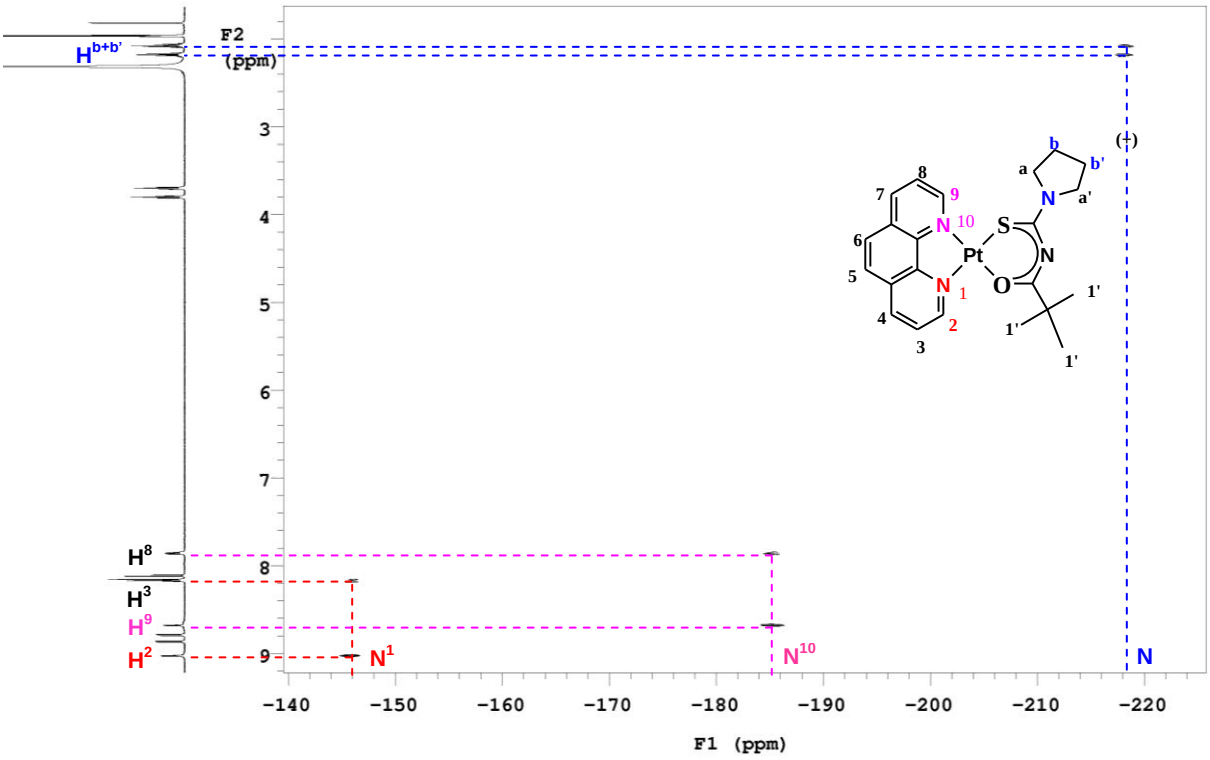

Figure 2.10: *$^{1}H,^{15}N$ HMBC plot of $[Pt^{II}(phen)(L^{1}\text{-}O,S)]Cl$ showing the ^{1}H and ^{15}N correlations in acetonitrile-d_6. Nitrogen chemical shifts are reported relative to nitromethane.*

The nitrogen as well as the corresponding proton chemical shifts are summarized in Table 2.2. The most deshielded nitrogen (N^1) correlates to the most deshielded proton (H^2) as expected from the assignments made earlier.

Table 2.2: *Summary of the ^{15}N and ^{1}H chemical shifts obtained $[Pt^{II}(phen)(L^{1}\text{-}O,S)]Cl$ from the $^{1}H,^{15}N$ HMBC experiments.*

	N^1	H^2	H^3	N^{10}	H^9	H^8	N	$H^{b+b'}$
δ / ppm	-145.80*	9.01	8.15	-185.27*	8.66	7.84	-218.15*	2.16 2.05

**Chemical shifts relative to nitromethane.*

In summary, from the ^{1}H, COSY, HMBC, NOESY and DOSY NMR spectra the unambiguous assignment of the protons H^2 and H^9 of [Pt^{II}(phen)(L^1-*O,S*)]Cl was not possible. In order to make the full assignment an assumption regarding the most deshielded proton must be made. This initial assignment can be substantiated to an extent by considering the atoms trans to the phenanthroline nitrogens. Oxygen is more electronegative than sulphur and is classified as a hard donor atom while sulphur is a soft donor atom according to Pearson's HSAB principal.[48] It is expected that the sulphur atom would form a stronger bond with the relatively soft platinum(II) metal centre compared to oxygen. The nitrogen trans to the sulphur would then be more deshielded because of the stronger Pt-S bond. The pyrrolidyl nitrogen also withdraws electron density from the sulphur atom and would further contribute to the deshielding of the nitrogen trans to sulphur (Diagram 2.1).

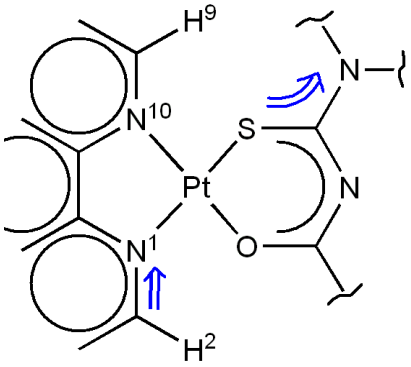

Diagram 2.1: *Deshielding of N^1 and H^2 due to the electron withdrawing effect the strong Pt-S bond in the trans position that is enhanced by the inductive effect of the pyrrolidyl nitrogen.*

With this in mind we assigned the most deshielded nitrogen to be N^1 and consecutively N^{10} to be the most shielded nitrogen. With these assumptions, full assignment of the proton spectrum can be done by using the ^{1}H,^{15}N HMBC and COSY correlation diagrams.

Confirmation of the assignments was obtained from the platinum satellites observed in the ^{1}H NMR spectra of these complexes. The platinum satellites were broad due to chemical shift anisotropy (CSA) at these high magnetic fields.[49] It is known that the CSA effects decrease with a lower magnetic field strength and therefore the platinum satellites are more resolved in the ^{1}H NMR spectra at 400MHz (Figure 2.11a). From the spectrum obtained at 400 MHz we roughly estimated the ^{1}H-^{195}Pt coupling constants for H^2 and H^9 to be 19 and 44 Hz respectively.

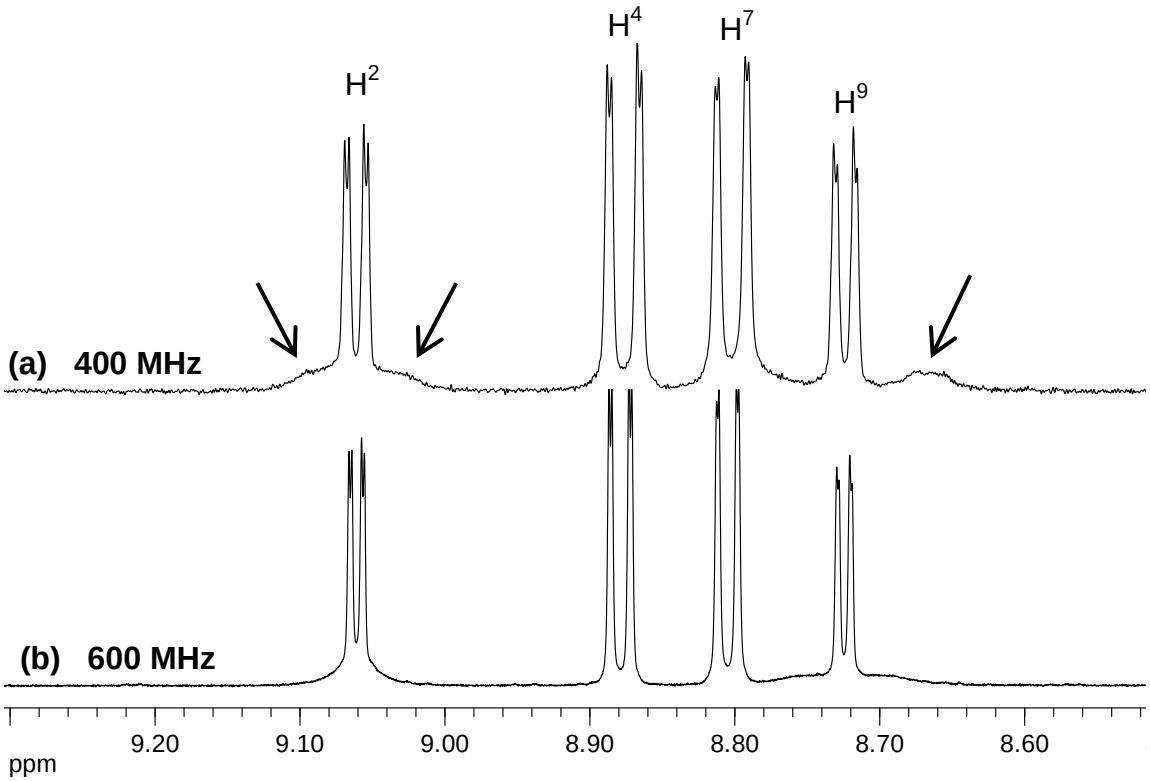

Figure 2.11: *The ^{1}H NMR spectrum of $Pt^{II}(phen)(L^{1}$-S,O)]Cl showing broad unresolved ^{195}Pt satellites that are more visible* ***(a)*** *at 400 MHz (11.74 T) than* ***(b)*** *at a higher magnetic field of 600 MHz (14.09 T).*

The difference in the magnitude of the ^{1}H-^{195}Pt coupling constants observed for H^2 and H^9 can be rationalised on the basis of electron density in the Pt-N bonds trans to the donor atoms of the *N*,*N*-di(alkyl)-*N'*-acylthiourea. The Pt-S bond is thought to be the strongest and withdraws more electrons from the Pt-N bond trans to the sulphur atom. This leads to less electron density in the region trans to the sulphur causing N^1 and H^2 to be the most deshielded. Less electron density implies that the coupling constant must decrease because of the through-bond coupling nature of scalar *J*-coupling.[50] The difference in electron density of the regions trans to the sulphur and oxygen atoms can clearly be seen from the chemical shift difference of the atoms in that region (Diagram 2.2).

$\Delta\delta_N = N^1 - N^{10}$

$= -147.80 \text{ ppm} - (-185.27 \text{ ppm})$

$= 37.47 \text{ ppm}$

$\Delta\delta_H = H^2 - H^9$

$= 9.01 \text{ ppm} - 8.66 \text{ ppm}$

$= 0.35 \text{ ppm}$

Diagram 2.2: *Calculated chemical shift difference between* $N^1 - N^{10}$ *and* $H^2 - H^9$.

The relatively large chemical shift difference between $N^1 - N^{10}$ (37.47 pm) and $H^2 - H^9$ (0.35 ppm) as well as the difference in ^1H-^{195}Pt coupling constants between H^2 and H^9 (15 Hz) reflects the significantly different electronic environments of the atoms trans to the Pt-S and Pt-O bonds. The significant difference in the two regions makes the assignment of the proton spectrum without direct experimental evidence more reliable.

2.5. DOSY spectroscopy and Computational Methodology

2.5.1 DOSY Spectroscopy

To analyze the association reactions in this study use was made of chemical shift dependence on analyte concentration as well as translational diffusion coefficients of the molecules of interest. The magnitude of a diffusion coefficient is dependent on the size, shape and solvation of the molecules and is exceptionally useful for studying molecular association in solution.[51,52] Diffusion coefficients are obtained from measuring the attenuation of the NMR signals (Figure 2.12) during a pulsed field gradient (PFG) experiment and are relatively easy to determine using diffusion ordered spectroscopy (DOSY).

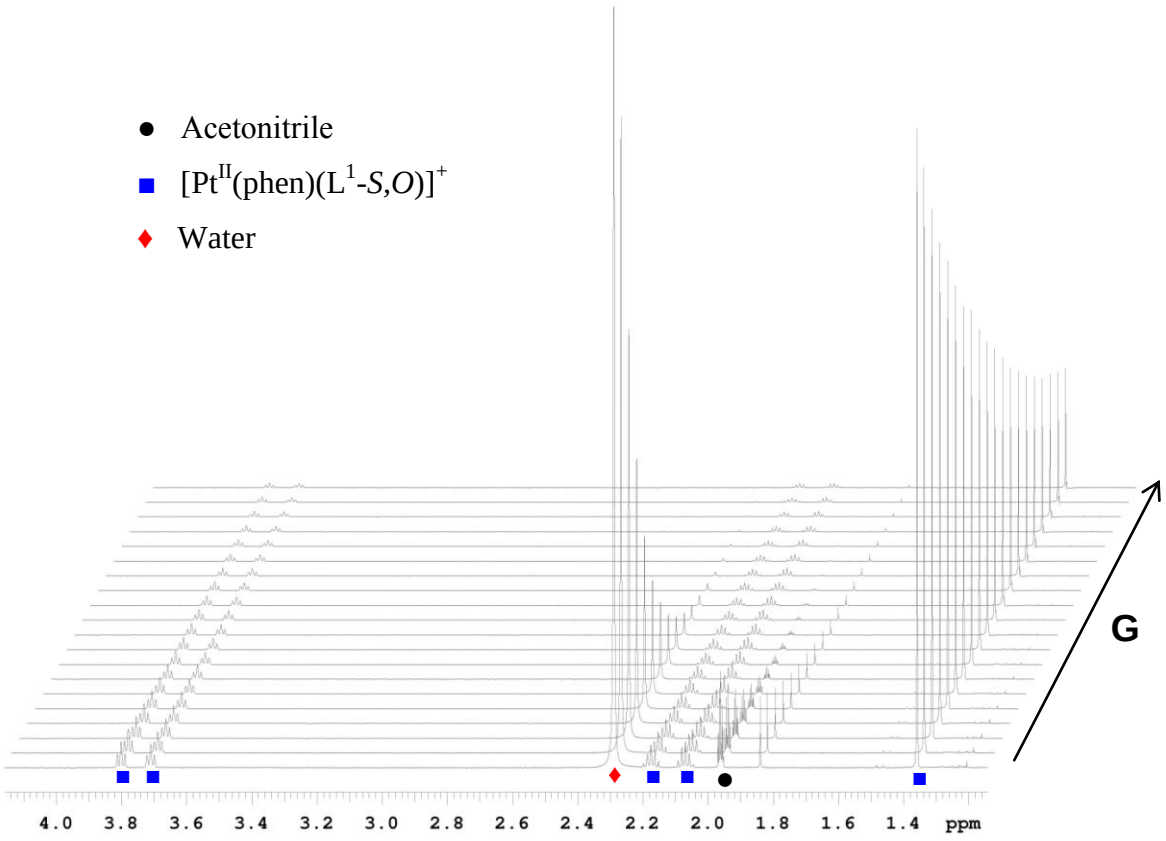

Figure 2.12: *Attenuation of the ^{1}H NMR signals of a mixture of $[Pt^{II}(phen)(L^{1}\text{-}S,O)]^{+}$, acetonitrile and water during a typical DOSY experiment with increasing gradient strength (0.0107-0.449 $G.m^{-1}$).*

The attenuation of the resonance signals and the PFG experiment can be explained by Scheme 2.6.[53] Scheme 2.6 illustrates only the translation of the hypothetical molecules **A** and **B** in the direction of the z-axis for simplification. To illustrate the concept assume molecule **A** diffuses faster than molecule **B** during the same diffusion delay time interval (Δ). The experiment consists of two pulsed field gradients (PFG) where there is a diffusion delay Δ between the two PFGs and the second PFG is the inverse of the first PFG. Complete refocusing of the magnetization components will occur when the local magnetic field of a nucleus is identical during the two gradient pulses. The local magnetic field is spatially dependant because of the field gradient (G_z) that is used. This implies that a molecule that diffuses after the diffusion delay between the two gradient pulses will experience a different local magnetic field when the second PFG is applied which leads to only partial refocusing of the magnetization, so resulting in the attenuation of the resonance signal. The attenuation follows an exponential decay as illustrated in Figure 2.12. The extent of attenuation is a function of the magnetic gradient pulse amplitude (G) and is proportional to the diffusion coefficient (D) as shown in equation 1

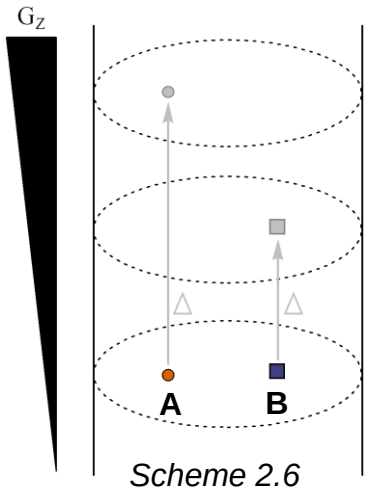

Scheme 2.6

$$I = I_0 \exp\left(\frac{-2\tau}{T_2} - (\gamma\delta G)^2 D\left(\Delta - \frac{\delta}{3}\right)\right) \qquad (1)$$

Where I_0 is the signal intensity with no gradient present, D the diffusion coefficient, Δ diffusion delay, δ the duration of the gradient pulses, γ the magnetogyric ratio, and G is the different gradient amplitudes used.[53]

A least-squares fit of equation 1 to the signal attenuation data allows for the calculation of the diffusion coefficient, D. The calculated diffusion coefficients are displayed as a two-dimensional plot with the proton spectrum as the one dimension and diffusion coefficients as the other (Figure 2.13).

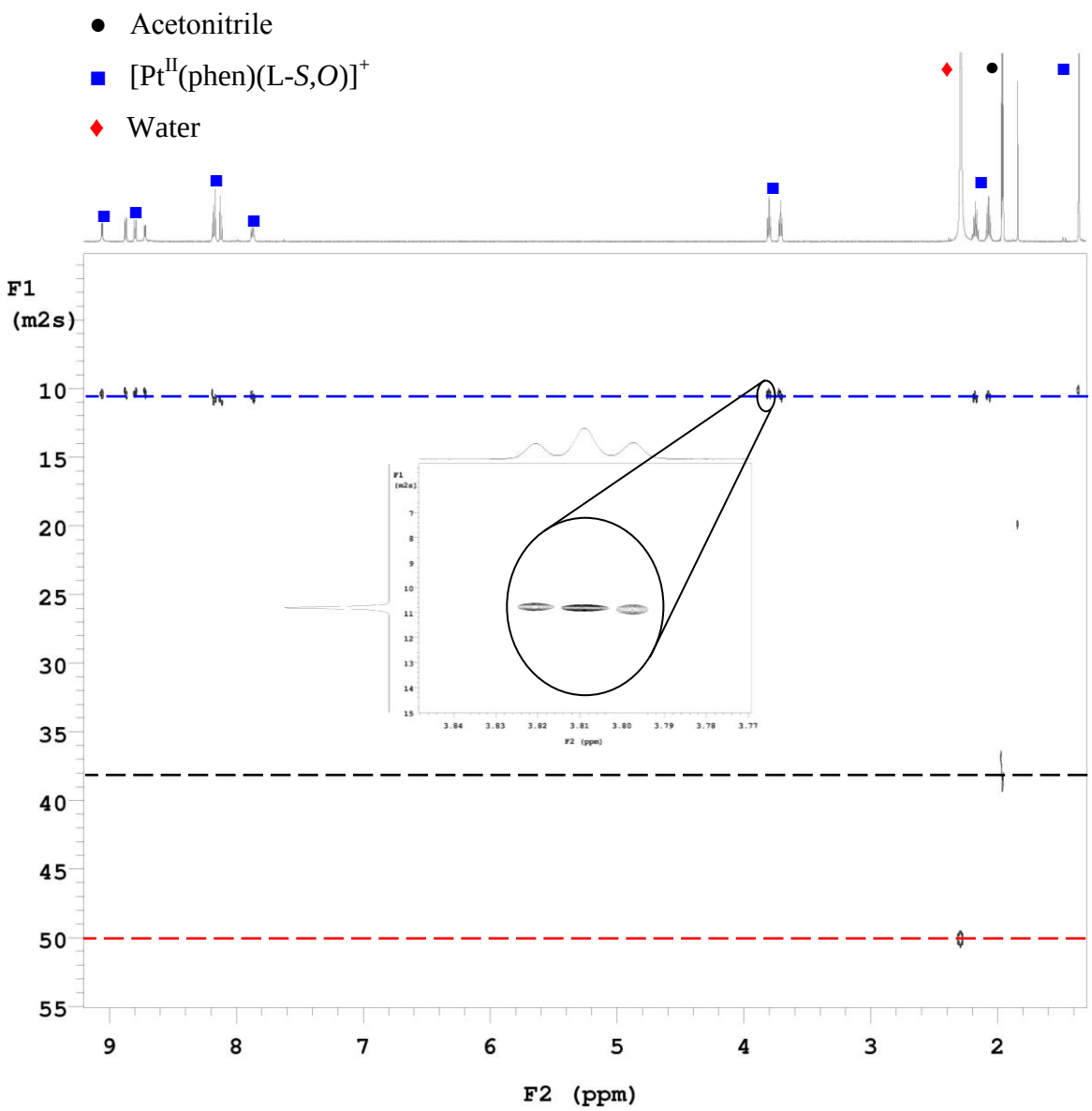

Figure 2.13: *DOSY plot of a mixture of $[Pt^{II}(phen)(L^1\text{-}S,O)]^+$, acetonitrile and water showing an average diffusion coefficient for a diffusion delay of 30 ms. The gradient pulse duration was 2 ms and 20 gradients intervals between 0.0107-0.449 $G.m^{-1}$ were used.*

From Figure 2.12 it can be seen that the rate of attenuation of the proton resonance signals for the different components is in the order water > acetonitrile > $[Pt^{II}(phen)(L^1\text{-}S,O)]^+$ (Figure 2.12). This is also reflected in the DOSY plot (Figure 2.13) where water has the largest diffusion coefficient compared to $[Pt^{II}(phen)(L^1\text{-}S,O)]^+$ with the smallest. Resonance signals belonging to the same molecule all give rise to the same diffusion

coefficient as illustrated by the dashed horizontal lines in the two-dimensional DOSY plot (Figure 2.13).

2.5.2 Computational Details of the Models for Aggregation

In the model system examined in this work, several simultaneous chemical equilibria may be present. From the average observed signal response, X_{obs}, equation 2 (where X_i = ^{1}H chemical shift, δ_i, or diffusion coefficient, D_i, and α_i = mole fraction of species i) and the total concentration of reagents, we want to calculate for the reactions defined in a chemical model the equilibrium constant(s), K_i, and chemical shifts, δ_i, or diffusion coefficients, D_i, of individual species (dimer aggregates, trimer aggregates, ion-pairs, etc).

$$X_{obs} = \sum_{i=n} \alpha_i X_i \qquad (2)$$

This particular type of mathematical problem can be solved in several ways.[54] For dimerization reactions we opted to use a program called, DIMER-K_D, written by Lawrence and Koch several years ago to fit data with a dimerization model[36] (the program utilizes the algorithm by Horman and co-workers who examined dimer formation of nucleic acids based on the following simple model[55]). This can be expressed as follows:

$$M + M \rightleftharpoons M_2 \qquad (3)$$

$$K_D = [M_2] / [M]^2 \qquad (4)$$

where [M] is monomer concentration, $[M_2]$ the dimer concentration, $[M]_0$ the total concentration and K_D is the equilibrium constant for the dimerisation of $[Pt^{II}(Phen)(L^1\text{-}S,O)]^+$ (M). The total concentration, $[M]_0$, of the molecules in solution is:

$$[M_0] = [M] + 2[M_2] \qquad (5)$$

Combining and rearranging eq. (4) and (5) results in an equation that is dependent on K_D and the mole fraction of M present as the dimer M_2 ($2[M_2] / [M]_0$):

$$\frac{1}{(2K_D[M]_0)^2} = \frac{2[M_2]}{[M]_0} + \frac{[M]_0}{2[M_2]} - 2 \qquad (6)$$

An average signal between the monomer and dimer moieties is observed (δ_{obs}) that can be attributed to the fast exchange between these moieties on the NMR time scale. This observed signal is the weighted average between the monomer (δ_m) and dimer chemical shifts (δ_d).

$$\delta_{obs} = \alpha_m \delta_m + \alpha_d \delta_d \qquad (7)$$

The assumption is made that the fraction of M present as the dimer ($\alpha_d = 2[M_2] / [M]_0$) is related to the measured chemical shift δ_{obs}

$$\alpha_d = (\delta_m - \delta_{obs}) / (\delta_m - \delta_d) \qquad (8)$$

or

$$\delta_{obs} = \delta_m - \alpha_d (\delta_m - \delta_d) \qquad (9)$$

Equation 9 should be a straight line, relating observed chemical shift (δ_{obs}) to the fraction of dimer present (α_d). For a series of concentrations, [M_0], different sets of α_d are calculated for each K_D. The value of K_D is varied and the final K_D value is defined as the best straight line fit for δ_i vs α_d. The dimerisation constant (K_D) is calculated from equations (6) and (8) by iterating the dimerisation constant and the dimer mole fraction (α_d) to best fit the experimental data.

When dealing with multiple equilibria we used a program called Dynafit version 3[56] that is freely available for academic purposes. The signal response that Dynafit version 3 can handle is however slightly different to that of equation 2; instead of using mole fraction in equation 2, Dynafit uses the concentration of the species, c_i. This problem

was circumvented by multiplying equation 2 by the total concentration, C_T, of the reagent of interest and after grouping terms, equation 10 is obtained.

$$C_T X_{obs} = \sum_{i=n} c_i X_i \qquad (10)$$

Dynafit numerically solves non-linear equaions related to the relevant equilibria using a modified Levenberg–Marquardt algorithm.[56] All the models were fitted to experimental data using non-linear least squares analysis.

2.6 Experimental

2.6.1 Instrumentation

^{1}H NMR, 2D NMR and DOSY experiments were done in 5mm tubes using a Varian Unity Inova 400 MHz spectrometer operating at 399.95 MHz or a Varian Unity Inova 600 MHz spectrometer equipped with an inverse detection pulsed field gradient (idpfg) probe operating at 599.99 MHz. DOSY experimental parameters: Pulse sequence: Dbppste_cc (Bipolar Pulse Pair Stimulated Echo with Convection Compensation), ^{1}H spectral width = 10 ppm, number of acquisitions varied from sample, recycling delay = 2 s, diffusion delay 30 ms, Gradient pulse duration 2 ms, 20 different values of G, the gradient magnitude, varying between 0.0107 and 0.449 Gm^{-1}. Diffusion coefficients were calculated using the Varian vnmrj software (version 2.1b). Melting points were determined using an Electrothermal IA9300 Digital Melting Point Apparatus. UV-VIS spectra were recorded on a single beam Agilent 8253E UV-visible spectrophotometer. The IR absorbance spectra were recorded on a Thermo Nicolet Nexus FT-IR spectrometer fitted with a Smart-ATR adaptor. Elemental analysis for C, H and N were done on an EA Euro 3000 Elemental Analyser. Electro spray mass spectra were obtained using a Waters API Quattro Micro Mass Spectrometer.

2.6.2 Sample preparation for ^{1}H NMR Spectroscopy

The ^{1}H NMR chemical shift concentration dependence and temperature dependence were obtained by diluting a stock [Pt^{II}(phen)(L^{1}-*S*,*O*)]Cl solution to the desired concentrations in separate 5mm NMR tubes. To ensure temperature equilibration samples were left for 15 to 20 minutes in the spectrometer before commencing measurements. Only a concentration dependence study was conducted for the DOSY experiments due to the change in solvent viscosity with temperature variation that directly influences the rate of diffusion. In order to examine the [Pt^{II}(phen)(L^{1}-*S*,*O*)]Cl and fluoranthene ^{1}H NMR chemical shift dependence a mole ratio titration was performed. To achieve this 300µl of a 10 mM Pt^{II}(phen)(L^{1}-*S*,*O*)]Cl was added to

separate NMR tubes with increasing amount of fluoranthene and diluted to a total volume of 500µl with CD_3CN.

2.6.3 Reagents

All reagents and solvents were commercially available and were used without further purification. [$PtCl_2$(1,10-phenanthroline)] was synthesized from commercially available $K_2[PtCl_4]$ (Aldrich) and 1,10-phenanthroline monohydrate. Commercially available potassium thiocyanate, benzoyl / ^{t}buthyl chloride and appropriate amines (Aldrich) were used to synthesize the corresponding *N,N*-di(alkyl)-*N'*-acylthiourea ligands. Commercially available fluoranthene (Aldrich) was used without further purification.

2.6.4 Characterization

The [Pt^{II}(phen)(L^1-*S,O*)]Cl complex and precursors have been successfully synthesized and characterized as shown below. Complete characterization of [Pt^{II}(phen)(L^1-*S,O*)]Cl was necessary since this complex were used further in the study. The IR spectra of [Pt^{II}(phen)(L^1-*S,O*)]Cl can be found in Appendix B. However, the remaining complexes of the series, [Pt^{II}(phen)(L^{2-5}-*S,O*)]Cl, were characterized only by melting point measurements and ^{1}H NMR spectroscopy since clean ^{1}H NMR spectra were obtained. The ^{1}H NMR spectra and assignments of all the complexes, precursors and fluoranthene are given in Figures 2.14-2.25 while the ^{1}H NMR data and melting points are summarized in Tables 2.3-2.9.

[$Pt^{II}Cl_2$(1,10-phenanthroline)]: 201 mg, Yield 87.4%, m.p. > 350°C. ^{1}H NMR (399.95 MHz, [D_6]DMSO, 25°C), δ=9.70 (dd, ^4J(H,H)=1.3 Hz, ^3J(H,H)=5.5 Hz, 2H; H^9, H^2), 9.04 (dd, ^4J(H,H)=1.3Hz, ^3J(H,H)=8.2 Hz, 2H; H^4, H^7), 8.29 (s, 2H; H^5, H^6), 8.17 ppm (dd, ^3J(H,H)=5.5 Hz, ^3J(H,H)=8.2 Hz, 2H; H^3, H^8). IR (ATR): υ (cm^{-1}), 3083 (arom. C-H stretch), 3059 (arom. C-H stretch), 1427 (arom. C-C stretch), 1220 (asym. C-N stretch) 1208 (sym. C-N stretch); elemental analysis calcd (%) for $C_{22}H_{25}N_4SOClPt$: C 32.3, N 6.3; found: C 32.6, N 6.0.

***N*-pyrrolidyl-*N'*-(*2,2*-dimethylpropanoyl)thiourea (HL^1)**: 564 mg, Yield 90.1%, m.p. 136-137°C; ^{1}H NMR (399.95 MHz, [D_6]DMSO, 25°C), δ=9.74 (s, 1H: NH), 3.63 (m, 2H: H^a), 3.42 (m, 2H: $H^{a'}$), 1.90 (m, 4H: H^b, $H^{b'}$), 1.16 (s, 9H: $H^{1'}$); ^{13}C NMR (50.31 MHz, $CDCl_3$, 25°C), δ=27.16 ($C^{3''}$), 39.62 ($C^{2''}$), 54.43 ($C^{3'}$), 52.52 (C^3), 26.16 ($C^{4'}$), 24.59 (C^4), 176.66 (C^S), 174.38 ppm (C^O); UV/Vis: λ_{max} (ε) 216(13 399), 276 nm (14 792 $dm^3mol^{-1}cm^{-1}$); Elemental analysis calcd (%) for $C_{10}H_{18}N_2OS$: C 57.8, H 8.5, N 13.1, S 14.96; found: C 57.0, H 8.8, N 13.3, S 14.8.

(*N*-pyrrolidyl-*N*-(2,2-dimethylpropanoyl)thiourea)(1,10-phenanthroline) platinum(II) chloride ([Pt^{II}(phen)(L^1-*S,O*)]Cl): The general method for the synthesis of mixed-ligand [Pt^{II}(diimine)(L^n-*S,O*)]PF_6 complexes described by Koch *et al*,[36] was modified for the preparation of [Pt^{II}(phen)(L^1-*S,O*)]Cl. A suspension of [$PtCl_2$(phen)] (0.045 g, 0.1 mmol) in 10 ml of acetonitrile was heated under reflux for 10 min, after which *N*-pyrrolidyl-*N*-(2,2-dimethylpropanoyl)thiourea (0.022 g, 0.101 mmol) in 2 ml acetonitrile was added dropwise and the mixture heated under reflux for 45 min. A suspension of sodium acetate (0.028 g, 0.15 mmol) in acetonitrile was added and the mixture was heated under reflux overnight. The cooled mixture was filtered through Celite to remove any Na/KCl precipitate formed. The filtrate was concentrated by evaporation to volume of *ca.* 2 ml. Diethyl ether (100 ml) was added and the precipitate was collected by centrifugation, resuspended several times with cold diethyl ether and centrifuged again. The yellow product was dried overnight in a vacuum oven at 70 °C.

[Pt^{II}(phen)(L^1-*S,O*)]Cl: 58 mg, Yield 93%, m.p. 134 – 135 °C ^{1}H NMR (599.99 MHz, CD_3CN), δ=9.01 (dd, ^4J(H,H)=0.9 Hz, ^3J(H,H)=4.5 Hz, 1H: H^2), 8.85 (dd, ^4J(H,H)=0.9 Hz, ^3J(H,H)=7.7 Hz, 1H: H^4), 8.77 (dd, ^4J(H,H)=0.6 Hz, ^3J = 7.8 Hz, 1H: H^7), 8.66 (d, ^3J(H,H)=5.3 Hz, 1H: H^9), 8.15 (dd, ^3J(H,H)=4.5 Hz, ^3J(H,H)=7.7 Hz 1H: H^3), 8.12 (m, 2H: H^5, H^6), 7.84 ppm (dd, ^3J(H,H)=5.3 Hz, ^3J(H,H)=7.3 Hz, 1H: H^8). IR (ATR): υ (cm^{-1}), 3086 (arom. C-H stretch), 3059 (arom. C-H stretch), 2969 (C-H stretch), 2927 (C-H stretch), 1482 (C-O stretch), 1380 (CH_3 umbrella deformation), 1434 (arom. C-C stretch) 1264 (asym. C-N stretch) 1228 (sym. C-N stretch); (+) ESI MS: *m/z* 588 (M^+, calc. 588.6)

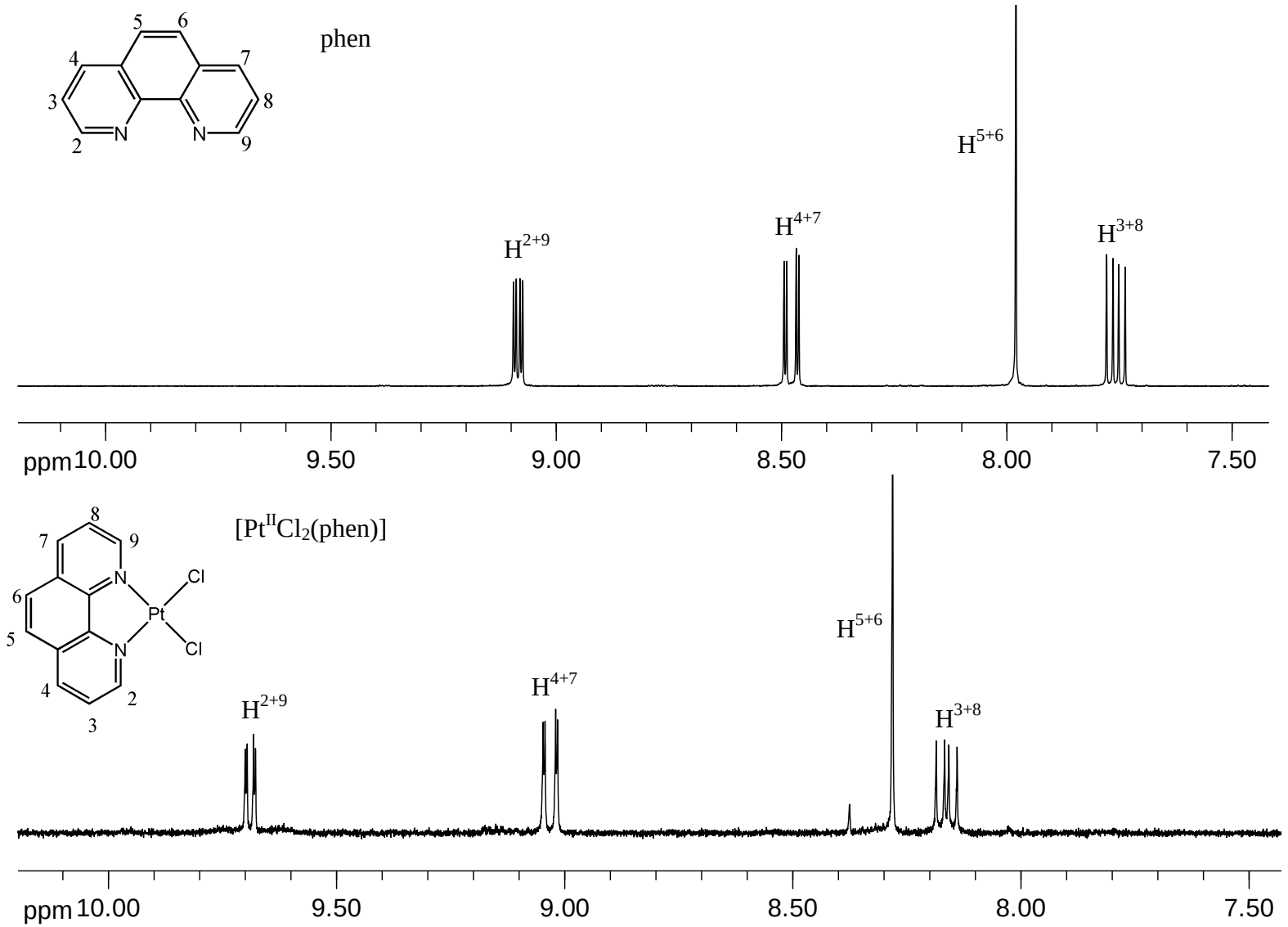

Figure 2.14: *^{1}H NMR spectrum and assignment of phen and [Pt^{II}Cl$_2$(phen)] in DMSO-d$_6$ at 25ºC*

Table 2.3: *^{1}H NMR data of phen and [$Pt^{II}Cl_2$(phen)] in DMSO-d_6 at 25ºC*

Solvent: DMSO-d_6	Assignment	Chemical Shift (ppm)	No of H's	Multiplicity	Coupling Constants (Hz)
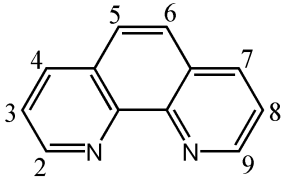 phen	H^{2+9}	9.10	2	dd	$J^3 = 4.3$; $J^4 = 1.8$
	H^{4+7}	8.50	2	dd	$J^3 = 8.1$; $J^4 = 1.8$
	H^{5+6}	8.00	2	s	–
	H^{3+8}	7.78	2	dd	$J^3 = 8.1$; $J^4 = 4.3$
m.p. >392 ºC	Assignment	Chemical Shift (ppm)	No of H's	Multiplicity	Coupling Constants (Hz)
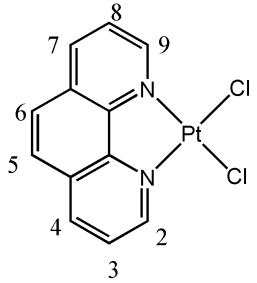 [$Pt^{II}Cl_2$(phen)]	H^{2+9}	9.70	2	dd	$J^3 = 5.5$; $J^4 = 1.3$
	H^{4+7}	9.04	2	dd	$J^3 = 8.3$; $J^4 = 1.3$
	H^{5+6}	8.29	2	s	–
	H^{3+8}	8.17	2	dd	$J^3 = 8.3$; $J^4 = 5.5$

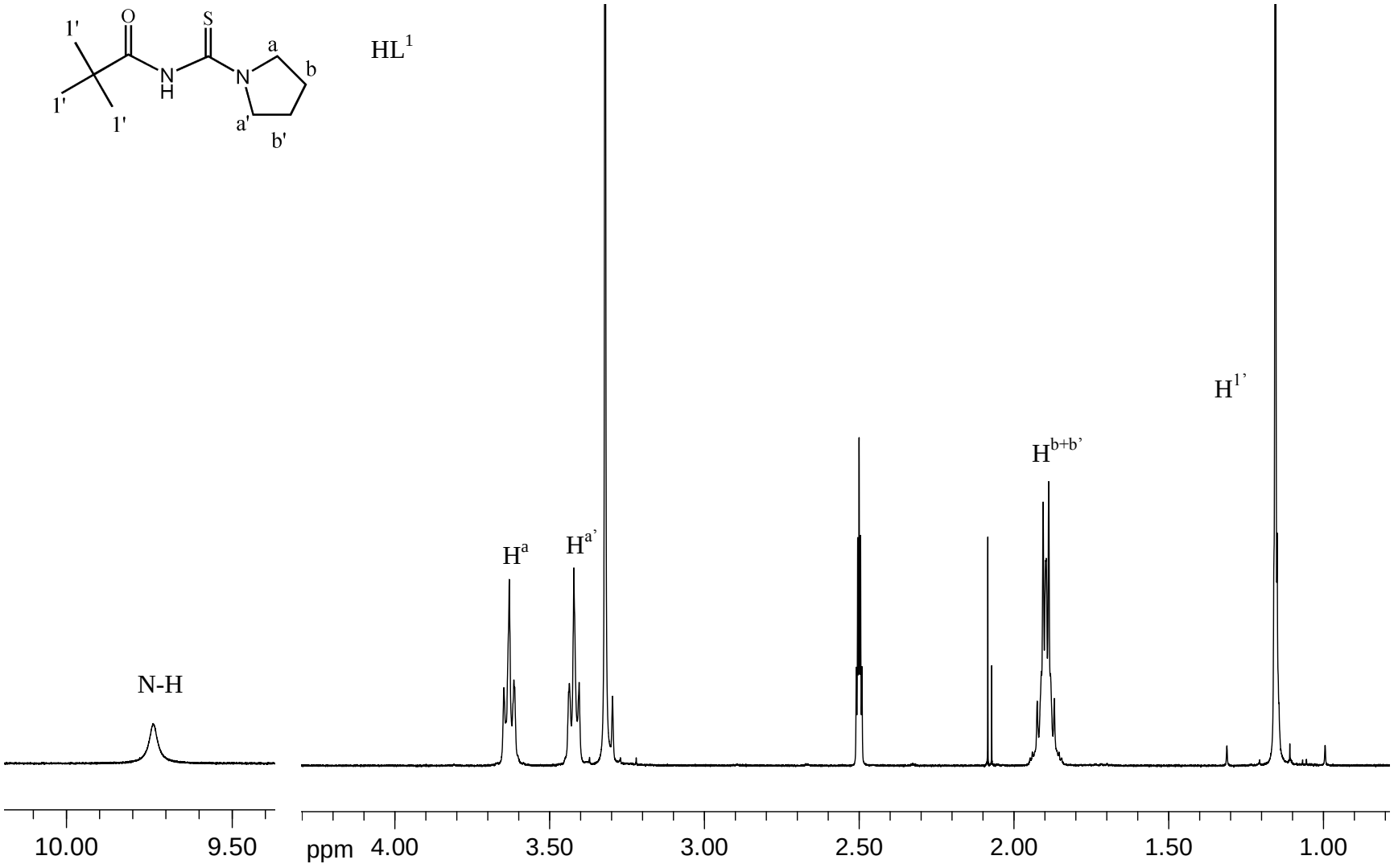

Figure 2.15: *^{1}H NMR spectrum and assignment of HL^{1} in DMSO-d_6 at 25ºC*

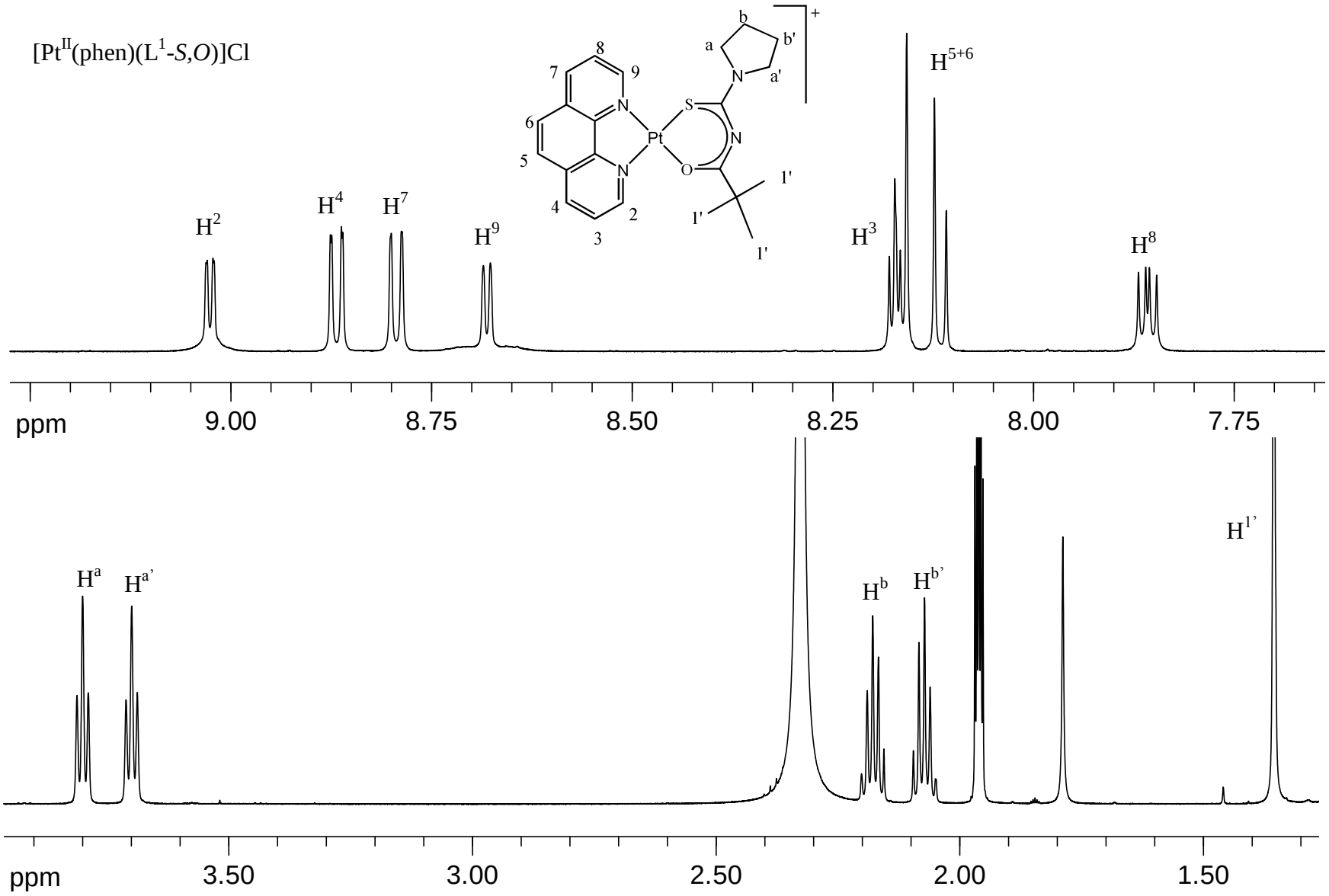

Figure 2.16: *^{1}H NMR spectrum and assignment of [Pt^{II}(phen)(L^1-S,O)]Cl in CD_3CN at 25ºC*

Table 2.4: *^{1}H NMR data of HL^{1} and $[Pt^{II}(phen)(L^{1}\text{-}S,O)]Cl$ in DMSO-d_6 at 25ºC*

Solvent: DMSO-d_6	Assignment	Chemical Shift (ppm)	No of H's	Multiplicity	Coupling Constants (Hz)
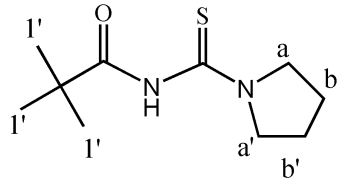	NH	9.74	1	broad s	–
	H^{a}	3.63	2	t	$J^{3} = 7.0$
	$H^{a'}$	3.42	2	t	$J^{3} = 6.7$
	$H^{b+b'}$	1.90	4	m	–
HL^{1}	$H^{1'}$	1.34	9	s	–
m.p. 134-135 ºC	Assignment	Chemical Shift (ppm)	No of H's	Multiplicity	Coupling Constants (Hz)
Solvent: CD_3CN	H^{2}	9.03	1	dd	$J^{3} = 5.2$; $J^{4} = 0.9$
	H^{4}	8.87	1	dd	$J^{3} = 8.2$; $J^{4} = 1.0$
	H^{7}	8.79	1	dd	$J^{3} = 8.2$; $J^{4} = 0.7$
	H^{9}	8.68	1	dd	$J^{3} = 5.2$
	H^{3}	8.17	1	dd	$J^{3} = 8.2$; $J^{4} = 4.4$
	H^{5+6}	8.14	2	m	–
	H^{8}	7.86	1	dd	$J^{3} = 8.2$; $J^{4} = 5.4$
	H^{a}	3.80	2	t	$J^{3} = 7.0$
	$H^{a'}$	3.70	2	t	$J^{3} = 7.0$
	H^{b}	2.18	2	q	$J^{3} = 6.9$
$[Pt^{II}(phen)(L^{1}\text{-}S,O)]Cl$	$H^{b'}$	2.07	2	q	$J^{3} = 6.9$
	$H^{1'}$	1.36	9	s	–

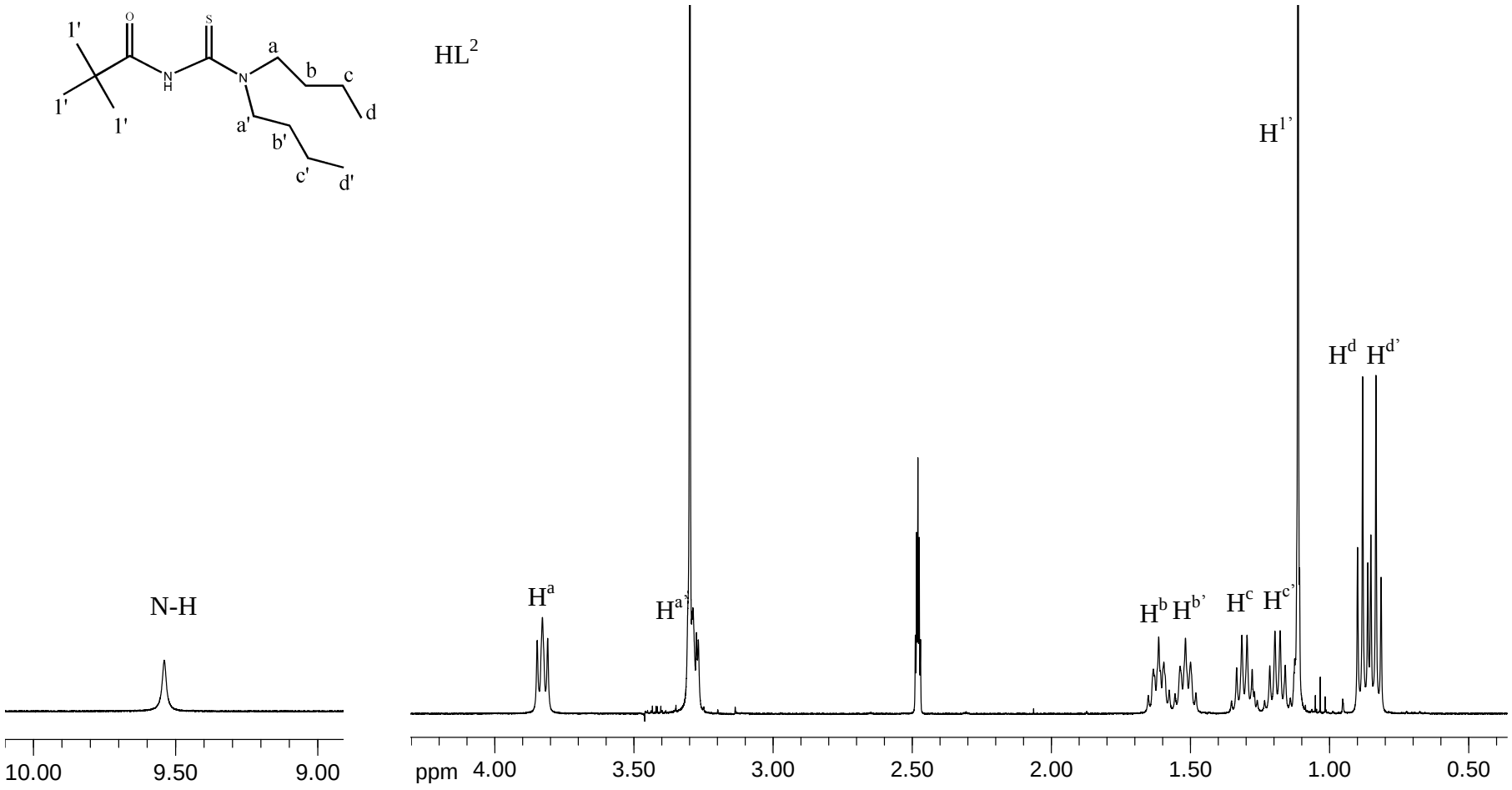

Figure 2.17: *^{1}H NMR spectrum and assignment of HL^2 in DMSO-d_6 at 25ºC*

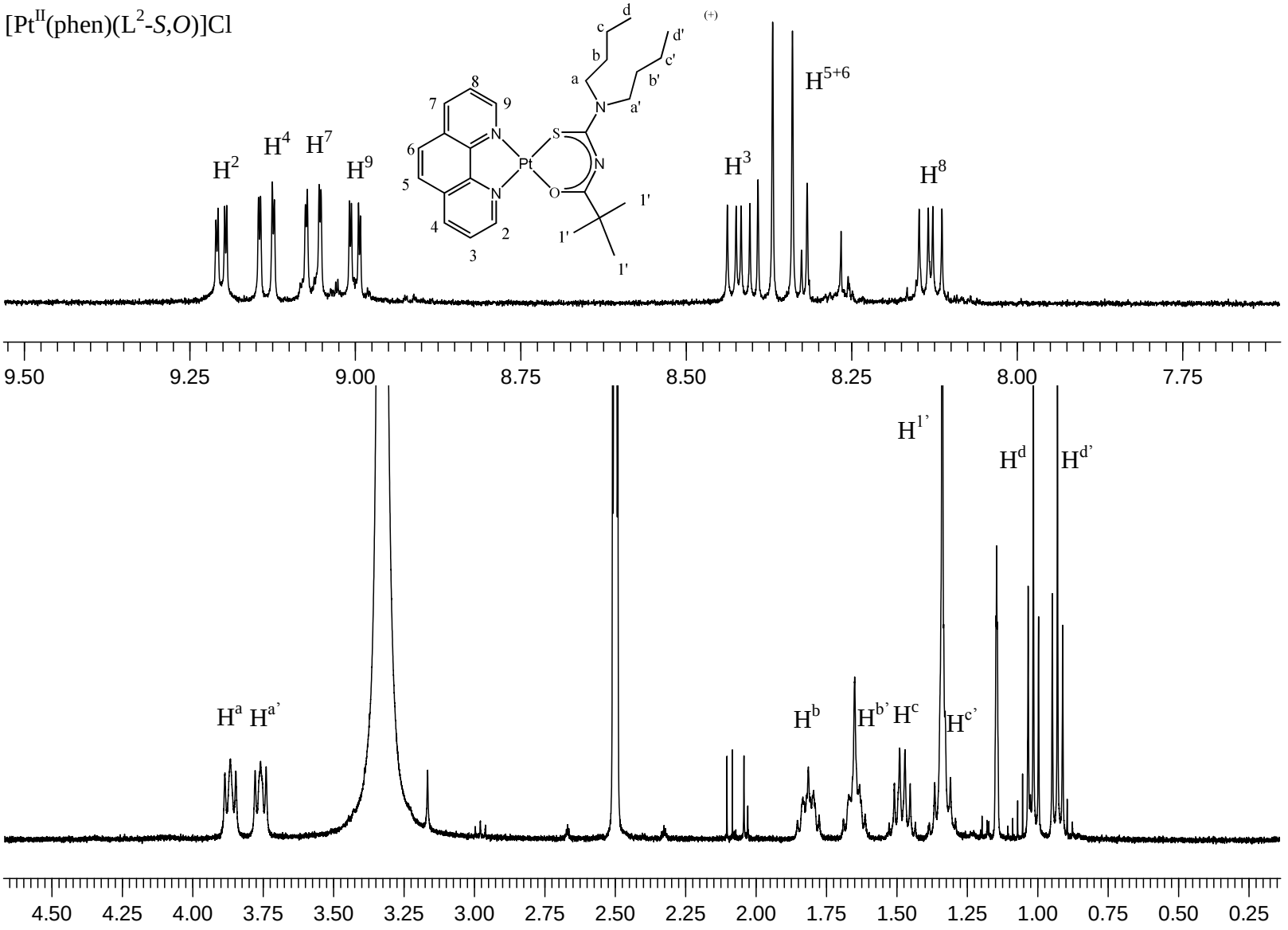

Figure 2.18: *^{1}H NMR spectrum and assignment of [Pt^{II}(phen)(L^{2}-S,O)]Cl in DMSO-d_6 at 25ºC*

Table 2.5: *^{1}H NMR data of HL^{2} and $[Pt^{II}(phen)(L^{2}\text{-}S,O)]Cl$ in DMSO-d_6 at 25ºC*

Yield 82%	Assignment	Chemical Shift (ppm)	No of H's	Multiplicity	Coupling Constants (Hz)
Solvent: DMSO-d_6 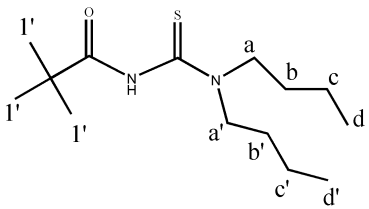 HL^{2}	NH	9.56	1	broad s	–
	H^{a}	3.87	2	t	$J^{3} = 7.5$
	$H^{a'}$	3.76	2	m	–
	H^{b}	1.81	2	q	$J^{3} = 7.5$
	$H^{b'}$	1.65	2	q	$J^{3} = 7.4$
	H^{c}	1.48	2	s	$J^{3} = 7.5$
	$H^{c'}$	1.34	2	s	$J^{3} = 7.5$
	$H^{1'}$	1.34	9	s	–
	H^{d}	1.02	3	t	$J^{3} = 7.4$
	$H^{d'}$	1.93	3	t	$J^{3} = 7.4$
m.p. 128-130 ºC	Assignment	Chemical Shift (ppm)	No of H's	Multiplicity	Coupling Constants (Hz)
Solvent: DMSO-d_6 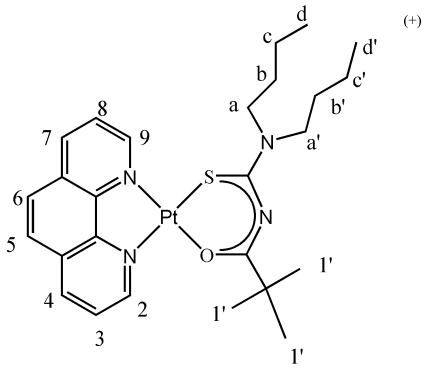 $[Pt^{II}(phen)(L^{2}\text{-}S,O)]Cl$	H^{2}	9.20	1	dd	$J^{3} = 5.1$; $J^{4} = 1.1$
	H^{4}	9.13	1	dd	$J^{3} = 8.3$; $J^{4} = 1.1$
	H^{7}	9.06	1	dd	$J^{3} = 8.4$; $J^{4} = 1.0$
	H^{9}	9.00	1	dd	$J^{3} = 5.2$; $J^{4} = 1.0$
	H^{3}	8.42	1	dd	$J^{3} = 8.2$; $J^{4} = 5.2$
	H^{5+6}	8.35	2	m	–
	H^{8}	8.13	1	dd	$J^{3} = 8.3$; $J^{4} = 5.5$
	H^{a}	3.87	2	t	$J^{3} = 7.9$
	$H^{a'}$	3.76	2	t	$J^{3} = 8.0$
	H^{b}	1.81	2	q	$J^{3} = 7.7$
	$H^{b'}$	1.65	2	q	$J^{3} = 7.7$
	H^{c}	1.48	2	s	$J^{3} = 7.5$
	$H^{c'}$	1.34	2	s	$J^{3} = 7.4$
	$H^{1'}$	1.34	9	s	–
	H^{d}	1.02	3	t	$J^{3} = 7.4$
	$H^{d'}$	1.93	3	t	$J^{3} = 7.4$

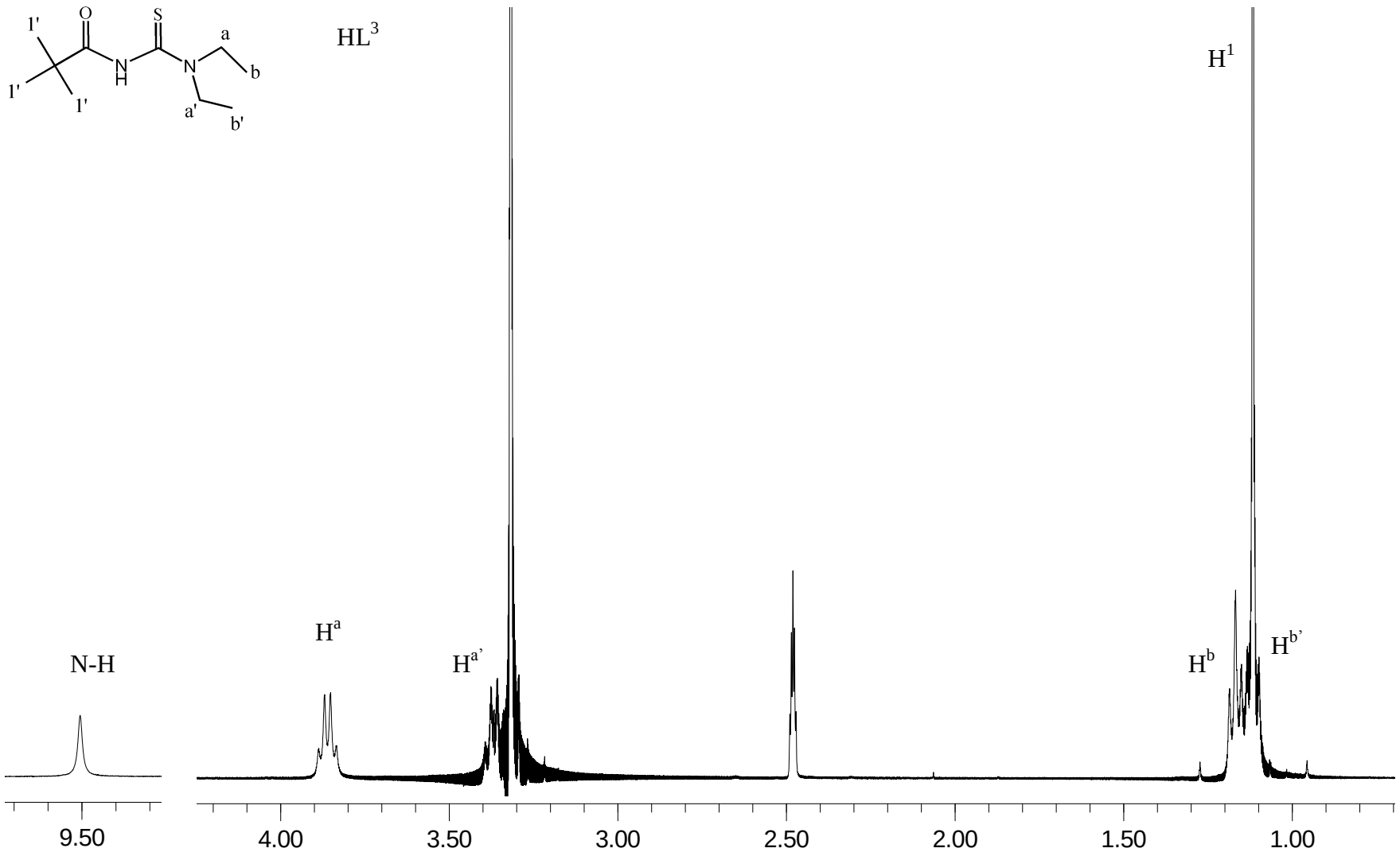

Figure 2.19: *^{1}H NMR spectrum and assignment of HL^{3} in DMSO-d_6 at 25ºC*

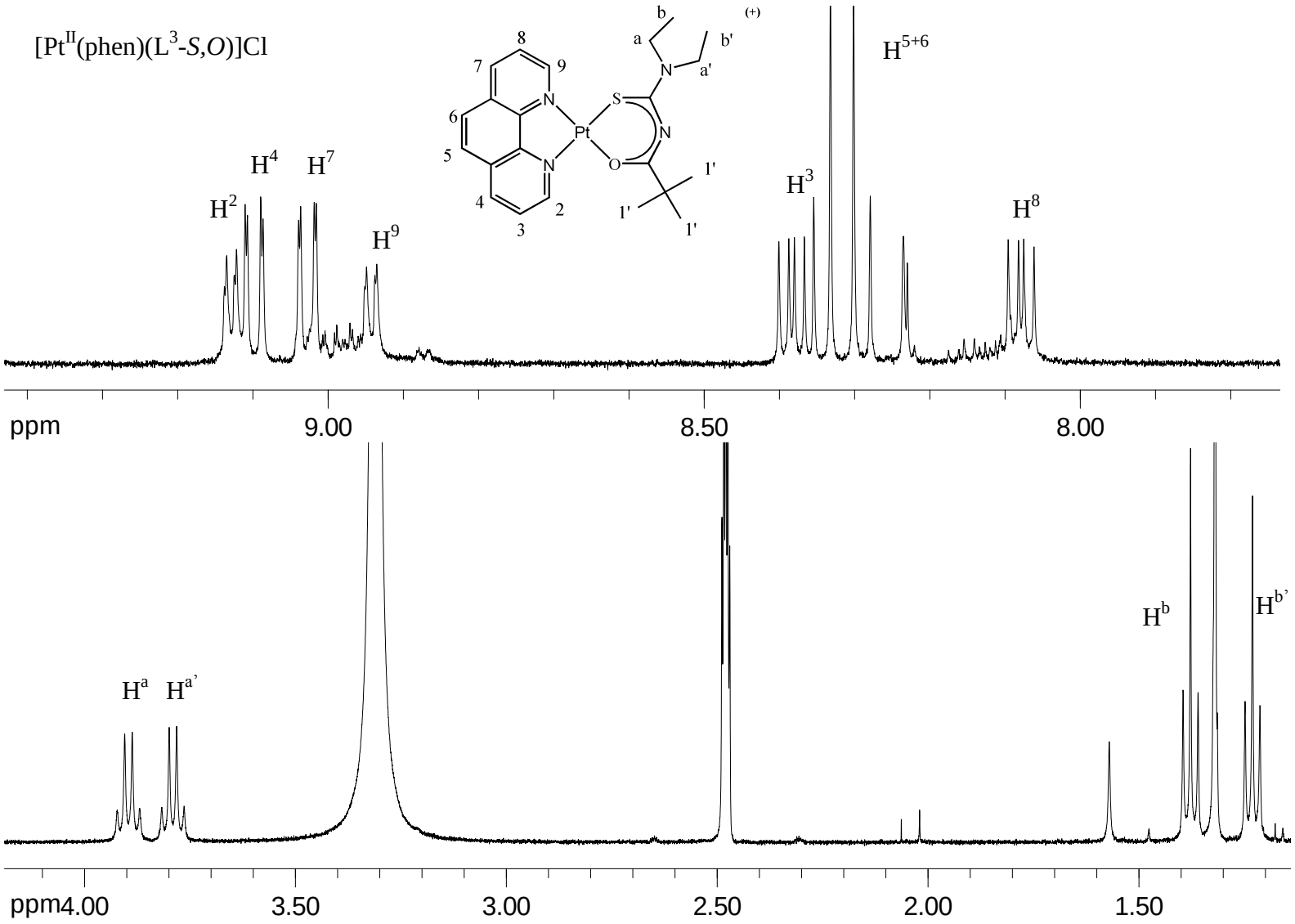

Figure 2.20: *^{1}H NMR spectrum and assignment of [Pt^{II}(phen)(L^3-S,O)]Cl in DMSO-d_6 at 25ºC*

Table 2.6: *^{1}H NMR data of HL^3 and $[Pt^{II}(phen)(L^3\text{-}S,O)]Cl$ in DMSO-d_6 at 25ºC*

Yield: 78%	Assignment	Chemical Shift (ppm)	No of H's	Multiplicity	Coupling Constants (Hz)
Solvent: DMSO-d_6	NH	9.51	1	broad s	–
	H^{a}	3.86	2	q	$J^3 = 7.0$
	$H^{a'}$	3.37	2	q	$J^3 = 7.0$
	H^{b}	1.17	3	t	$J^3 = 7.0$
	$H^{b'}$	1.12	3	t	$J^3 = 7.0$
	$H^{1'}$	1.12	9	s	–
HL^3					
m.p. 136-139 ºC	Assignment	Chemical Shift (ppm)	No of H's	Multiplicity	Coupling Constants (Hz)
Solvent: DMSO-d_6	H^{2}	9.12	1	dd	$J^3 = 4.1$; $J^4 = 1.2$
	H^{4}	9.10	1	dd	$J^3 = 7.0$; $J^4 = 1.2$
	H^{7}	9.03	1	dd	$J^3 = 7.2$; $J^4 = 1.1$
	H^{9}	8.94	1	dd	$J^3 = 4.4$; $J^4 = 1.1$
	H^{3}	8.38	1	dd	$J^3 = 8.3$; $J^3 = 5.3$
	H^{5+6}	8.32	2	m	–
	H^{8}	8.08	1	dd	$J^3 = 8.3$; $J^3 = 5.5$
	H^{a}	3.90	2	q	$J^3 = 7.1$
	$H^{a'}$	3.79	2	q	$J^3 = 7.0$
	H^{b}	1.38	3	t	$J^3 = 7.1$
	$H^{1'}$	1.32	9	s	–
	$H^{b'}$	1.23	3	t	$J^3 = 7.0$
$[Pt^{II}(phen)(L^3\text{-}S,O)]Cl$					

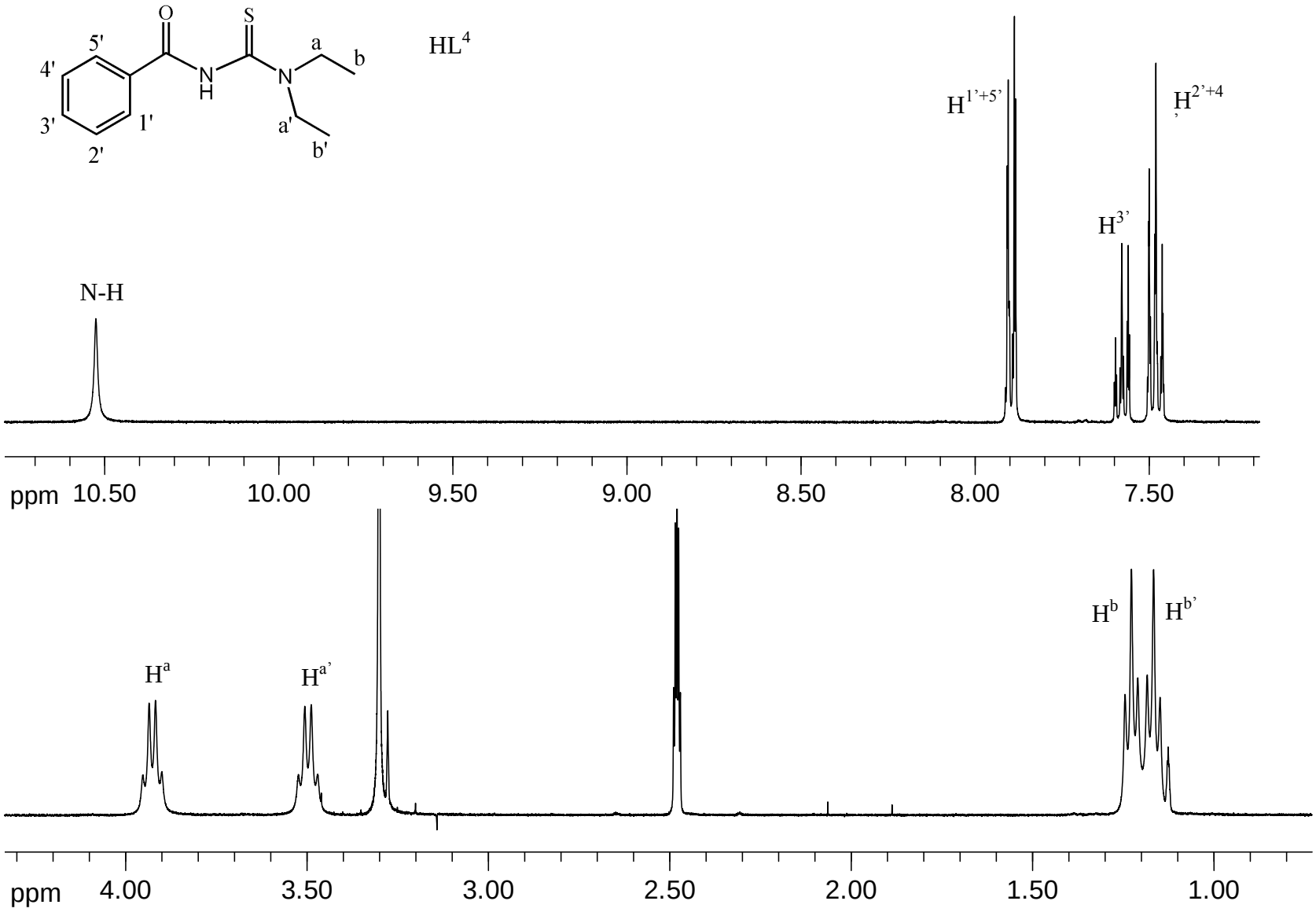

Figure 2.21: *^{1}H NMR spectrum and assignment of HL^4 in DMSO-d_6 at 25ºC*

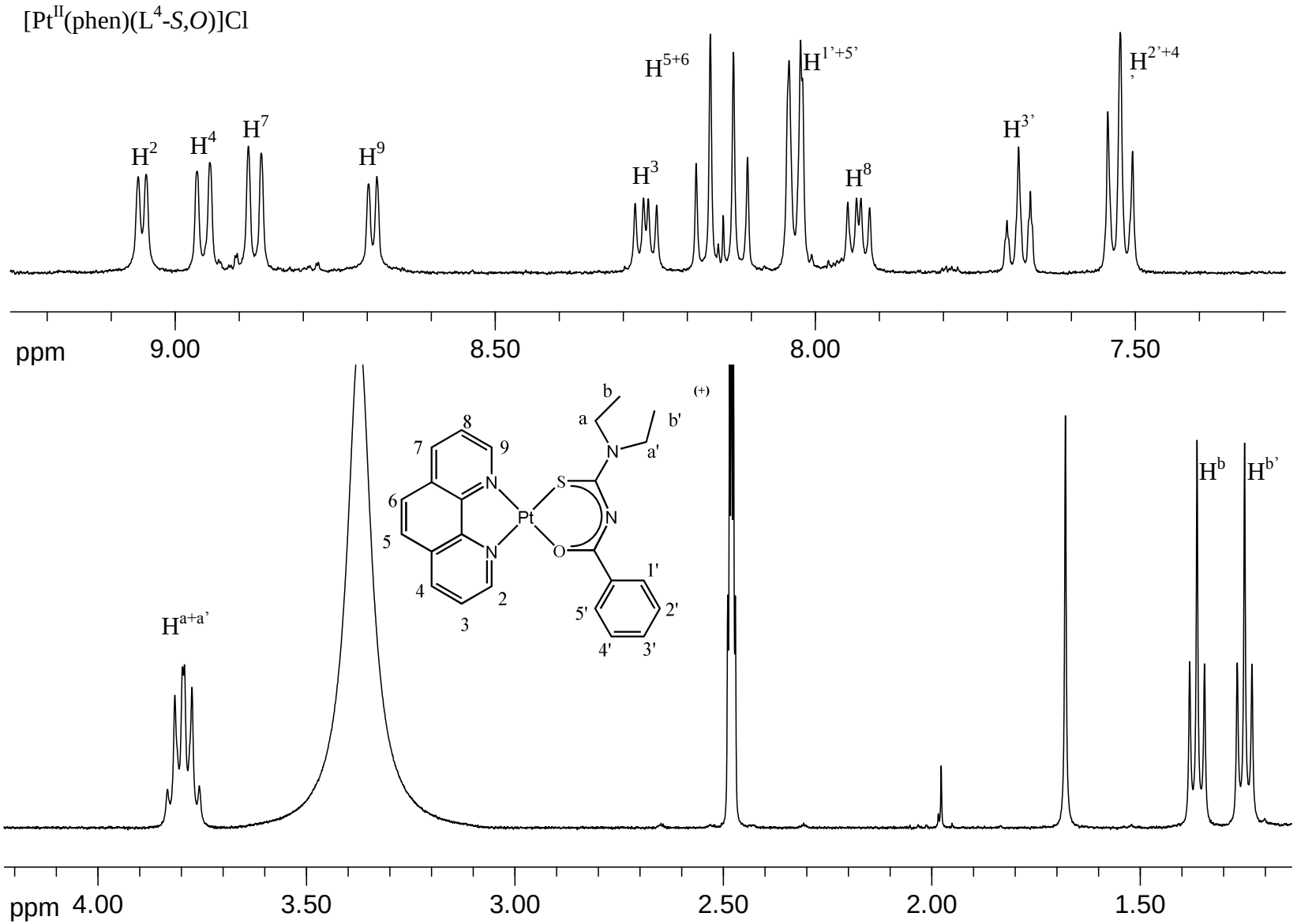

Figure 2.22: *^{1}H NMR spectrum and assignment of [Pt^{II}(phen)(L^4-S,O)]Cl in DMSO-d_6 at 25ºC*

Table 2.7: *^{1}H NMR data of HL^4 and $[Pt^{II}(phen)(L^4\text{-}S,O)]Cl$ in DMSO-d_6 at 25ºC*

Yield: 79%	Assignment	Chemical Shift (ppm)	No of H's	Multiplicity	Coupling Constants (Hz)
Solvent: DMSO-d_6	NH	10.55	1	broad s	–
	$H^{1'+5'}$	7.91	2	m	–
	$H^{3'}$	7.60	1	tt	$J^3 = 7.4$; $J^4 = 1.7$
	$H^{2'+4'}$	7.50	2	m	–
	H^{a}	3.95	2	q	$J^3 = 7.0$
	$H^{a'}$	3.52	2	q	$J^3 = 7.0$
	H^{b}	1.25	3	t	$J^3 = 7.0$
HL^4	$H^{b'}$	1.19	3	t	$J^3 = 7.0$
m.p. 244-247 ºC	Assignment	Chemical Shift (ppm)	No of H's	Multiplicity	Coupling Constants (Hz)
Solvent: DMSO-d_6	H^{2}	9.05	1	d	$J^3 = 4.9$
	H^{4}	8.96	1	d	$J^3 = 7.8$
	H^{7}	8.88	1	d	$J^3 = 8.0$
	H^{9}	8.69	1	d	$J^3 = 5.2$
	H^{3}	8.25	1	dd	$J^3 = 8.2$; $J^4 = 5.2$
	H^{5+6}	8.15	2	m	–
	$H^{1'+5'}$	8.03	2	d	$J^3 = 7.2$
	H^{8}	7.93	1	dd	$J^3 = 8.2$; $J^4 = 5.5$
	$H^{3'}$	7.68	1	t	$J^3 = 7.3$
	$H^{2'+4'}$	7.52	2	t	$J^3 = 7.7$
	$H^{a+a'}$	3.79	4	m	–
	H^{b}	1.36	3	t	$J^3 = 7.1$
$[Pt^{II}(phen)(L^4\text{-}S,O)]Cl$	$H^{b'}$	1.25	3	t	$J^3 = 7.1$

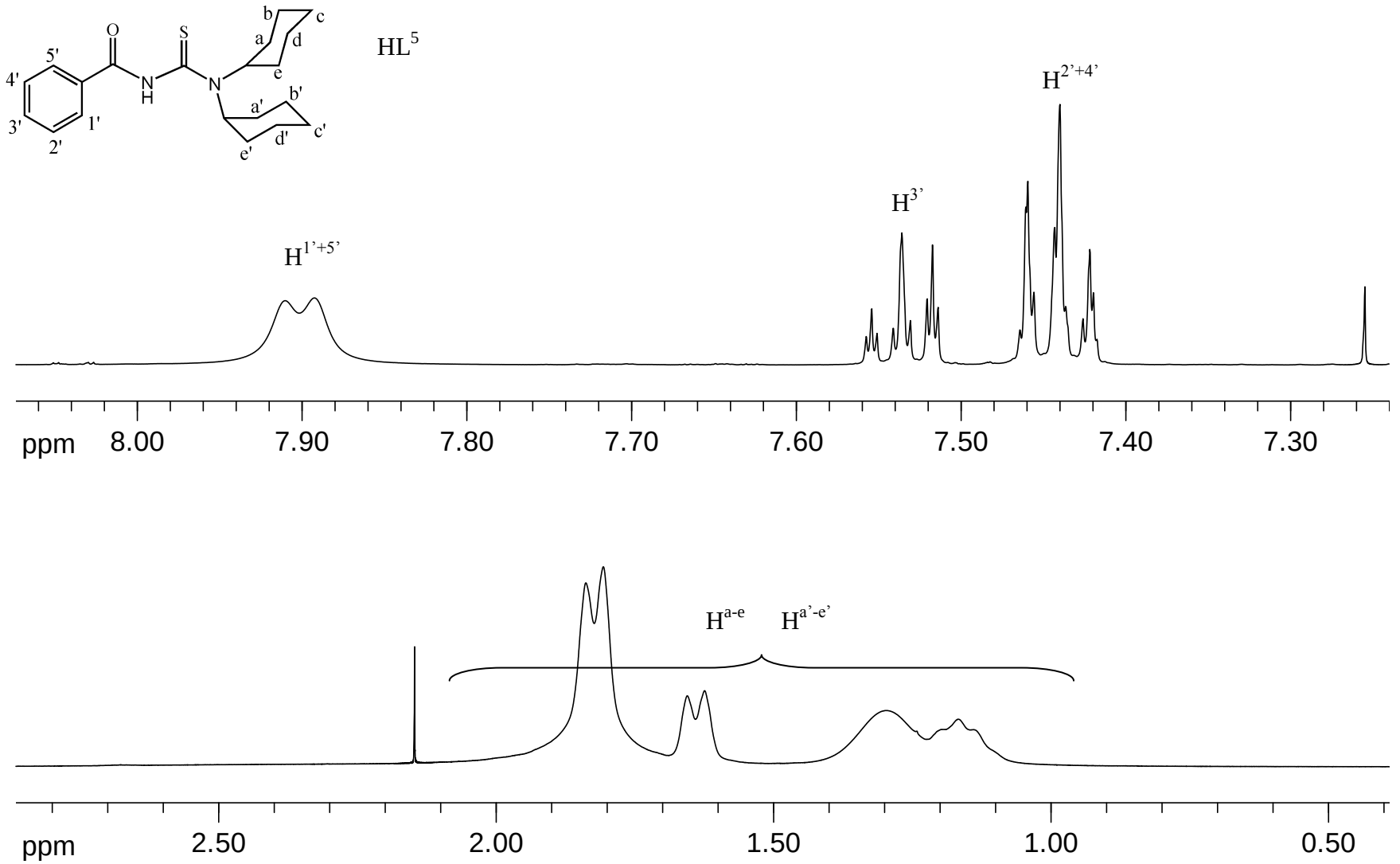

Figure 2.23: *^{1}H NMR spectrum and assignment of HL^{5} in $CDCl_3$ at 25ºC*

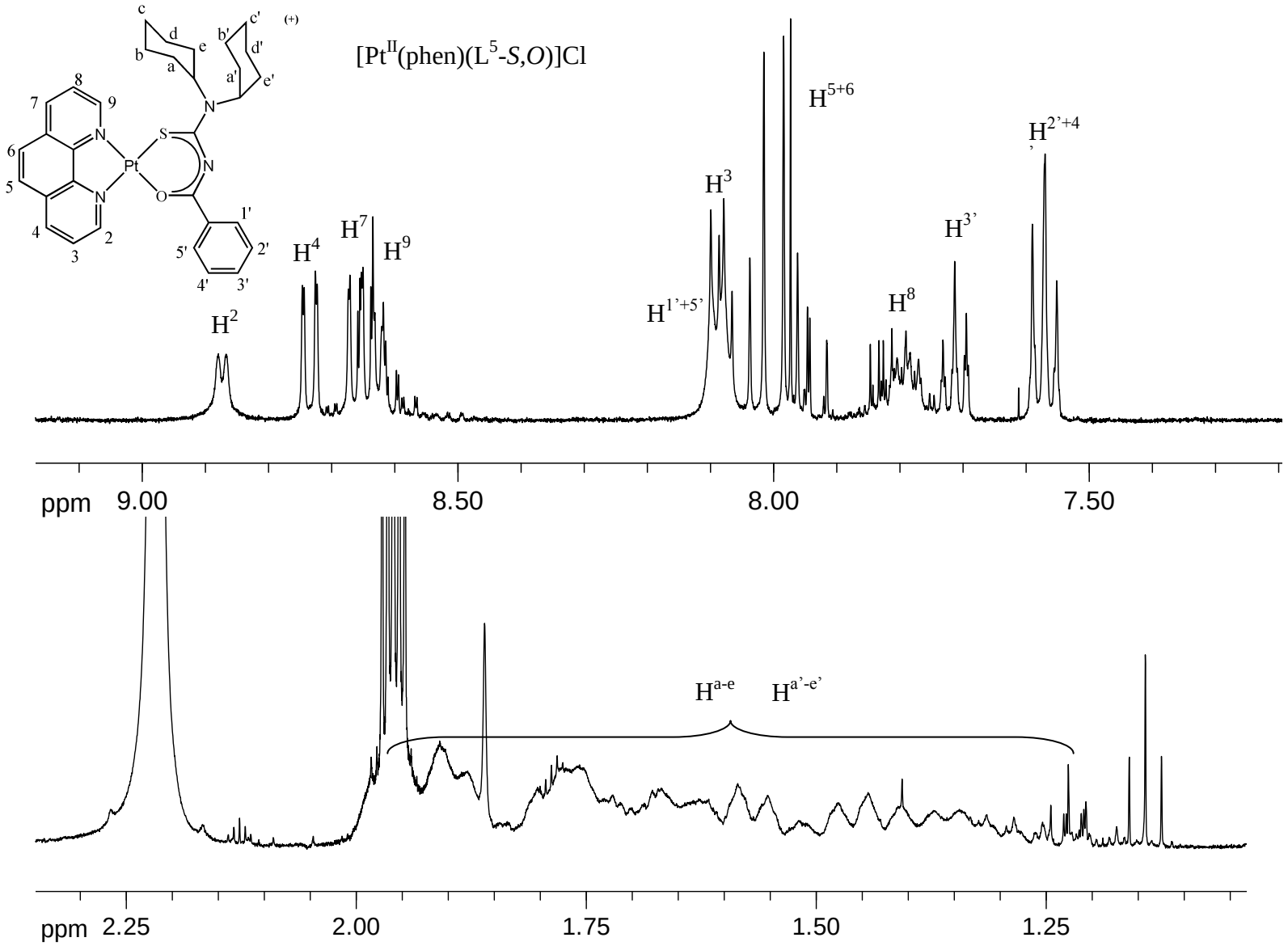

Figure 2.24: *^{1}H NMR spectrum and assignment of [Pt^{II}(phen)(L^5-S,O)]Cl in $CDCl_3$ at 25ºC*

Table 2.8: *^{1}H NMR data of HL^5 and $[Pt^{II}(phen)(L^5\text{-}S,O)]Cl$ in $CDCl_3$ at 25ºC*

Yield: 76%	Assignment	Chemical Shift (ppm)	No of H's	Multiplicity	Coupling Constants (Hz)
Solvent: $CDCl_3$ 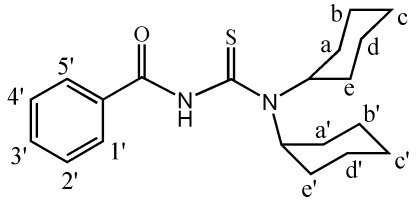 HL^5	$H^{1'+5'}$	7.90	2	m	–
	$H^{3'}$	7.54	1	tt	$J^3 = 7.4$; $J^4 = 1.7$
	$H^{2'+4'}$	7.44	2	m	–
	H^{abcde}+	0.44-	20	m	–
	$H^{a'b'c'd'e'}$	5.08			
m.p. 182-185 ºC	Assignment	Chemical Shift (ppm)	No of H's	Multiplicity	Coupling Constants (Hz)
Solvent: $CDCl_3$ 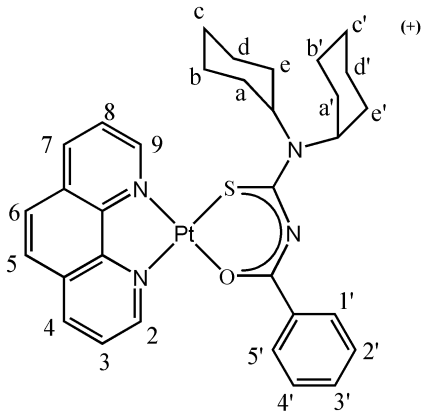 $[Pt^{II}(phen)(L^5\text{-}S,O)]Cl$	H^2	8.87	1	d	$J^3 = 5.2$
	H^4	8.73	1	dd	$J^3 = 8.2$; $J^4 = 1.1$
	H^7	8.66	1	dd	$J^3 = 8.2$; $J^4 = 1.0$
	H^9	8.63	1	d	$J^3 = 5.4$
	H^3	8.07	1	dd	$J^3 = 8.2$; $J^4 = 5.2$
	H^{5+6}	8.01	2	m	–
	$H^{1'+5'}$	8.09	2	d	$J^3 = 8.2$
	H^8	7.79	1	m	–
	$H^{3'}$	7.71	1	tt	$J^3 = 7.4$; $J^4 = 1.2$
	$H^{2'+4'}$	7.57	2	t	$J^3 = 7.7$
	H^{abcde}+	1.21-	20	m	–
	$H^{a'b'c'd'e'}$	2.00			

Figure 2.25: *^{1}H NMR spectrum and assignment of fluoranthene in CD_3CN at 25ºC*

Table 2.9: *^{1}H NMR data of fluoranthene in CD_3CN at 25ºC*

	Assignment	Chemical Shift (ppm)	No of H's	Multiplicity	Coupling Constants (Hz)
Solvent: CD_3CN 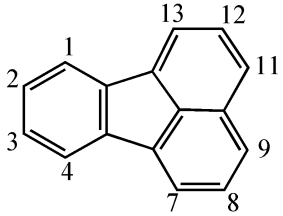 Fluoranthene	H^{3+17}	8.07	2	dd	$J^3 = 7.1$; $J^4 = 0.5$
	H^{3+16}	8.01	2		–
	H^{9+11}	7.94	2	dd	$J^3 = 8.3$; $J^4 = 0.5$
	H^{3+17}	7.43	2	dd	$J^3 = 8.3$; $J^4 = 6.9$
	H^{8+12}	7.41	2		–

Chapter 3

Self-association of $[Pt^{II}(phen)(L^{1}\text{-}S,O)]^{+}$ in acetonitrile and acetonitrile/water mixtures

Chapter 3

Self-association of $[Pt^{II}(phen)(L^1\text{-}S,O)]^+$ in acetonitrile and acetonitrile/water mixtures

3.1 Introduction

Non-covalent cation-π interactions have been the subject of extensive interest in the last decade in view of their well established role and importance in biological systems[16,20,21,57,58] as well as in supramolecular chemistry and molecular recognition phenomena.[14,15,17,21] There are several manifestations of this type of non-covalent bonding interaction, the simplest and most extensively studied system involves group I and II metal cations or protonated amine with benzene and other aromatic molecules in the gas and solution phase. [20,59] The detailed nature of cation-π interactions has been reviewed and in the *gas phase* for example, the $K^+\cdots$benzene interaction energies can exceed $K^+\cdots H_2O$ interaction energies,[60,61] and it has been convincingly shown that 'organic' cations, such as ammonium ions, can strongly interact with suitably designed synthetic arene-based receptors as well as in numerous biological structures.[62,63] In aqueous solution, cations are obviously solvated resulting in the attenuation of the cation-π interaction leading to elongation of the interaction distance between the cation and arene centre as compared to such interactions in the gas phase.[59] In the case of "π-stacking" and/or aggregation of metalloporphyrins, Hunter and Sanders[40] derived an elegant simple electrostatic model which demonstrate that so-called "π-π" interactions in planar metalloporphyrins actually arise from favourable π-σ attractions which overcome π-π repulsions in such molecules. This model has resulted in a set of rules with which to predict the nature and relative interaction geometry of such aggregation phenomena, at least in the case of planar metalloporphyrins.

In this study the chemistry of planar, formally cationic mixed-ligand platinum(II) complexes of the general structure $[Pt(diimine)(L^n\text{-}S,O)]^+$ (where diimine is 2,2'-bipyridine or 1,10-phenanthroline and HL^n-*S,O* represents various chelating *N*-acyl-

N,N'-dialkylthioureas) is of interest. Such mixed ligand platinum(II) complexes have been shown to display interesting biological activity ranging from significant potential anti-malarial activity,[18] to interesting DNA intercalation with demonstrable *in vivo* activity toward bacterial *E. coli* AB1886 *(uvr A)* cultures;[19] moreover preliminary work shows that such complexes undergo some interesting DNA-mediated biomineralization.[64] Koch and co-workers have previously studied a series of [Pt^{II}(diimine)(L^n-*S,O*)]PF_6 salts which were found to display well defined aggregation behaviour in acetonitrile solutions, which they ascribed to cation-π interactions leading to the formation of non-covalent 'dimer aggregates' in solution.[36] For this system they found that the Gibbs free energy associated with the 'dimer aggregate' formation increases by approximately 2.4 kJmol^{-1} per aromatic ring of the diimine bound to platinum(II); these Gibbs free energies are slightly higher than energies reported by Rebeck *et al* for only π-π stacking interactions of 1.8 kJmol^{-1}.[65]

By contrast to the well known group I and II metal cations and protonated amine systems which show significant cation-π interactions,[20,59] outer-sphere complexes with uncharged aromatic molecules with planar complex cations such as [Pt^{II}(diimine)(L^n-*S,O*)]$^+$ and even [Pt^{II}(diimine)$_2$]$^{2+}$ have received comparatively little attention in the literature.[17,36,66] The *in vitro* anti-malarial activity of [Pt^{II}(diimine)(L^n-*S,O*)]$^+$ is postulated to arise by inhibition of *β*-hematin (synthetic hemozoin or malaria pigment) formation in view of the cationic platinum(II) complexes forming moderately strong outer-sphere complexes with ferriprotoporphyrin IX in 40 % aqueous dimethyl sulphoxide (DMSO) solution.[18]

In this context, the potential cation-π self-association of [Pt^{II}(phen)(L^1-*S,O*)]Cl (Scheme 2.5) in acetonitrile as a model system was studied by means of ^{1}H NMR concentration dependence studies and specifically with Diffusion Ordered Spectroscopy (DOSY). ^{1}H NMR is particularly well suited for this type of investigation because the relevant thermodynamic parameters can be estimated from the concentration dependence of ^{1}H chemical shifts,[55,66,67] while the relative spatial orientation of the complex cation within an aggregate in solution can be inferred.[36] DOSY experiments have been used as an independent method to estimate the thermodynamic properties of this system[21,67] and

to obtain the estimated hydrodynamic volumes of aggregates, which gives a measure of the number of molecules present in an 'aggregate'.[68,69]

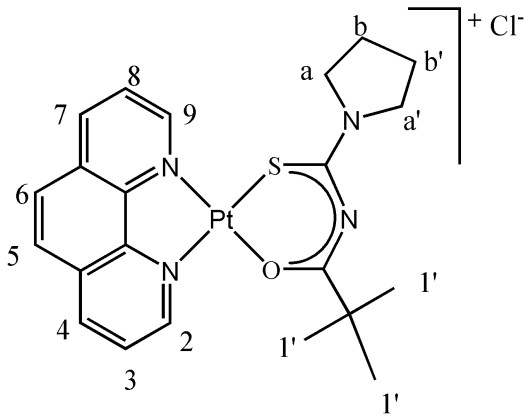

Scheme 2.5: *Structure and numbering scheme for [Pt^{II}(phen)(L^1-S,O)]Cl.*

3.2 Results and discussion

3.2.1 Self-association of [Pt^{II}(phen)(L^n-*S,O*)]$^+$: A High Resolution ^{1}H NMR Study

The ^{1}H NMR spectra obtained as a function of [Pt^{II}(phen)(L^1-*S,O*)]$^+$ concentration at 267.1 K in CD_3CN are shown in Figure 3.1. The marked concentration dependence of the chemical shift of particularly the H^2 and H^9 resonance signals of the coordinated 1,10-phenanthroline moiety suggests that self-association/aggregation processes are occurring with increasing concentration, as previously demonstrated for related complexes.[36] Moreover the spectra reveal that the aggregated species existing in solution are in fast-exchange (in chemical shift) on the NMR time-scale since only one set of ^{1}H resonances are observed over the concentration and temperature range studied. Possible dissociation reactions of the [Pt^{II}(Phen)(L^1-*S,O*)]$^+$ complex over time, such as Cl^- coordination to the platinum(II) metal centre following chelate ring opening reactions, may be excluded since no spectral changes consistent with dissociation were observed over a 5 day period at any fixed concentration for the temperature range 278 - 301 K (see Apendix A).

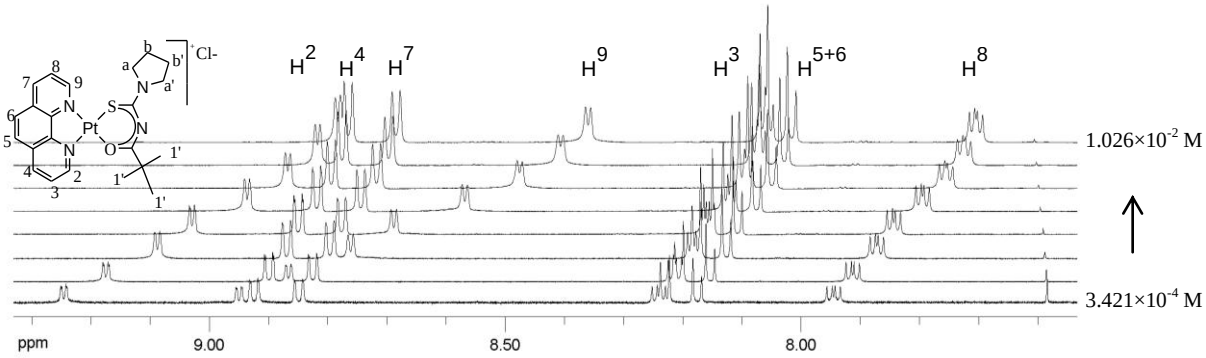

Figure 3.1: *^{1}H NMR spectra (599.99 MHz) of [Pt^{II}(phen)(L^1-S,O)]$^+$ in CD$_3$CN at 273.4 K with increasing complex concentration. Only a partial spectrum is shown as several nuclei (N-pyrrolidyl-N-(2,2-dimethylpropanoyl)thiourea protons) exhibit no or little chemical shift concentration dependence*

Significantly *all* the ^{1}H resonances of the 1,10-phenanthroline group show different degrees of δ_{obs} concentration dependence, depending on their relative positions in the 1.10-phenanthroline ring system (Figure 3.2a), while the chemical shifts of the protons of the coordinated *N*-pyrrolidyl-*N*-(2,2-dimethylpropanoyl)thiourea ligands show much smaller concentration dependences (Figure 3.2b).

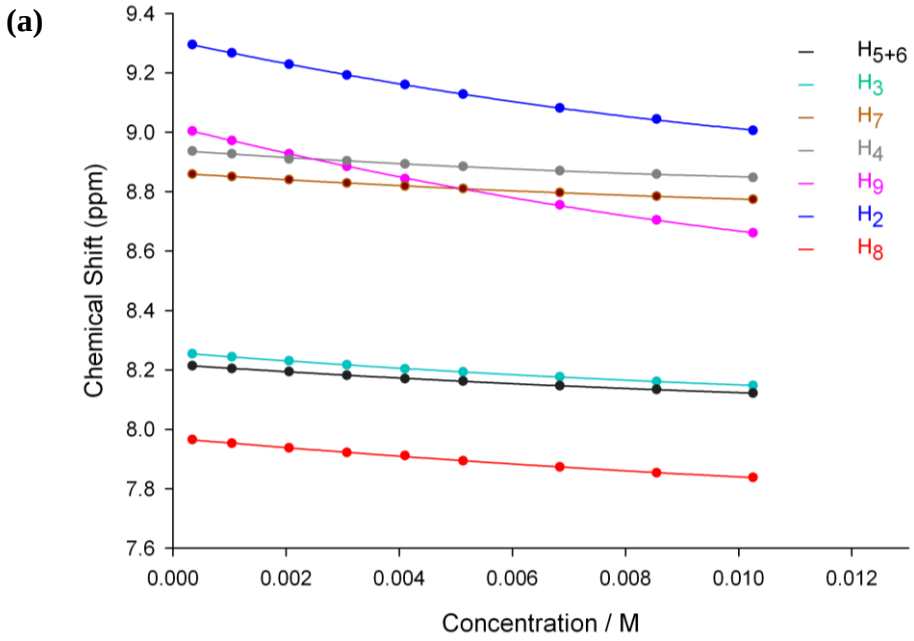

Figure 3.2: *Concentration dependence of the protons of [Pt^{II}(phen)(L^1-S,O)]$^+$ in CD$_3$CN at 299 K with increasing complex concentration, where **(a)** is the phenanthroline protons in the aromatic region.*

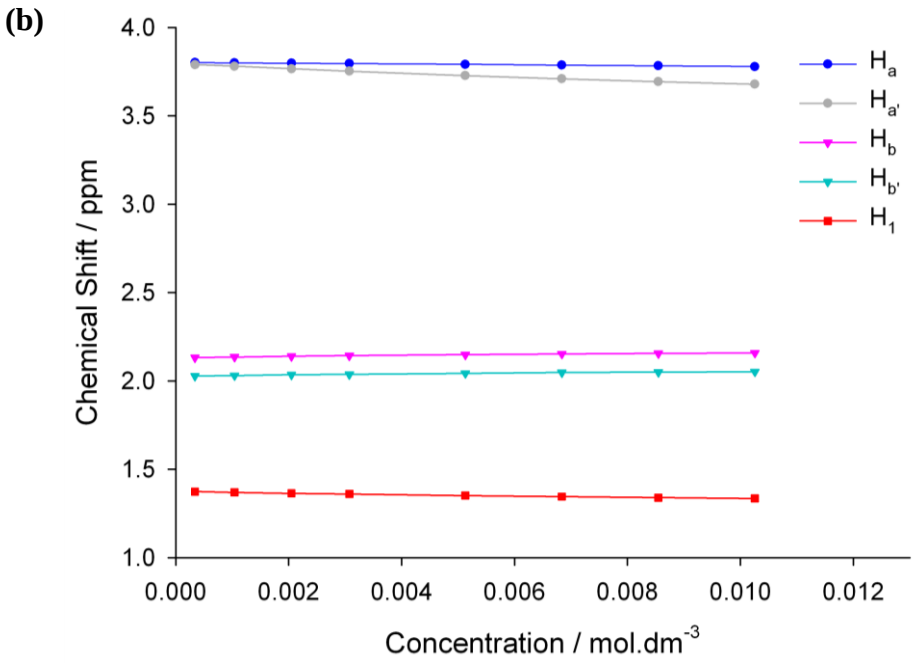

Figure 3.2: *Concentration dependence of the protons of [Pt^{II}(phen)(L^1-S,O)]$^+$ in CD$_3$CN at 299 K with increasing complex concentration, where* ***(b)*** *the N,N-di(alkyl)-N'-acylthiourea protons in the aliphatic region.*

Several intermolecular processes in solution may be invoked to account for the concentration dependence of the δ_{obs}, notably self-association or aggregation of [Pt^{II}(phen)(L^1-*S,O*)]$^+$ cations and/or ion-pairing between the complex cation and Cl$^-$ ion (due to the relatively low dielectric constant of acetonitrile[70], $\varepsilon \approx 37.5$ at 298 K).

The concentration dependence of the δ_{obs} for the [Pt^{II}(phen)(L^1-*S,O*)]Cl salt in acetonitrile solution is postulated to be due essentially to 'dimer aggregate' (D) formation consisting of two planar complex [Pt^{II}(phen)(L^1-*S,O*)]$^+$ cations participating in cation-π stacking interactions in solution (*vide infra*). Self-association of [Pt^{II}(phen)(L^1-*S,O*)]$^+$ leading to higher order aggregates such as 'trimer' or even 'tetramer' aggregates would result in more highly charged species which is thought unlikely in acetonitrile. Nonetheless, to critically examine our postulate of the formation of only dimer aggregates, as well as to exclude the possibility of ion-pairing and/or higher order aggregates being present in solution, an attempt to fit various models including dimer, trimer, and tetramers, as well as a model in which [Pt^{II}(phen)(L^1-*S,O*)]$^{+\cdots}$Cl$^-$ ion-pairing occurs, to the data shown in Figure 3.3 using non-linear least-

squares regression methods, was undertaken. With the exception of the simple dimer (D) model (relation 11), all other models resulted in absurdly large relative percentage errors for calculated equilibrium constants associated with possible ion-pairing and/or higher than dimer self-association processes, disqualifying such more complicated models.

The excellent fit between the δ_{obs} and calculated values obtained with only the dimer (D) model shown in Figure 3.3 (see also equation 12) and further, the plausible calculated chemical shifts of the monomer and dimer of the H^2 protons (9.316 ± 0.029 and 7.851 ± 0.089 ppm respectively at 299.2 K) provides a compelling argument for the dimer model postulated here.

$$2M \underset{}{\overset{K_D}{\rightleftharpoons}} M_2 \qquad (11)$$

$$C_{T(Pt)}\delta_{obs} = c_M\delta_M + 2c_{M2}\delta_{M2} \qquad (12)$$

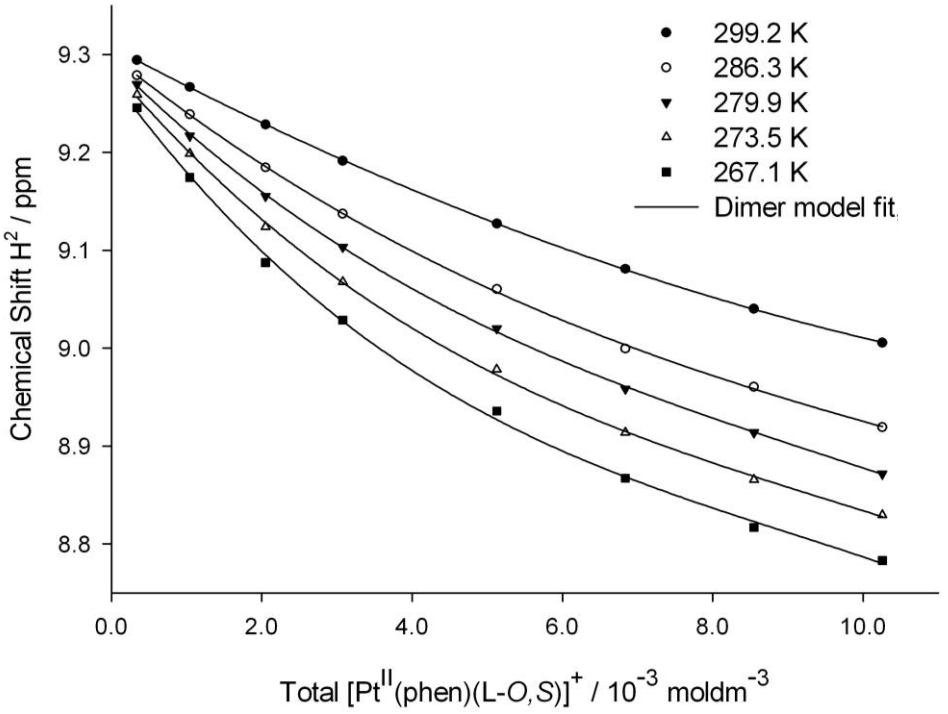

Figure 3.3: *Excellent agreement was obtained between the dimer model least-squares fits and the experimental (symbols) chemical shift dependence of the 1,10-phenanthroline H^2 proton on the concentration of [Pt^{II}(phen)(L^1-S,O)]$^+$.*

The chemical shift of all the ^{1}H resonance signals is also dependent on the temperature. As the temperature decreases an upfield shift of all the ^{1}H resonances was observed and depending on the position of the proton in the complex the extent/magnitude of the δ_{obs} temperature dependence varied (Figure 3.4), similar to that observed for the concentration dependence studies. The ^{1}H δ_{obs} temperature dependence of the [Pt^{II}(phen)(L^1-*S,O*)]Cl is further evidence of a self-association/aggregation process occurring.

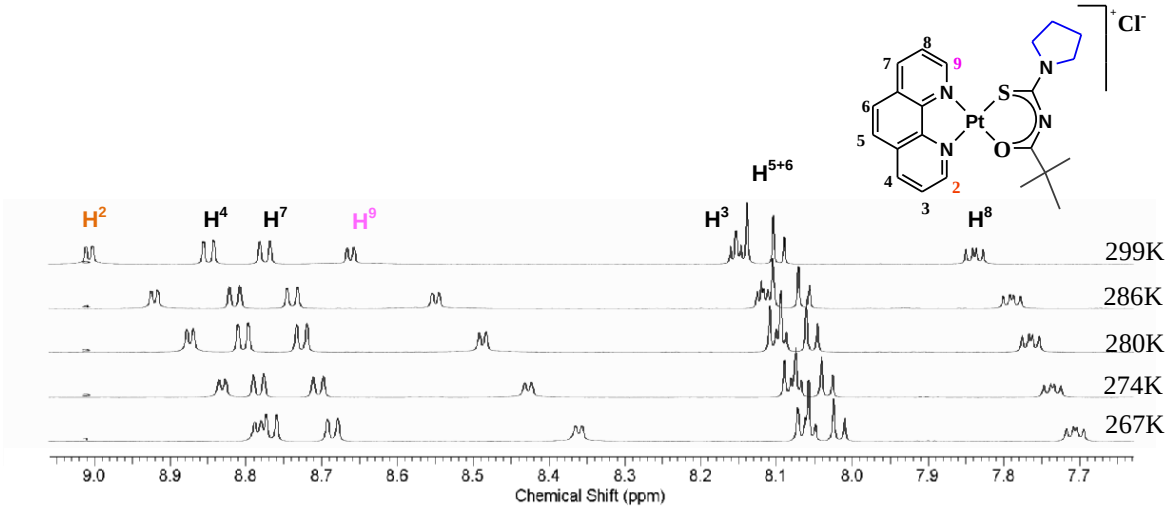

Figure 3.4: *^{1}H NMR spectra (599.99 MHz) of [Pt^{II}(phen)(L^1-S,O)]$^+$ in CD_3CN (1.026×10^{-2} M) as a function of temperature. Only a partial spectrum is shown as several nuclei (N-pyrrolidyl-N-(2,2-dimethylpropanoyl)thiourea protons) exhibit no or little chemical shift temperature dependence.*

Raising the temperature from 267.1 to 299.2 K, the K_D decreases from 56 ± 8 M^{-1} to 17 ± 2 M^{-1}, indicating as expected that dimer formation is exothermic (Table 3.1). The standard reaction enthalpy, Δ_rH^o, and entropy, Δ_rS^o, can be estimated by fitting the Van't Hoff equation (13) to the temperature dependent K_D data. Over the relatively small temperature range used here (Δ 32.1 K), it is expected that the Δ_rH^o and Δ_rS^o are temperature independent yielding a linear plot of ln(K_D) versus T^{-1}.

This is confirmed by the good linear trend obtained using the Van't Hoff equation (Figure 3.5), which further validates the dimer aggregate model; the standard reaction enthalpy (slope) and entropy (intercept) of reaction 11 are listed in Table 3.1.

$$\ln(K_D) = -\frac{\Delta_r H^O}{RT} + \frac{\Delta_r S^O}{R} \qquad (13)$$

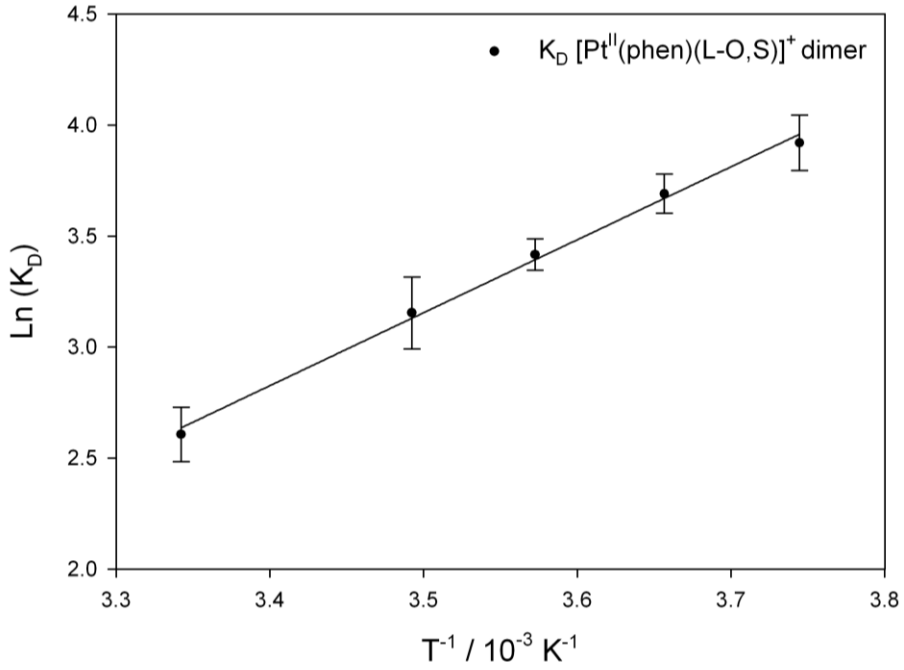

Figure 3.5: *The good linear fit obtained with the Van't Hoff equation is further validation for the self-association of [Pt^{II}(phen)(L^1-S,O)]$^+$ in CD$_3$CN. The 95% confidence interval of the slope and intercept for the [Pt^{II}(phen)(L^1-S,O)]$^+$ dimer equal 3087.1 (±374.2)x -7.5 (±1.3)*

Table 3.1: *Calculated dimerization constants, K_D for [Pt^{II}(phen)(L^1-S,O)]$^+$ in CD$_3$CN and thermodynamic data.*

Temp / K	K_D / M^{-1}	$\Delta_r H^o$ / $Jmol^{-1}$	$\Delta_r S^o$ / $Jmol^{-1}$	$\Delta_r G^o$ / $Jmol^{-1}$
299.2	17 (± 2)	-25129 (± 3112)	-61 (± 11)	-6998
286.3	27 (± 5)			-7777
279.9	29 (± 3)			-8167
273.5	46 (± 7)			-8556
267.1	56 (± 8)			-8946

The relatively large, negative Δ_rS^o is indicative of an association reaction consistent with the inference that only dimer aggregates are formed. By comparison, ion-pair processes are typically associated with a positive Δ_rS^o changes, as solvated molecules are "released" upon ion-pair formation.[21,71] Furthermore, it is clear from the thermodynamic data (Table 3.1) ($\Delta_rH^o < 0$, $T\Delta_rS^o < 0$) that the dimer formation reaction is enthalpy driven and that this thermodynamic behaviour is indicative of cation-π binding.[21]

3.2.2 ^{1}H Diffusion Ordered Spectroscopy (DOSY) Study of the Self-association of [Pt^{II}(phen)(L^n-*S*,*O*)]$^+$

Given the relatively simple dimer model, it is reasonable to expect that molecular diffusion processes might be affected by increased dimer formation, as a function of increasing complex concentration. This expectation is confirmed by diffusion ordered ^{1}H NMR spectroscopy (DOSY) which is shown here also to be an independent method with which to verify conclusions drawn from the concentration and temperature ^{1}H NMR chemical shift dependence studies. Experiments with diffusion delay times varying from 30 to 200 ms resulted in no significant differences in DOSY spectra nor in calculated diffusion coefficients (Figure 2.13 see page 32); it is therefore reasonable to conclude that only an averaged diffusion coefficient, D_{obs}, is observed.[72] Unlike the ^{1}H chemical shift experiments discussed above, all protons of the complex [Pt^{II}(phen)(L^1-*S*,*O*)]$^+$ in equilibrium with the dimer yield the "same" diffusion coefficient and this method is therefore not dependent on the individual proton chemical shifts. The D_{CD3CN} obtained here (39.5×10^{-10} m^{2}s^{-1}) differs by less than 7% from the value obtained by Kato and co-workers[73] (4.3×10^{-9} m^{2}s^{-1}), and consequently the D_{CD3CN} were used as an internal 'standard'. The D_{obs} for the complex is proportional to the sum of the product of the individual diffusion coefficients, D_i, and the concentration of the species (i) present (equation 14). Estimation of the K_D from diffusion data is based on the same mathematical algorithm[55] as for the ^{1}H chemical shift dependence described above.

$$C_{T(Pt)}D_{obs} = c_M D_M + 2c_{M2}D_{M2} \qquad (14)$$

As the concentration of [Pt^{II}(phen)(L^1-*S,O*)]$^+$ increases experimental diffusion coefficients decrease (Figure 3.6), consistent with a dimer model. The least-squares fit with the dimerization model (relation 11) is in good agreement with the diffusion data (Figure 3.6) and the calculated K_D from diffusion data at 299.2 K is 15 ± 8 M^{-1} (ΔG = -6737 $Jmol^{-1}$).

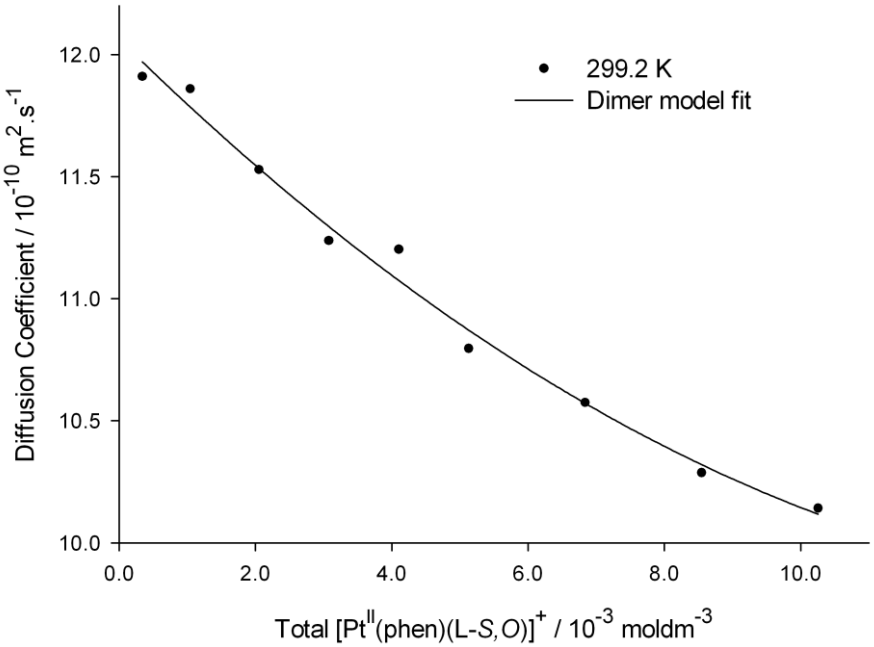

Figure 3.6: *Good agreement was obtained between the dimer model least-squares fit and the experimental (symbols) diffusion coefficient dependence on the concentration of [Pt^{II}(phen)(L^1-S,O)]$^+$ at 299.2 K.*

This compares well with the K_D calculated from the chemical shift data 17 ± 2 M^{-1} (ΔG = -7048 $Jmol^{-1}$) and supports the simple dimer model. The agreement is reasonably acceptable given that the relative percent error of measured diffusion coefficients is at best 4%, albeit much larger than the relative percentage error in the measurement of a ^{1}H NMR chemical shift (0.2%), arguably leading to a less precise value of K_D from DOSY NMR data (Figure 3.6). The satisfactory agreement between the two methods of estimating K_D indicates that this model is internally consistent.

In principle the hydrodynamic radius and volume of a complex may be estimated from DOSY data at a given concentration. The *hydro-dynamic* radius is the radius of an

equivalent sphere which includes both solvent (*hydro*) and *dynamic* features of a structure.[75,75] The diffusion coefficient is related to molecular size by the well known Stokes-Einstein equation (15), from which the hydrodynamic radius, r_H, and volume, v_H, of the molecules/aggregates in question can be estimated,

$$D = \frac{kT}{6\pi\eta r_H} \qquad (15)$$

where k is the Boltzmann constant, T is the absolute temperature and η the solvent viscosity.[68] This equation assumes a spherical molecule and is obviously a rather crude approximation of our square planar complexes. It is assumed that the solvent viscosity does not change significantly with solute concentration, which is justified for the relatively low solute concentrations used and justified by the negligible change in D_{CD3CN} values ($39.53 \pm 0.72 \times 10^{-10}$ m^{2}s^{-1}) obtained for all solutions of differing solute concentration examined at 299.2 K. The hydrodynamic radii estimated (Table 3.2) from the D_{obs} represent an "average" of the monomer and dimer.

Table 3.2: *Diffusion coefficients D ($\times 10^{-10}$ m^{2}s^{-1}), hydrodynamic radii r_H (Å) and hydrodynamic volumes V_H (Å^3) for [Pt^{II}(phen)(L^1-S,O)]$^+$ in CD_3CN at different complex concentrations (mM).*

Conc / mM	D / 10^{-10} m^{2}s^{-1}	r_H / Å	V_H / Å^3
10.26	10.14 (± 0.07)	5.82	824.1
8.55	10.29 (± 0.09)	5.73	789.6
6.84	10.58 (± 0.08)	5.58	726.8
5.13	10.80 (± 0.11)	5.46	683.2
4.10	11.20 (± 0.11)	5.27	611.5
3.08	11.24 (± 0.13)	5.25	605.6
2.05	11.53 (± 0.17)	5.12	561.0
1.04	11.86 (± 0.12)	4.97	515.2
0.34	11.91 (± 0.18)	4.95	508.7

From the least-squares fit of the data in Figure 3.6, the [Pt^{II}(phen)(L^1-*S,O*)]$^+$ monomer and dimer individual diffusion coefficients were estimated at *ca.* 12.1 ± 0.6 × 10^{-10} and 5.9 ± 0.8 × 10^{-10} m^2s^{-1} respectively from which the hydrodynamic radii for the monomer and dimer could be estimated to be 4.8 (± 2.3) and 10.1 (± 3.5) Å respectively.

The r_H value for the [Pt^{II}(phen)(L^1-*S,O*)]$^+$ complex is reasonable when compared to the $r_{H\ X\text{-}Ray}$ estimated from single crystal X-ray data of *cis*-[Pt^{II}(*N*-pyrrolidyl-*N*-(2,2-dimethylpropanoyl)thiourea)$_2$] and [Pt^{II}(en)(phen)]$Cl_2{\cdot}2H_2O$ as shown below,[76,77] which is 5.8 Å (Diagram 3.1), whereas the calculated r_H of the dimer is reasonable when considering two [Pt^{II}(phen)(L^1-*S,O*)]$^+$ species in close contact. The $r_{H\ X\text{-}Ray}$ were estimated by measuring the distance from the platinum atom to the centre of a line connecting the two outer most atoms of the structure. This was done for *cis*-[Pt^{II}(L^1)$_2$] to estimate the contribution of L^1 to the radius of [Pt^{II}(phen)(L^1-*S,O*)]$^+$ and likewise the contribution of the phenanthroline ligand was estimated from [Pt^{II}(en)(phen)]$Cl_2{\cdot}2H_2O$.

Diagram 3.1: *Estimation of the r_H of [Pt^{II}(phen)(L^1-S,O)]$^+$ from two closely related crystal structures*

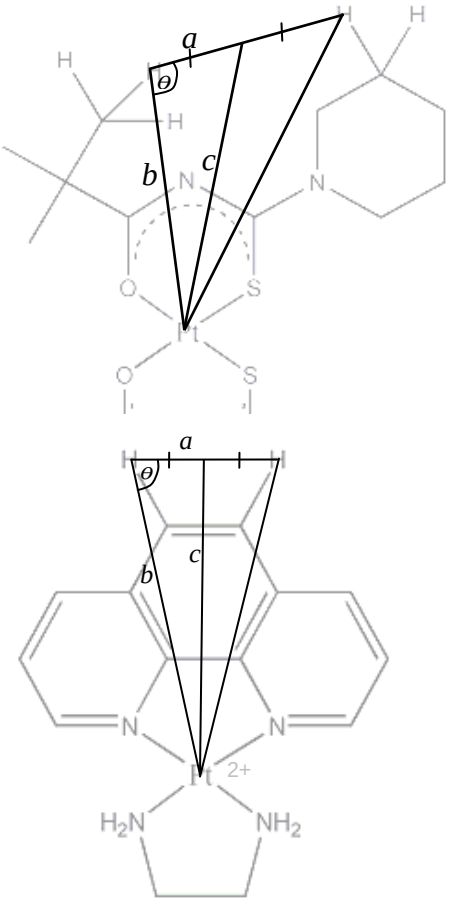

From crystal structure of Mautjana *et al*:[76]

Θ = 80.52°

a = 4.00Å/2 = 2.00Å

b = 5.604Å

Cosine rule:

$c^2 = a^2 + b^2 - 2ab(\cos \theta)$

c = 5.63Å

From crystal structure of Kato *et al*:[77]

Θ = 78.38°

a = 2.536/2 = 1.268Å

b = 6.199Å

Cosine rule:

$c^2 = a^2 + b^2 - 2ab(\cos \theta)$

c = 6.06Å

Estimated r_H = (5.63 + 6.05) / 2 = 5.84Å

The consistency of the DOSY data with that obtained from the concentration dependence of the δ_{obs}(^{1}H) of the [Pt^{II}(phen)(L^1-*S,O*)]$^+$ complex is convincing support of dimer formation through cation-π association of these planar platinum(II) complexes.

3.2.3 Self-association Mass Spectroscopy in vacuo

The cation-π interaction of the [Pt^{II}(phen)(L^1-*S,O*)]Cl complex has been shown to be relatively favourable in solution so that it may be expected to be even more so in the gas phase.[59] In this study ESI(+) MS (Electron Spray Ionization) was used and it is thought that the detection of aggregates may be possible due to relatively gentle ionization of this technique.

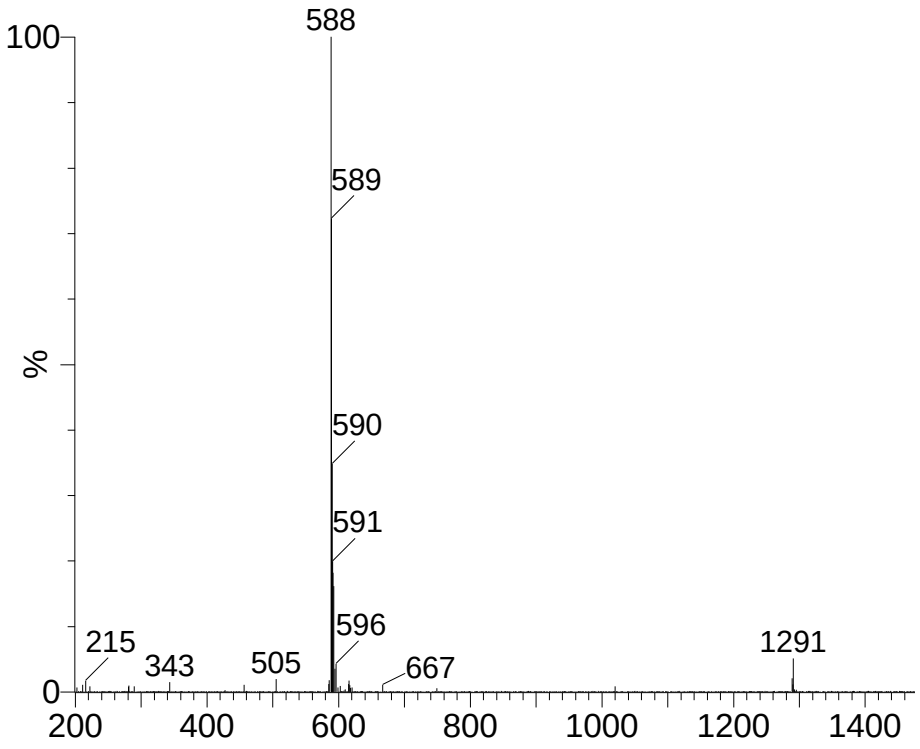

***Figure 3.7**: ESI(+) Mass Spectrum of [Pt^{II}(phen)(L^1-S,O)]Cl in acetonitrile.*

The molecular ion (M^+ = [Pt^{II}(phen)(L^1-*S,O*)]$^+$) is the peak at m/z of 588 while the peak with a m/z equal to 1291 is argued to be a dimer aggregate consisting of two [Pt^{II}(phen)(L^1-*S,O*)]$^+$ species, one Cl$^-$ ion and two acetonitrile molecules (Figure 3.7). This aggregate has an overall charge of +1 and can thus be observed. A dimer in the

form {[Pt^{II}(phen)(L^1-*S*,*O*)]$^+$}$_2$ is also expected to form but this dimer would result in a m/z value equal to that of the molecular ion (588) and would not be distinguishable from M^+. Aggregates were observed by Koch and co-workers for similar complexes where they have found peaks in the (+)FAB spectrum corresponding to dimer aggregates.[36] The presence of solvent molecules in an aggregate observed in the ESI mass spectrum is not something new and was also observed by Kettrup and co-workers for CuEDTA in water.[78] The observation of dimer aggregates in the mass spectrum of [Pt^{II}(phen)(L^1-*S*,*O*)]Cl confirms the tendency of these complexes to aggregate not only in solution but also in vacuum.

3.2.4 Self-association Study using UV-*VIS* Spectroscopy

UV-VIS spectroscopy is a well known method for studying molecular association in solution and has been used to determine association constants for various complexes.[79,80] A UV-VIS concentration dependence study was attempted for [Pt^{II}(phen)(L^1-*S*,*O*)]Cl with the objective of comparing the findings with the dimerization constants calculated from the chemical shift and diffusion coefficient concentration dependence study. Unfortunately, this complex exhibited two intense bands (presumably charge-transfer) at 210nm and 275nm even at very low concentrations. An attempted concentration dependence study revealed that the self-association at such low concentrations does not occur to a considerable degree, or at least cannot be adequately investigated by UV-VIS spectroscopy.

3.2.5 Proposed Dimer Structure

Unfortunately numerous attempts to obtain crystals suitable for single crystal x-ray diffraction failed to date, so that direct structural support for the geometrical nature of the dimer aggregate is lacking at present. Nevertheless from the relative ^{1}H chemical shift trends observed (Figure 3.1 see pages 60-1) it is possible to infer a most likely structure of the dimer aggregate in solution.

The relatively small concentration dependence of the δ_{obs} for the butyl and *N*-pyrrolidyl protons (Figure 3.2b) compared to the large chemical shift concentration dependence of

the 1,10-phenanthroline protons, particular H^2 and H^9 (Figure 3.2a), suggests that these complexes stack *regiospecifically* in a face-to-face manner involving the phenanthroline sides of the complex. An unlikely 'T-shaped' edge-on geometry[40] for the dimer can be ruled out given the chemical shift trends observed (Figure 3.2). The coplanar stacking arrangement postulated will maximize the cation-π attractions and minimize π-π repulsion to result in an offset cation-π stacking geometry between adjacent complexes, consistent with related metalloporphyrins suggested by the Sanderson[40] model, as in Scheme 3.2. Depicted in the scheme are the most reasonable dimer aggregate structures postulated in solution; since the system is in fast exchange in chemical shift, only an average structure can be proposed from NMR data in view of several possible geometric stacking interactions conceivable.

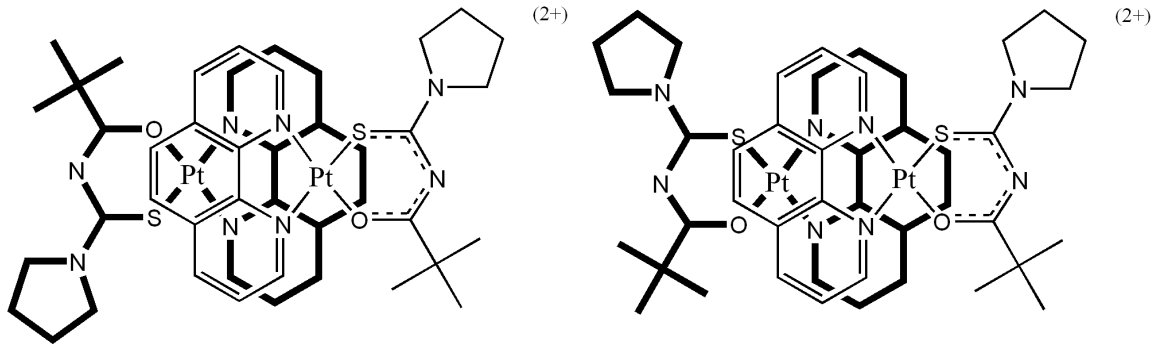

Scheme 3.2: *Proposed average [Pt^{II}(phen)(L^1-S,O)]$^+$ dimer aggregate structures in solution.*

3.2.6 Effect of Solvent Composition on the Extent of Association

When water is added to acetonitrile it is expected that the solvation characteristics of the charged [Pt^{II}(diimine)(L^n-*S,O*)]$^+$X$^-$ complexes will change and therefore influence the extent of self-association.[81] To investigate this, the ratio of water to acetonitrile was gradually changed from pure acetonitrile to water/acetonitrile mixtures ranging from 10-100% (v/v) D_2O.

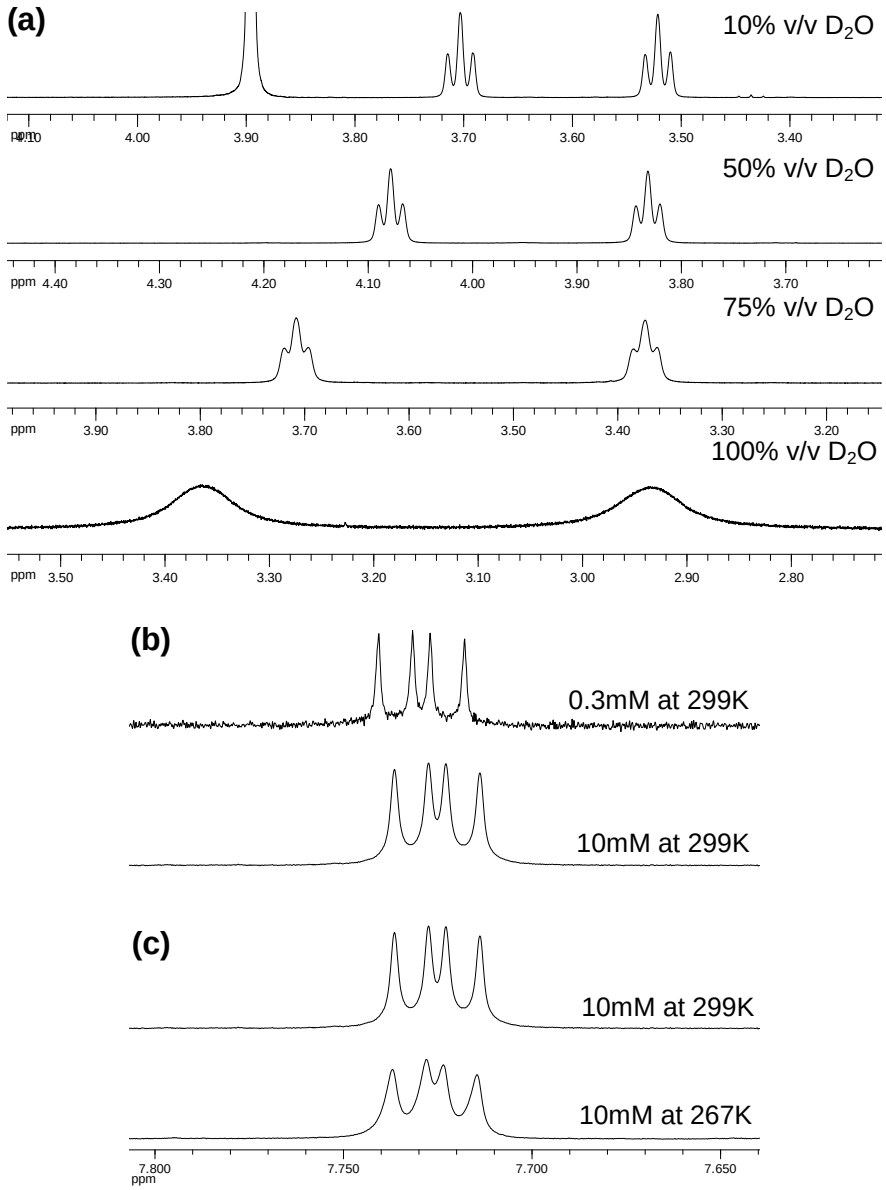

Figure 3.8: *Broadening of the ^{1}H NMR resonance signals of [Pt^{II}(phen)(L^1-S,O)]$^+$ due to the increased dimerization as a result from **(a)** an increase in D_2O content, **(b)** an increase in concentration and **(c)** a decrease in temperature.*

Interestingly the ^{1}H NMR signals broaden as the D_2O content of the solution is increased (Figure 3.8a). Magnetic field inhomogeneity or intermediate chemical exchange is normally the reason for the broad resonance signals observed in a NMR spectrum. Magnetic field inhomogneity of the external magnetic field can be greatly reduced with proper shimming and was not the reason for the broad resonance signals observed since a sharp solvent peak was observed. *Intra*- and *inter*-molecular

interactions associated with the formation of aggregates with higher molecular weight can conceivably result in a decrease in the molecular tumbling rate. If the rate of tumbling is not high this results in shorter T_2 relaxation times. A decrease in T_2 relaxation times due to molecular motion results in broadening of the observed resonance signals. The half-height line-width ($\Delta\upsilon$) of a resonance signal is inversely proportional to the T_2 relaxation time.[53]

$$\Delta\nu_{1/2} \ \alpha \ \frac{1}{T_2} \qquad (16)$$

An increase in concentration of [Pt^{II}(phen)(L^1-*S,O*)]Cl (Figure 3.8b) as well as an decrease in temperature (Figure 3.8c) leads to a shift towards more aggregate formation which presumably results in shorter T_2 relaxation times reflected in broadening of the resonance signals observed. Broad signals due to slow or intermediate chemical exchange effects could also be responsible for the broadening however, the rate of exchange would presumably not be significantly affected by the [Pt^{II}(phen)(L^1-*S,O*)]Cl concentration and thus intermediate chemical exchange is not thought to be responsible for the broadening of the resonance signals observed.

3.2.6.1 Water/acetonitrile mixtures up to 30% (v/v) D_2O

The change in chemical shift with an increase in [Pt^{II}(phen)(L^1-*S,O*)]Cl concentration is more dramatic with a increase in the percentage of D_2O in the solvent (Figure 3.9). An excellent fit between the δ_{obs} and calculated values was obtained for only the dimer (D) model as shown in Figure 3.9, while reasonable calculated monomer and dimer limiting chemical shifts for the H^2 protons were obtained.

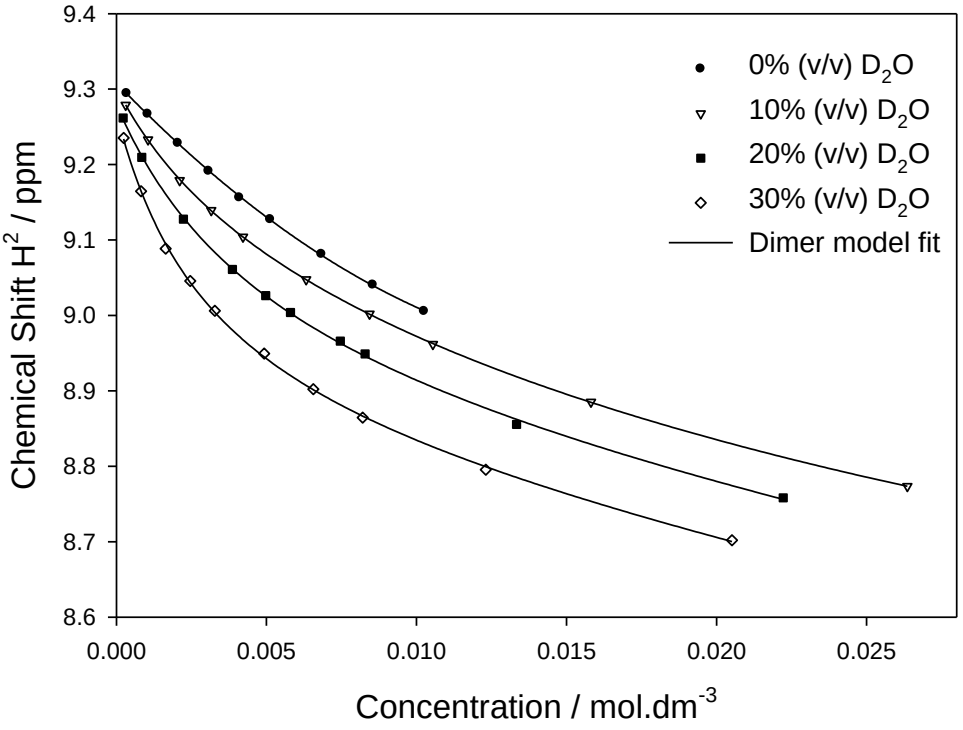

Figure 3.9: *Chemical shift concentration dependence of the 1,10-phenanthroline H^2 proton on the concentration of [Pt^{II}(phen)(L^1-S,O)]$^+$ in CD$_3$CN:D$_2$O mixtures (299K).*

Using the "dimer" model, where M = [Pt^{II}(phen)(L^1-*S,O*)]$^+$ monomer and M$_2$ = {[Pt^{II}(phen)(L^1-*S,O*)]$^+$}$_2$, dimerization constants (K_D) and chemical shifts (δ_i) for the relevant protons were estimated to within a 95% confidence limit for each temperature and 0% to 30% v/v D$_2$O solutions as seen in Figure 3.10. The dimer model fits the experimental data exceptionally well while the dimerization constants calculated for the 0-30% (v/v) D$_2$O:CD$_3$CN solvent mixtures at various temperatures show a systematic increase with D$_2$O content as well as a decrease in temperature summarized in Table 3.3; the relative percentage errors for all K_D values are estimated < 13%.

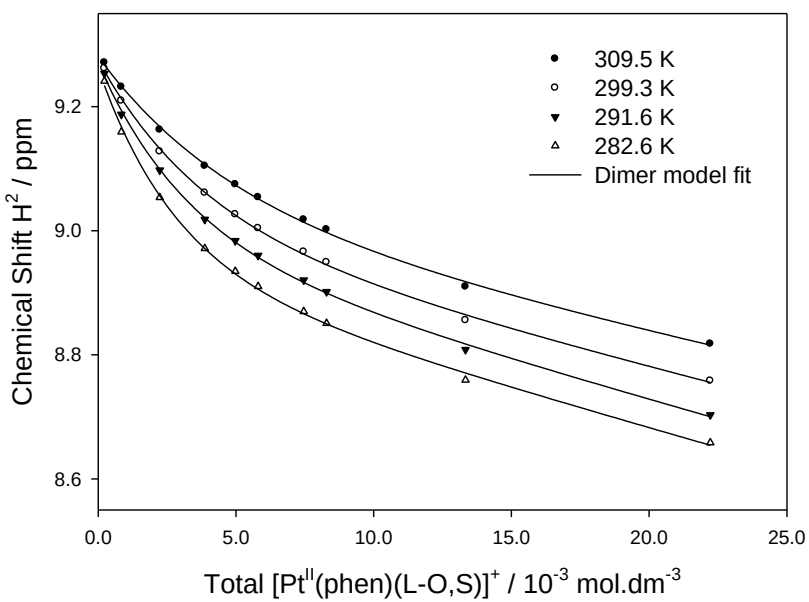

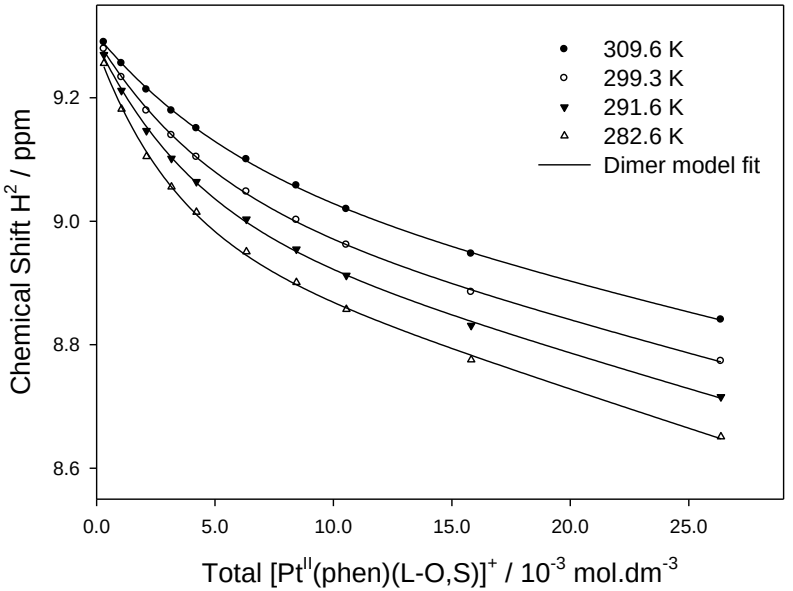

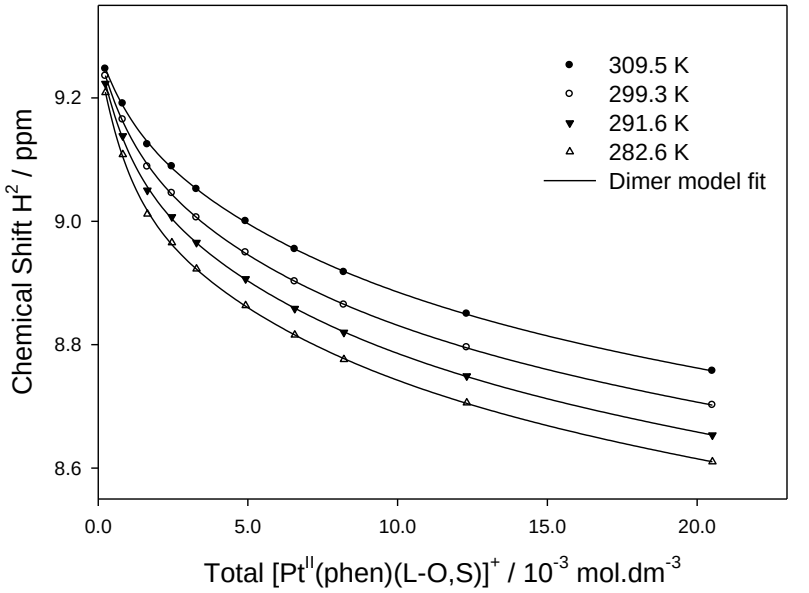

Figure 3.10: *Excellent agreement was obtained between the dimer model least-squares fits and the experimental (symbols) chemical shift dependence of the 1,10-phenanthroline H^2 proton on the concentration of $[Pt^{II}(phen)(L^1\text{-}S,O)]^+$ in (a) 10:90, (b) 20:80 and (c) 30:70 v/v D_2O:CD_3CN mixtures.*

Table 3.3: *Calculated dimerization constants, K_D for $[Pt^{II}(phen)(L^1\text{-}S,O)]^+$ in different D_2O:CD_3CN mixtures.*

	K_D			
Temp / K	0% v/v D_2O	10% v/v D_2O	20% v/v D_2O	30% v/v D_2O
309.6	12 (± 1)	20 (± 2)	29 (± 3)	54 (± 5)
299.3	17 (± 2)	27 (± 3)	39 (± 4)	71 (± 8)
291.6	22 (± 2)	33(± 3)	43 (± 4)	87 (± 9)
282.6	29 (± 3)	41(± 5)	64 (± 7)	109 (± 10)

The dimerization constants for the mixed D_2O:CD_3CN solutions at 299K increases from 17 M^{-1} to 71 M^{-1}. The increase in dimerization constant with increasing D_2O percentage confirms the suggestion for the observed broadening of resonance signals (Figure 3.8a). It is reasonable to argue that the increase in the dimerization constant can be attributed to the water molecules 'stabilizing' the doubly charged dimers to a greater extent due to a higher dielectric constant of H_2O/D_2O (ε = 78.5) compared to acetonitrile (ε = 37.5).[70] Furthermore, the larger dimerization constant in the water mixtures could also be due to hydrophobicity of the $[Pt^{II}(phen)(L^1\text{-}S,O)]Cl$ complex. Hydrophobicity is the association of non-polar groups or molecules in an aqueous environment which arises from the tendency of water to energetically exclude non-polar molecules, due to solvation energy penalties.[82]

Dimerisation constants were determined as a function of temperature, from which the thermodynamic properties can be calculated using the Van't Hoff plot (Figure 3.11), from equation 13. The good fit of the Van't Hoff equation to the experimental data (Figure 3.11) confirms the validity of the dimer model and that no significant ion pairing or higher order aggregation is present in the D_2O:CD_3CN mixed solutions up to 30%. The thermodynamic data obtained from the Van't Hoff plots is summarized in Table 3.4.

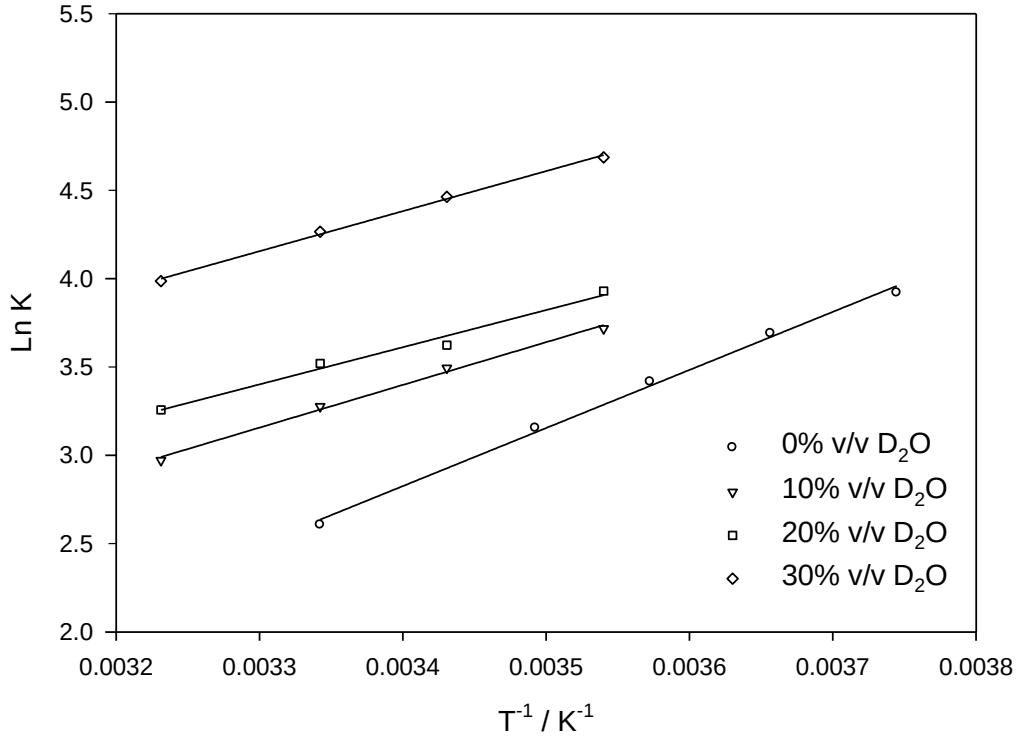

Figure 3.11: *Van't Hoff plots of solutions 0% - 30% D_2O. The good linear fit obtained with the Van't Hoff equation is further validation for the self-association of $[Pt^{II}(phen)(L^1\text{-}S,O)]^+$ in CD_3CN.*

From Table 3.4 it can be seen that the Gibbs free energy for the dimer formation changes significantly as the solvent composition is changed. The more negative ΔG values for the higher concentration of D_2O percentage solutions shows that the dimer formation is more favourable for solutions containing more D_2O. The negative enthalpy ($\Delta H < 0$) implies that the dimer formation is enthalpy driven. The entropy is negative ($\Delta S < 0$) which is expected for an association process where two molecules form essentially one aggregate.

Table 3.4: *Thermodynamic data for the self-association of $[Pt^{II}(phen)(L^1\text{-}S,O)]^+$ in D_2O:CD_3CN mixed solutions at 299.3K.*

%D_2O	**K_D (299K)**	**ΔH (J/mol)**	**ΔS (J/mol)**	**ΔG (J/mol)**
0	17 (± 2)	-25129 (± 3112)	-61 (± 11)	-6998
10	27 (± 3)	-19685 (± 2438)	-40 (± 7)	-7981
20	39 (± 4)	-20089 (± 2489)	-38 (± 7)	-8571
30	71 (± 8)	-18854 (± 2335)	-27 (± 5)	-10389

This explains why the entropy term is negative but not the why the magnitude of the entropy decreases with increasing D_2O content. The trend is unexpected since the extent of dimerization increases as the concentration of D_2O increases. A possible explanation for this unexpected trend lies in the solvation of these complexes in solution. When the two solvated monomer molecules combine to form a dimer aggregate, it can be anticipated that solvent molecules from the salvation sphere of the complex must be "released" upon dimer formation since fewer molecules might be needed to solvate the dimer aggregate. This could result in a positive contribution towards the total entropy. This effect should be more significant for the solutions containing more D_2O in order to explain the trend in the entropy observed. Such reasoning is at this stage however speculative, and needs further investigation.

In summary the total entropy for the dimer formation is thought to be a combination of the large negative entropy due to the dimerization process and a smaller positive contribution due to the release of solvent molecules in the dimerization process that becomes more significant with increasing D_2O percentage solutions.

The enthalpy of the dimer formation shows a decrease in magnitude as the D_2O content increases except for the 20% v/v D_2O:CD_3CN solution which is within the experimental error. The dimer formation is more favourable for the solutions containing more D_2O that can be attributed to the entropy that becomes more positive with increasing amount of D_2O resulting in the overall aggregate formation to be more favoured.

3.2.6.2 Water/acetonitrile mixtures > 30% (v/v) D_2O

The solvent combinations were extended from 30% to 50, 75 and 100% v/v D_2O. The concentration dependence of H^2 for the solutions containing 50, 75 and 100% v/v D_2O:CD_3CN (Figure 3.12) were conducted. Excellent trends in the experimental data were obtained to which various models could be potentially fitted (Figure 3.12). However, the dimerization model does not fit the data while higher order aggregation models (trimers, tetramers etc.) and combinations thereof were attempted without success.

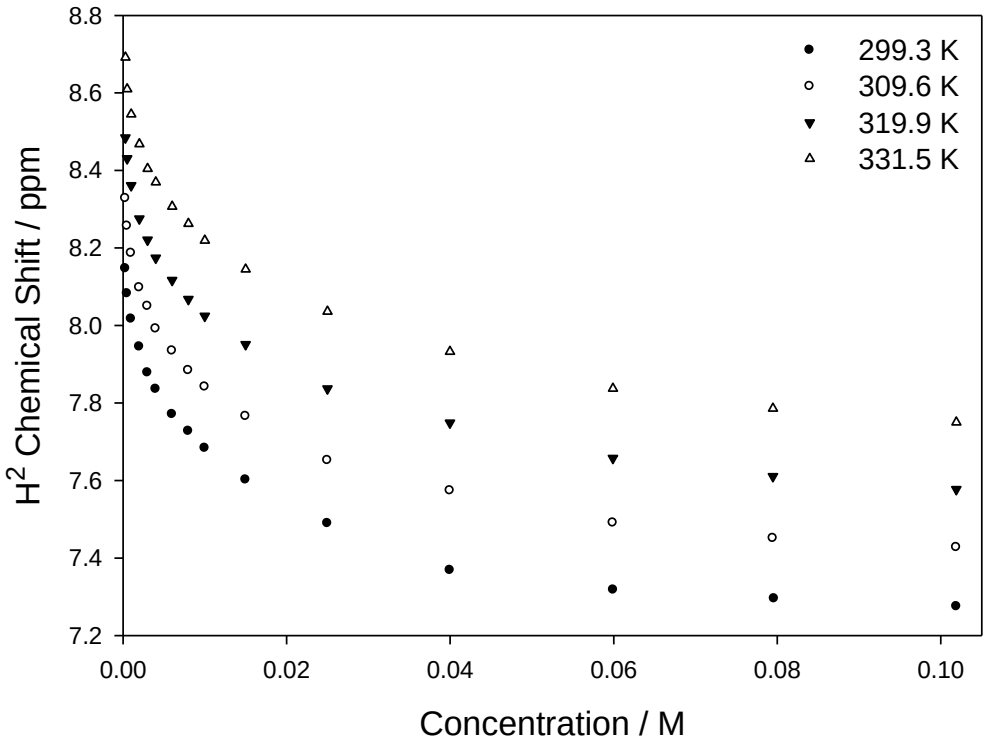

Figure 3.12: *Chemical shift dependence of the 1,10-phenanthroline H^2 proton on the concentration of $[Pt^{II}(phen)(L^1\text{-}S,O)]^+$ in solutions containing only D_2O.*

The change in chemical shift observed for the solutions containing only D_2O were drastic (± 0.66 ppm) while the resonance signals are very broad indicating that the extent of aggregation is clearly not supported by a simple dimer model (Figure 3.13). The broadness of the resonance signals suggests that the extent of association/aggregation is drastically larger as observed in Figure 3.8.

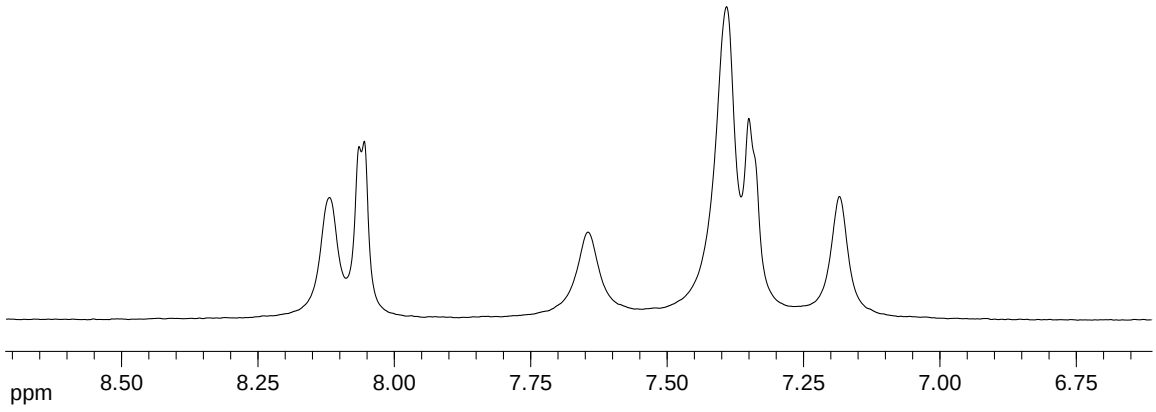

Figure 3.13: *Proton spectrum of $[Pt^{II}(phen)(L^1\text{-}S,O)]^+$ in D_2O showing the phenanthroline protons in the aromatic region of the spectrum.*

It is possible that $[Pt^{II}(phen)(L^1\text{-}S,O)]Cl$ forms super size aggregates or micelles in the 100% (v/v) D_2O solutions as suggested by the broad ^1H resonance signals observed (Figure 3.13) as well as the large aggregates observed in the TEM image of a 1.0 mM solution of $[Pt^{II}(phen)(L^1\text{-}S,O)]Cl$ in water stained with uranyl acetate (Figure 3.14).

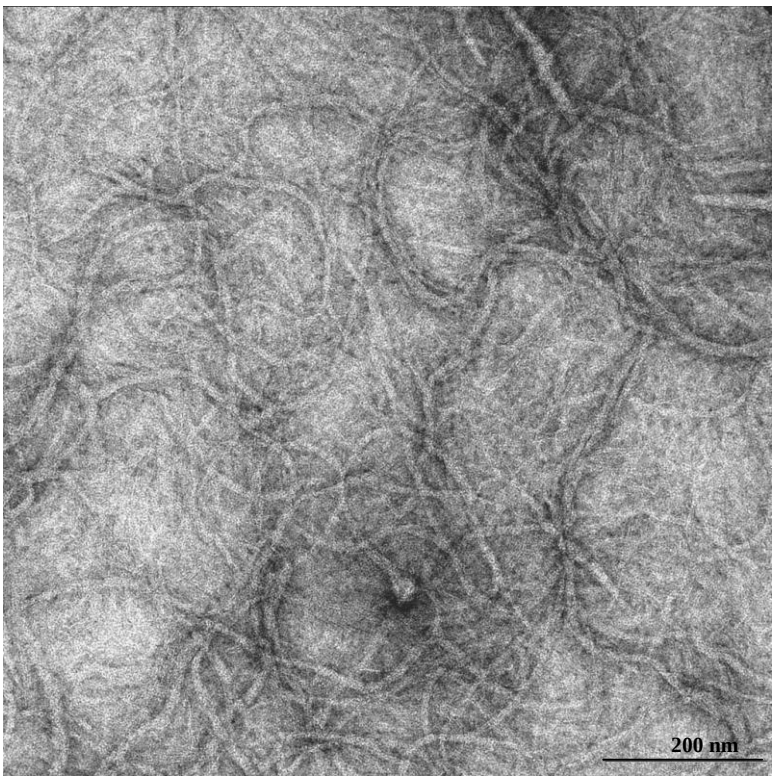

Figure 3.14: *TEM image of $[Pt^{II}(phen)(L^1\text{-}S,O)]Cl$ in H_2O stained with uranyl acetate.*

This will be subject of future study and is beyond the scope of this work. In the next chapter the hetero-association of $[Pt^{II}(phen)(L^1\text{-}S,O)]^+$ and fluoranthene in acetonitrile will be discussed.

Chapter 4

Non-covalent hetero-association of $[Pt^{II}(phen)(L^{1}\text{-}S,O)]^{+}$ and fluoranthene

Chapter 4

Non-covalent hetero-association of $[Pt^{II}(phen)(L^1\text{-}S,O)]^+$ and fluoranthene

4.1 Introduction

Compounds that DNA intercalate[7-10] and prevent hemazoin formation[26,27] are just two examples of the importance of hetero-association in biological systems. It was convincingly demonstrated in the previous chapter that $[Pt^{II}(phen)(L^1\text{-}S,O)]^+$ non-covalently self-associates, to form $\{Pt^{II}(phen)(L^1\text{-}S,O)]^+\}_2$, in acetonitrile solution. We attributed the self-association interaction to be driven by cation-π attraction. However, the $[Pt^{II}(phen)(L^1\text{-}S,O)]^+$ complex is positively charged and it is reasonable to expect equal charge repulsion. It is therefore envisaged that the extent of $[Pt^{II}(phen)(L^1\text{-}S,O)]^+$ association with neutral π-systems would be larger. Association of group I and II metal cations and protonated amine systems with uncharged π-systems is well known.[20,59] However, planar complex cations such as $[Pt^{II}(diimine)(L^n\text{-}S,O)]^+$ and even $[Pt^{II}(diimine)_2]^{2+}$ have received comparatively little attention in the literature.[17,36,66]

In this context, we examined potential cation-π interactions between the $[Pt^{II}(phen)(L^1\text{-}S,O)]Cl$ complex (Scheme 2.5 see page 59) and fluoranthene ($C_{16}H_{10}$) in acetonitrile as a model system, by means of ^1H NMR concentration dependence studies to probe these phenomena. ^1H NMR is particularly well suited for this type of investigation since from the concentration dependence of ^1H chemical shifts the relevant thermodynamic parameters can be estimated,[66,55] while the relative spatial orientation of the complex cation within an aggregate in solution can be inferred.[36] This model system is representative of competing non-covalent cation-π interactions leading to self-association of the complex $[Pt^{II}(phen)(L^1\text{-}S,O)]^+$ cation on the one hand, and cation-π interactions between fluoranthene and the complex in solution, on the other.

4.2 Results and Discussion

4.2.1 ^{1}H NMR Concentration Dependence Study

Addition of small quantities of aromatic molecules such as fluoranthene ($C_{16}H_{10}$) to a solution of [Pt^{II}(phen)(L^1-*S,O*)]Cl in acetonitrile, leads to changes in the ^{1}H NMR spectrum of the complex (Figure 4.1), resulting in significant shielding of H^2 and H^9 protons of the [Pt^{II}(phen)(L^1-*S,O*)]$^+$ cation in proportion to the relative mole ratio of [Pt^{II}(phen)(L^1-*S,O*)]$^+$ to fluoranthene. Such behaviour suggests substantial non-covalent association between fluoranthene and the [Pt^{II}(phen)(L^1-*S,O*)]$^+$ complex, through cation-π interactions. Since only single resonances for all ^{1}H of the [Pt^{II}(phen)(L^1-*S,O*)]Cl complex are observed at these temperatures in solution, the system is in fast exchange in chemical shift as observed for the self-association of the [Pt^{II}(phen)(L^1-*S,O*)]$^+$.

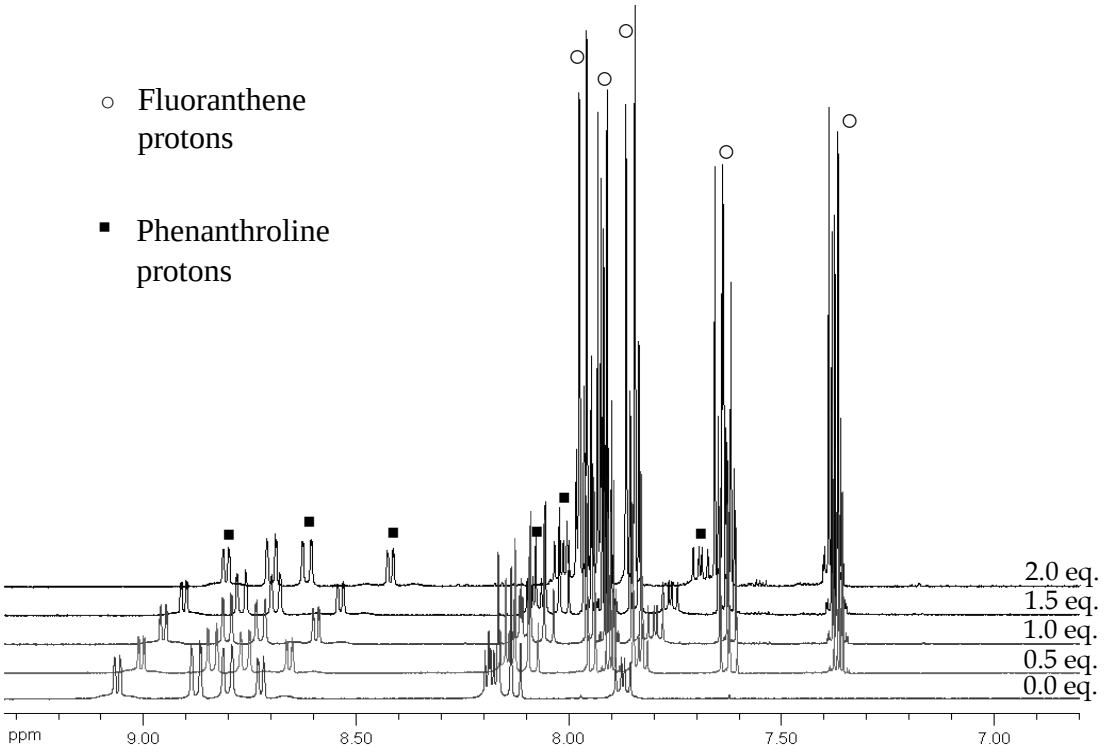

Figure 4.1. *^{1}H NMR spectra of a [Pt^{II}(phen)(L^1-S,O)]Cl (7.62 mM) and fluoranthene mixture in CD_3CN at 299.2K as a function of the molar equivalence of fluoranthene to [Pt^{II}(phen)(L^1-S,O)]Cl*

We have investigated this phenomenon quantitatively by means of the concentration dependence of the ^{1}H resonances (δ_{obs}) of the platinum complex as a function of added fluoranthene, with the view of estimating the association constants between the π-electron rich fluoranthene and the planar complex cation in acetonitrile.

With the addition of fluoranthene (F) to a solution of [Pt^{II}(phen)(L^1-*S,O*)]Cl in acetonitrile, the simplest additional reactions to aggregation of the complex cation (M), are the aggregation of fluoranthene itself to form at least a fluoranthene dimer (F_2) (equation 15) and outer-sphere complex formation between M and F, though cation-π interactions (equation 16).

$$2F \underset{}{\overset{K_A}{\rightleftharpoons}} F_2 \qquad (15)$$

$$M + F \underset{}{\overset{K_B}{\rightleftharpoons}} MF \qquad (16)$$

$$M + M \underset{}{\overset{K_D}{\rightleftharpoons}} M_2 \qquad (3)$$

To test if fluoranthene undergoes aggregation in acetonitrile (15), the ^{1}H chemical shift concentration dependence was studied in the temperature range 266 to 298 K. Changes in ^{1}H chemical shifts of fluoranthene were found to be very small (relative to the data in Figure 4.2) resulting in a total Δ 0.015 ppm over the range of 1.05 mM to 0.1 M fluoranthene. The relatively poor solubility of fluoranthene in acetonitrile prevented examination of higher concentrations, and hence precluded a reliable estimate of an aggregation (of at least dimer formation) constant from this data, so that we reasonably estimate a $K_A < 0.1$ M^{-1} at 266 K. Such a K_A value implies that the mole fraction of un-associated fluoranthene (α_F) is > 0.98 at the highest practical fluoranthene concentration of 0.1 M. Clearly any π-π stacking of fluoranthene in acetonitrile can be taken to be essentially negligible in a total concentration range up to 0.1 M fluoranthene achievable in acetonitrile-d_3.

Addition of increasing amounts of fluoranthene to an acetonitrile solution containing a constant amount of [Pt^{II}(phen)(L^{1}-*S*,*O*)]Cl (7.62 mM) caused a considerable change in the chemical shift of the H^{2} and H^{9} protons of 1,10-phenanthroline (Figure 4.2a).

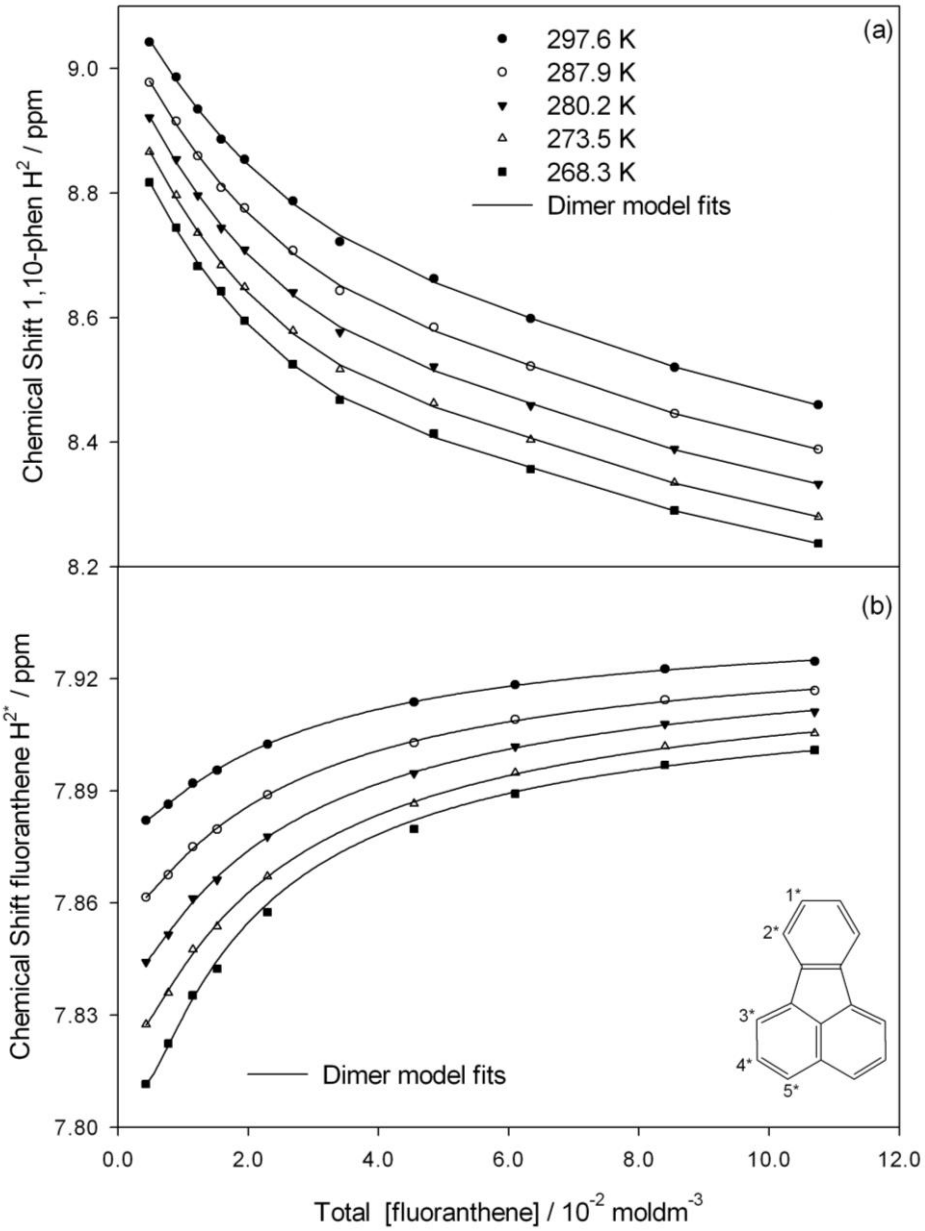

Figure 4.2: *Excellent agreement was obtained between the experimental (symbols) chemical shift dependence of* ***(a)*** *the 1,10-phenanthroline H^{2} proton and* ***(b)*** *the fluoranthene H^{2*} proton as a function of fluoranthene concentration and the self- and hereto association dimer model least-squares fits.*

To initially simplify matters, we assumed that only self- and hetero non-covalent dimer formation (relations 3 and 16) occur. Therefore, the δ_{obs} change of the H^2 and H^9 protons of 1,10-phenanthroline in the [Pt^{II}(phen)(L^1-*S,O*)]$^+$ complex as a function of increasing fluoranthene concentration can be expressed by equation 17, where M = [Pt^{II}(phen)(L^1-*S,O*)]$^+$ monomer, M_2 = [Pt^{II}(phen)(L^1-*S,O*)]$^+$ dimer and MF = [Pt^{II}(phen)(L^1-*S,O*)]$^+$/fluoranthene dimer.

$$C_{T(Pt)}\delta_{obs} = c_M\delta_M + 2c_{M2}\delta_{M2} + c_{MF}\delta_{MF} \qquad (17)$$

If the addition of fluoranthene only caused the dissociation of the [Pt^{II}(phen)(L^1-*S,O*)]$^+$ dimer in some manner and hence increased the [Pt^{II}(phen)(L^1-*S,O*)]$^+$ monomer concentration, c_M, the δ_{obs} change of the H^2 proton (Figure 4.2a) should undergo de-shielding. The data in Figure 4.2a clearly shows the converse, indicating significant [Pt^{II}(phen)(L^1-*S,O*)]$^+$/fluoranthene non-covalent aggregate formation (relation 16). Confirmation of [Pt^{II}(phen)(L^1-*S,O*)]$^+$ and fluoranthene non-covalent association can be obtained by analyzing the fluoranthene H^{2*} proton chemical shift data (Figure 4.2b).

The change in the δ_{obs} of the H^{2*} proton of fluoranthene as a function of increasing fluoranthene concentration may be expressed by equation 18, where F = fluoranthene and MF = [Pt^{II}(phen)(L^1-*S,O*)]$^+$/fluoranthene complex.

$$C_{T(F)}\delta_{obs} = c_F\delta_F + c_{MF}\delta_{MF} \qquad (18)$$

Increasing the concentration of fluoranthene leads to de-shielding of H^{2*} of fluoranthene after which the extent of de-shielding levels off (Figure 4.2b), in contrast to when no [Pt^{II}(phen)(L^1-*S,O*)]$^+$ is present in solution. The relative concentration ratio of MF to F determines if the δ_{obs} (equation 18) is relatively more shielded or de-shielded. The concentration ratio of MF to F is largest when the total fluoranthene concentration is lowest, so that as the total fluoranthene concentration increases, the concentration ratio decreases, resulting in the monomer term ($c_F\delta_F$) contributing relatively more to the δ_{obs} with each addition of fluoranthene so resulting in progressive de-shielding of the H^{2*}

proton (Figure 4.2b). The concentration dependence of the fluoranthene chemical shift data is thus consistent with [Pt^{II}(phen)(L^{1}-*S,O*)]$^{+}$/fluoranthene aggregation.

The least-squares fit of the self- and hetero-association model (relations 3 and 16) to the proton chemical shift data (Figures 4.2) at several temperatures are in excellent agreement with the experimental data. When fluoranthene self-association (relation 15) is included in the least-squares model fit the program Dynafit only converged with K_A values very close to zero confirming that the extent of possible fluoranthene dimerization is *negligible* compared to reactions 3 and 16 (Figure 4.3).

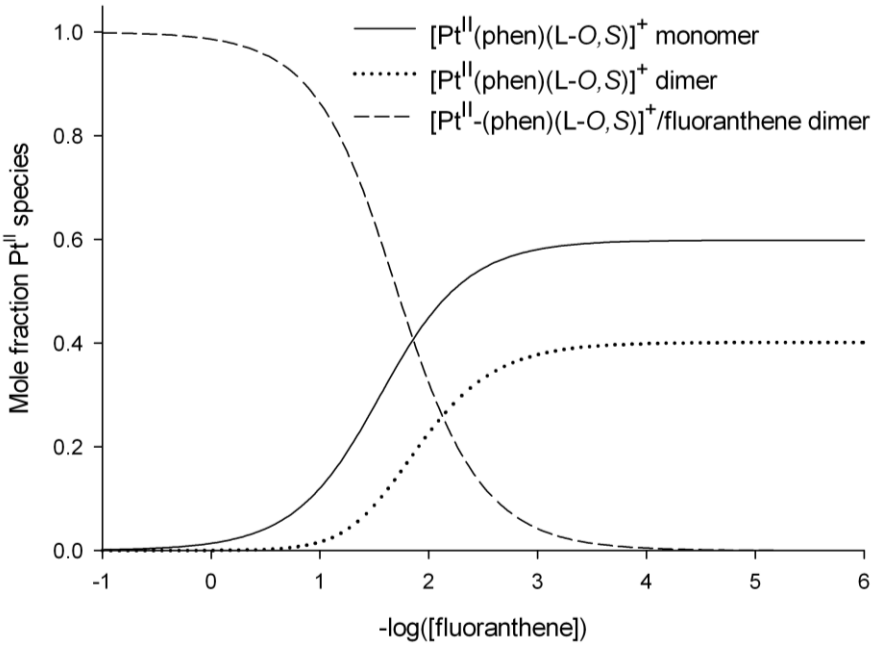

Figure 4.3: *Species distribution diagram when increasing amounts of fluoranthene is added to a [Pt^{II}(phen)(L^{1}-S,O)]$^{+}$ solution, with determined constants K_D and K_B of 56 (±13) M^{-1} and 72 (±7) M^{-1} respectively at 267.1 K. Fluoranthene π-π stacking is negligible in the concentration range below 0.1 M.*

Thermodynamic data for the self- and hetero-association model (relations 3 and 16) is obtained by the good fit with the Van't Hoff equation 13 (Figure 4.4), from which the standard reaction enthalpy and entropy of the [Pt^{II}(phen)(L^{1}-*S,O*)]$^{+}$/fluoranthene π-cation interaction was estimated (Table 4.1). The $\Delta_r S^o$ of relation M + F ⇌ MF (16) is negative, suggesting association between reactants. It is clear from the thermodynamic data (Table 4.1) that this hetero-association reaction is enthalpy driven, indicative of

cation-π binding.[21] The cation-π interaction is however crucial for these non-covalent complexes to form as demonstrated here that fluoranthene self-association is negligible under these reaction conditions.

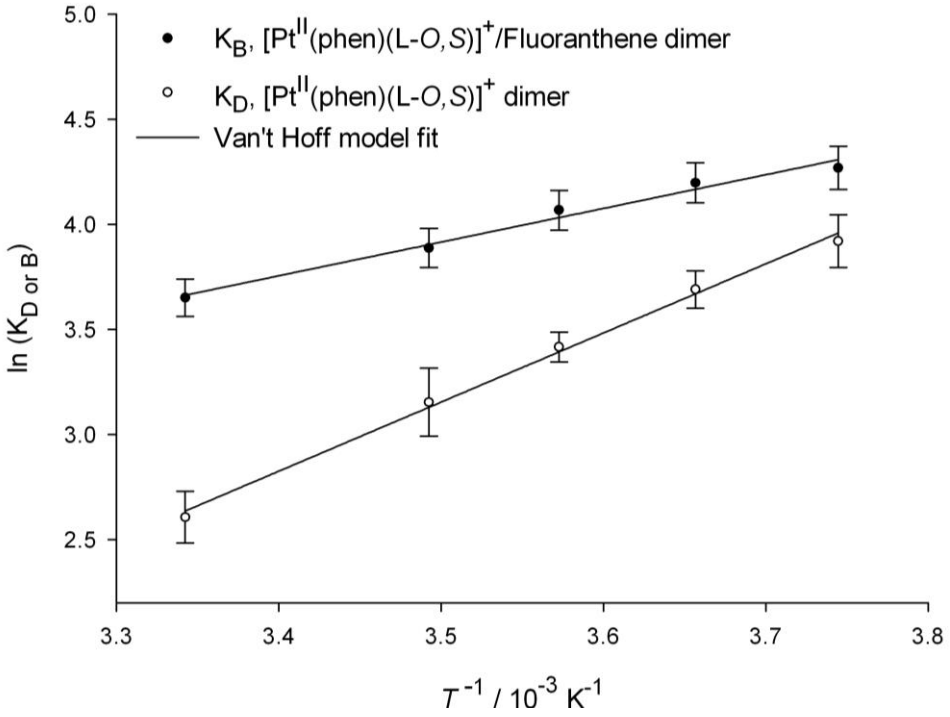

Figure 4.4: *The good linear fit obtained with the Van't Hoff equation is further validation for the other-sphere dimer formation of [Pt^{II}(phen)(L^{1}-S,O)]$^{+}$ and fluoranthene in CD$_3$CN. The 95% confidence interval of the slopes and intercepts for the [Pt^{II}(phen)(L^{1}-S,O)]$^{+}$ and [Pt^{II}(phen)(L^{1}-S,O)]$^{+}$/fluoranthene dimers equal 3087.1 (±374.2)x -7.5 (±1.3) and 1602.91 (±383.0)x -7.1 (±1.4)*

Table 4.1: *Calculated dimerization constants, K_B for [Pt^{II}(phen)(L^{1}-S,O)]$^{+}$/fluoranthene in CD$_3$CN and thermodynamic data.*

Temp / K	K_B / M^{-1}	Δ_rH^o / $Jmol^{-1}$	Δ_rS^o / $Jmol^{-1}$	Δ_rG^o / $Jmol^{-1}$
297.6	39 (± 4)	-13560 (± 3180)	-17 (± 11)	-9111
287.9	49 (± 5)			-9265
280.2	58 (± 6)			-9388
273.4	67 (± 7)			-9496
267.6	71 (± 7)			-9588

Overall our data indicates that only 1:1 {[Pt^{II}(phen)(L^1-*S,O*)]$^+$}$_2$ and [Pt^{II}(phen)(L^1-*S,O*)]$^+$/fluoranthene cation-π complexes are present in our solutions in the concentration range studied. The dimerization constant for the hetero-association of [Pt^{II}(phen)(L^1-*S,O*)]$^+$ and fluoranthene can in principle also be calculated from the ^{1}H fluoranthene chemical shift concentration dependence (see appendix A). However, the change in chemical shift is too small to calculate reliable association constants.

4.2.2 Proposed Non-covalent Hetero-dimer Structure in Solution

Remarkable ^{1}H chemical shift changes of the phenanthroline protons of the [Pt^{II}(phen)(L^1-*S,O*)]Cl complex with increasing amounts of fluoranthene were observed especially those of H^2 and H^9 (Figure 4.5a). Interestingly the aliphatic protons of the *N,N*-di(alkyl)-*N'*-acylthiourea ligand show almost no change in the chemical shift (Figure 4.5b). This can be rationalized by assuming that the fluoranthene molecule associates with [Pt^{II}(phen)(L^1-*S,O*)]$^+$ through π-π stacking with the 1,10-phenanthroline ligand as well as cation-π interaction with the platinum(II) metal centre.

The ^{1}H chemical shift trends in Figure 4.8a also show an interesting break at a concentration of ±0.03 M. The bottom range of 0.004 to 0.03 M fluoranthene added to the [Pt^{II}(phen)(L^1-*S,O*)]$^+$ complex solution exhibits more dramatic and different changes in chemical shift than the latter part. This can be ascribed to the two reactions of self-association of [Pt^{II}(phen)(L^1-*S,O*)]$^+$ and hetero-association between [Pt^{II}(phen)(L^1-*S,O*)]$^+$ and fluoranthene competing at lower fluoranthene concentrations. In the lower fluoranthene concentration range the self-association of [Pt^{II}(phen)(L^1-*S,O*)]$^+$ has a very significant effect on the chemical shift observed where the hetero-association is dominant for the latter part of higher fluoranthene concentration (>0.03 M) due to the large excess of fluoranthene in solution.

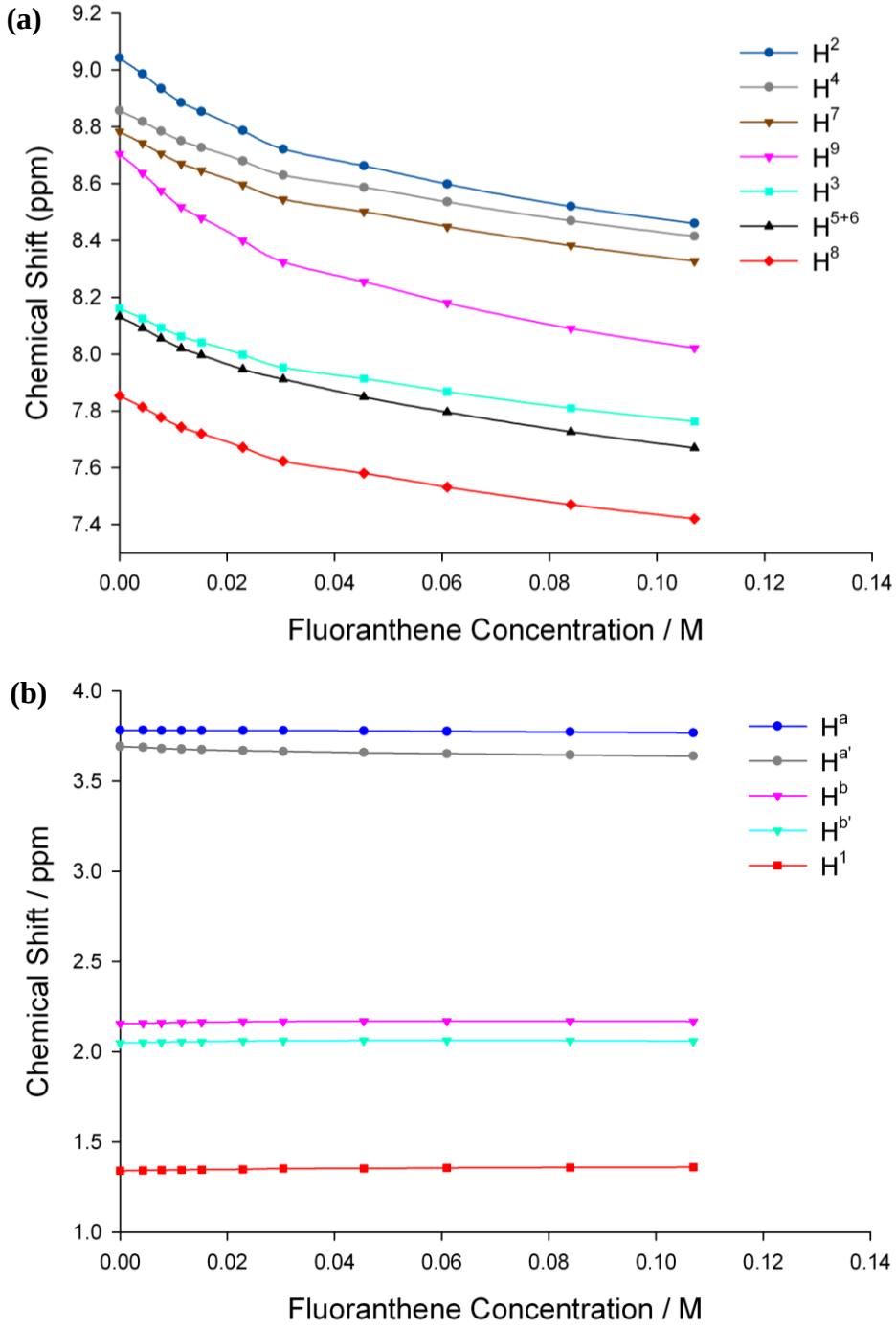

Figure 4.5: *Concentration dependence of the protons of [Pt^{II}(phen)(L^{1}-S,O)]Cl in CD_3CN at 299 K with increasing fluoranthene concentration, where* ***(a)*** *is the phenanthroline protons in the aromatic region and* ***(b)*** *the N,N-pyrolidyl-N'-^{t}butylthio-urea protons in the aliphatic region.*

These trends can be used to propose the average structure of the outer-sphere [Pt^{II}(phen)(L^{1}-*S,O*)]$^{+}$/fluoranthene hetero-dimer in solution.

The chemical shift trends observed as a result of the fluoranthene concentration dependence (Figure 4.5) suggests that the 1:1 cation-π complex has an average structure highlighted in Scheme 4.1 in which fluoranthene stacks *regiospecifically* in a coplanar manner to maximize π–σ attraction and minimize π-π repulsions in an offset stacking geometry, similar to that postulated for [Pt^{II}(phen)(L^{1}-*S,O*)]$^{+}$ dimer aggregate as shown in Scheme 2.5 (see page 59).

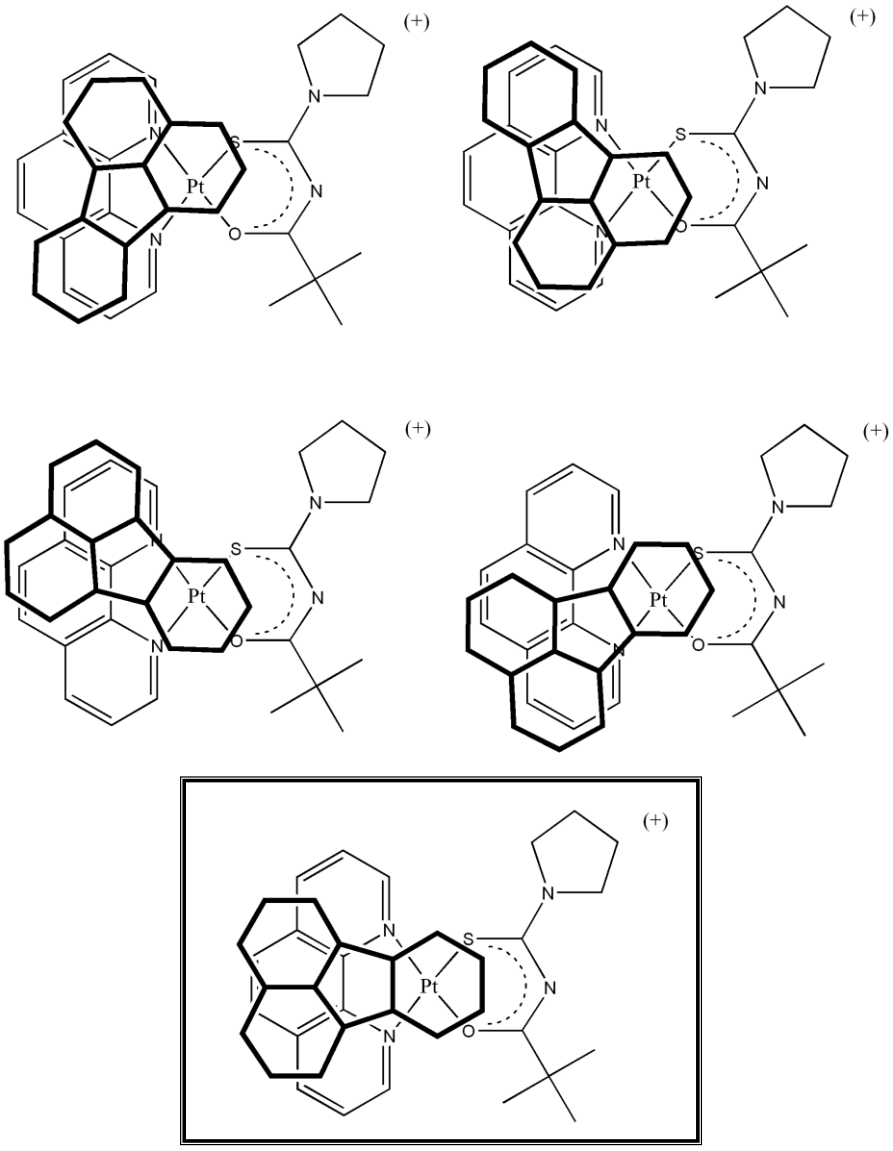

Scheme 4.1: *Proposed possible average [Pt^{II}(phen)(L^{1}-S,O)]$^{+}$/fluoranthene dimer aggregate structures in solution. The highlighted structure is used as the average structure of the [Pt^{II}(phen)(L^{1}-S,O)]$^{+}$/fluoranthene dimer aggregate.*

The association structures in Scheme 4.1 are consistent with literature where Kobayashi and co-workers used NMR and molecular orbital calculations to propose a fluoranthene/benzene noncovalent dimer structure (Figure 4.6a) in solution.[83] The benzene molecule associates with the naphthalene side of fluoranthene through π-π stacking interactions. In Scheme 4.1 we also propose π-π stacking between the phenanthroline ligand and the naphthalene side of the fluoranthene moiety.
Moreover Elschenbroich and co-workers used ^{1}H NMR, EPR and single crystal X-ray diffraction to characterize the Cr(fluoranthene)$_2$ complexes.[84]

(a)

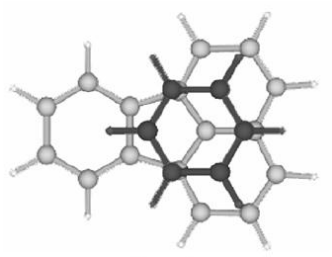

Top view

(b)

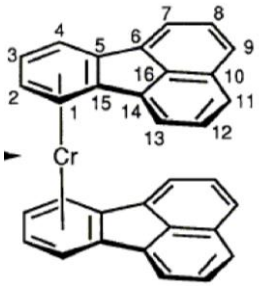

Figure 4.6: *Literature structures of two complexes with fluoranthene where* ***(a)*** *fluoranthene / benzene dimer*[83] *and* ***(b)*** *most stable Cr(fluoranthene)$_2$ isomer.* [84]

The most stable isomer of the coordination of the Cr(fluoranthene)$_2$ complex (Figure 4.6b) is where Cr coordinates to the benzene part of fluoranthene. This result is further indirect confirmation for our proposed structure for the [Pt^{II}(phen)(L^1-*S,O*)]$^+$/fluoranthene dimer with the platinum(II) metal centre associated with the benzene part of fluoranthene through cation-π interaction.

The spectrum of fluoranthene in chloroform[85] corresponds well with our spectrum obtained in acetonitrile-d_6 (Figure 4.7) and was consecutively used for the assignment of the fluoranthene specrtum in CD_3CN (Table 4.2).

Table 4.2: *^{1}H NMR chemical shifts of fluoranthene in CD_3CN compared to literature values recorded in $CDCl_3$.*

Assignment	δ_F (ppm) in CD_3CN	δ_F (ppm) in $CDCl_3$[85]	δ_F (ppm) in C_6D_6[84]	δ_{CrF_2} (ppm) in C_6D_6[84]
H^{3*}	8.07	7.93	7.73	4.86
H^{2*}	8.01	7.90	7.64	6.83
H^{5*}	7.94	7.83	7.61	7.35
H^{4*}	7.71	7.63	7.37	7.08
H^{1*}	7.43	7.38	7.24	4.45

Interestingly, the multiplicity of protons H^{1+4} and H^{2+3} is significantly different than expected. The signals of these protons are expected to be two sets of doublets due to the symmetry of the fluoranthene molecule. The unexpected coupling of these protons can be attributed to second order coupling. The energy transitions giving rise to second order coupling cannot be seen by inspection and can be calculated when the spin system of the moiety is known. This however is beyond the scope of this study.

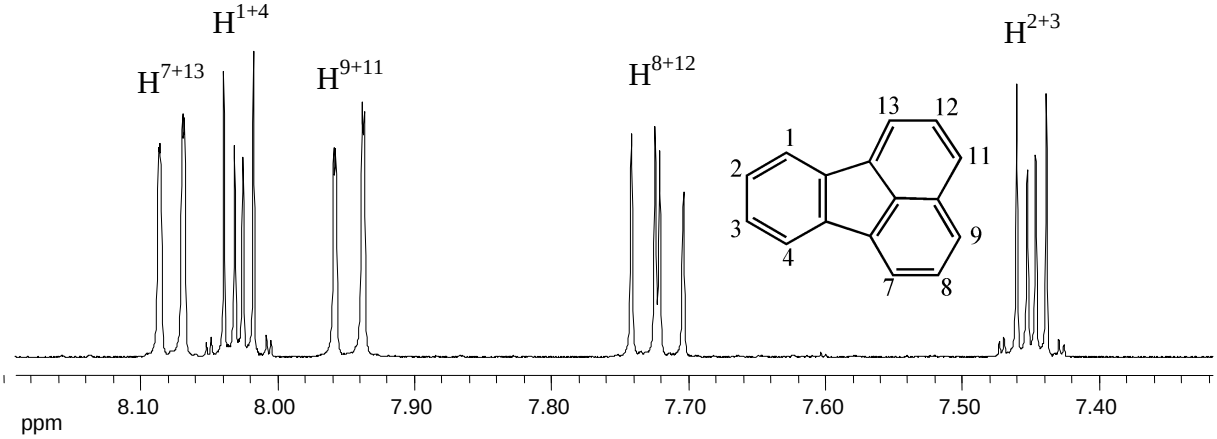

Figure 4.7: *^{1}H NMR spectrum and assignment of fluoranthene in CD_3CN at 25ºC*

4.2.3 Comparison of the Self- and Hetero-association of [Pt^{II}(phen)(L^1-*S,O*)]$^+$ and Fluoranthene in Acetonitrile

In the mixed solution of [Pt^{II}(phen)(L^1-*S,O*)]Cl and fluoranthene we have the two competing outer-sphere self- and hetero-association reactions expressed by equations 3 and 16:

$$M + M \overset{K_D}{\rightleftharpoons} M_2 \qquad (3)$$

$$M + F \overset{K_B}{\rightleftharpoons} MF \qquad (16)$$

The dimerization constants as well as the thermodynamic parameters of the two competing outer-sphere association reactions are summarized in Table 4.3.

Table 4.3: *Calculated dimerization constants, K_D and K_B and thermodynamic data for the self- and hetero-association of [Pt^{II}(phen)(L^1-S,O)]$^+$ and fluoranthene in CD_3CN.*

Temp / K	K / M^{-1}	$\Delta_r H^o$ / Jmol^{-1}	$\Delta_r S^o$ / Jmol^{-1}	$\Delta_r G^o$ / Jmol^{-1}
Self-association M + M ⇌ M_2 (3)				
299.2	17 (± 2)	-25129 (± 3112)	-61 (± 11)	-6998
Hetero-association M + F ⇌ MF (16)				
297.6	39 (± 4)	-13560 (± 3180)	-17 (± 11)	-9111

The proposed {[Pt^{II}(phen)(L^1-*S,O*)]$^+$}$_2$ and [Pt^{II}(phen)(L^1-*S,O*)]$^+$/fluoranthene dimer structures (Figure 4.2b) illustrate two major non-covalent interactions, π-π and cation-π interactions, of which the cation-π interaction is argued to be the more dominant interaction in these association reactions. The self-association of [Pt^{II}(phen)(L^1-*S,O*)]$^+$ consists of two centres of cation-π interactions balanced by the electrostatic repulsion of the charged molecules. The [Pt^{II}(phen)(L^1-*S,O*)]$^+$/fluoranthene dimer has only one cation-π interaction with extended π-π interactions (Scheme 4.2).

(a) 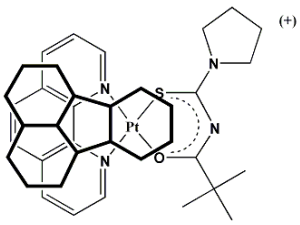 **(b)** 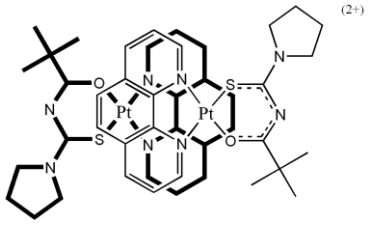

Scheme 4.2: *Proposed structures of the two competing outher-sphere dimers in solution where* ***(a)*** *is the [Pt^{II}(phen)(L^1-S,O)]$^+$ dimer and* ***(b)*** *[Pt^{II}(phen)(L^1-S,O)]$^+$/fluoranthene dimer.*

The thermodynamic parameters (Table 4.3) of the self- and hetero-association reactions 3 and 16, reveal that the [Pt^{II}(phen)(L^1-*S,O*)]$^+$/fluoranthene non-covalent complex has a larger dimerization constant, K_B, hence a larger standard reaction Gibbs energy ($\Delta_r G^o$). This may possibly be attributed to the charge repulsion present in the self-association interaction of [Pt^{II}(phen)(L^1-*S,O*)]$^+$ cations to form the doubly charged dimer that is absent for the [Pt^{II}(phen)(L^1-*S,O*)]$^+$/fluoranthene singly charged dimer aggregate. Both of the dimerization reactions exhibited negative reaction entropies ($\Delta S < 0$) as expected however, the entropy for the more favourable hetero-association is smaller compared to the self-association reaction (Table 4.3). Further studies are required to explain the entropy observed in detail however, it may be reasonable to think that the behaviour of counter ions and solvation of the monomers and aggregates would be significantly different in the two systems. Interestingly the enthalpy for the self-association reaction M + M $\rightleftharpoons$ M_2 is almost double that of the hetero-association M + F $\rightleftharpoons$ MF and one is tempted to think that this is due to the two centres of cation-π interactions in the [Pt^{II}(phen)(L^1-*S,O*)]$^+$ dimer counterbalanced by the equal charge repulsion compared to only one centre of cation-π interaction in the [Pt^{II}(phen)(L^1-*S,O*)]$^+$/fluoranthene dimer. However, this discussion of the thermodynamics of these systems is speculative and more information on the systems is necessary to explain the thermodynamic data in detail.

Chapter 5

Conclusions

Chapter 5

Conclusions

5.1 Conclusions

A series of [Pt^{II}(phen)(L^n-*S,O*)]Cl complexes (where phen is 1,10-phenanthroline and HL-*S,O* represents various chelating *N*-acyl-*N,N'*-dialkylthioureas) was successfully synthesized and characterized. From this series of complexes the Pt^{II}(1,10-phenanthroline)(*N*-pyrrolidyl-*N*-(2,2-dimethyl-propanoyl)thiourea)]Cl ([Pt^{II}(phen)(L^1-*S,O*)]Cl) complex was identified to be the most soluble in water as well as stable in dimethylsulphoxide solutions. [Pt^{II}(phen)(L^1-*S,O*)]Cl was consecutively used for the development of a viable system for studying the intermolecular associations of these complexes in solution. High resolution ^{1}H NMR as well as Diffusion Ordered Spectroscopy (DOSY NMR) were found to be particularly well suited for this type of investigation. ESI(+) mass spectra of [Pt^{II}(phen)(L^1-*S,O*)]Cl in acetonitrile revealed the existence of monomeric and dimeric species. ^{1}H NMR studies on [Pt^{II}(phen)(L^1-*S,O*)]Cl indicate that the complex forms regiospecific dimers in acetonitrile solutions which are in fast exchange in chemical shift. The chemical shift temperature dependence established that the dimerization reaction is enthalpy driven while the excellent linear Van't Hoff plot confirmed the dimerization model proposed.

The DOSY spectroscopy study also showed the existence of dimer aggregates in acetonitrile and is a method independent of the proton used for the determination of the association constants since all the protons of the same moiety exhibit the same diffusion coefficient. The ^{1}H NMR chemical shift and DOSY diffusion coefficient dependence data for [Pt^{II}(phen)(L^1-*S,O*)]$^+$ validates its self-association into a [Pt^{II}(phen)(L^1-*S,O*)]$^+$ dimer in acetonitrile solutions resulting in a K_D of 17 ± 2 M^{-1} at 299.2K.

The effect of D_2O on the extent of self-association of [Pt^{II}(phen)(L^1-*S,O*)]$^+$ was investigated by gradually changing the ratio of D_2O to CD_3CN in a mixed solvent

system. A broadening of the ^{1}H resonance signals was observed for increasing D_2O percentages, concentration and temperature suggesting an increase in the extent of dimer formation/aggregation. The dimer model accounted for the experimental data exceptionally well in 0 - 30% (v/v) D_2O:CD_3CN with the dimerization constants, K_D, calculated at 299.2K increasing from 17 M^{-1} to 71 M^{-1}. The increase in dimerization constants was attributed to the water molecules 'stabilizing' the doubly charged dimer to a greater extent due to a higher polarity compared to acetonitrile. A decrease in the magnitude of the reaction entropy was observed for increasing percentages of D_2O. The positive contribution to the overall negative reaction entropy was ascribed to the 'release' of solvent molecules upon dimer formation since fewer molecules are needed to solvate the dimer aggregate.

The ^{1}H concentration dependence of $[Pt^{II}(phen)(L^1\text{-}S,O)]Cl$ at higher percentages [D_2O:CD_3CN (50 – 100% v/v)] resulted in excellent trends in the experimental data. However, at higher percentages [D_2O:CD_3CN (50 - 100%)] the dimerization model does not fit the data, suggesting that higher order aggregation takes place; models which invoke trimers, tetramers etc. and combinations thereof were attempted without success. Possible micelle or super-sized aggregate formation in these solutions is suggested by the transmission electron microscopy images obtained for these solutions which will be further investigated in the future.

The ^{1}H NMR chemical shift dependence data of $[Pt^{II}(phen)(L^1\text{-}S,O)]^+$ on fluoranthene concentration validates the hetero-association of $[Pt^{II}(phen)(L^1\text{-}S,O)]^+$ and fluoranthene in acetonitrile solutions. Moreover $[Pt^{II}(phen)(L^1\text{-}S,O)]^+$ and fluoranthene form a 1:1 π-cation complex with an association constant, K_B (71 ± 8 M^{-1}) larger than the K_D (56 ± 8 M^{-1}) obtained for the self-association of $[Pt^{II}(phen)(L^1\text{-}S,O)]^+$ into a dimer at 267 K. Higher order aggregates and ion-pairing were found to be negligible on the basis of the excellent least-squares fit of the dimer model to the ^{1}H NMR data and resulting linear Van't Hoff plots. The thermodynamic parameters calculated in this work indicate that π-cation interactions between cationic $[Pt^{II}(phen)(L^1\text{-}S,O)]^+$ and uncharged aromatic molecules, such as fluoranthene studied here (Δ_rG^o ~ 9.6 $kJmol^{-1}$), are more favourable than self-association of the $[Pt^{II}(phen)(L^1\text{-}S,O)]^+$ (Δ_rG^o ~ 8.9 $kJmol^{-1}$), compared to

negligible π-π stacking of fluoranthene in acetonitrile. The data is consistent with essentially coplanar 1:1 aggregate strucrures in solution, resulting from regiospecific stacking interactions. This model system is representative of competing non-covalent π-cation interactions leading to self-association of the complex $[Pt^{II}(phen)(L^1\text{-}S,O)]^+$ cation on the one hand, and π-cation interactions between the complex $[Pt^{II}(phen)(L^1\text{-}S,O)]^+$ cation and fluoranthene solution, on the other.

In this study it was found that $[Pt^{II}(phen)(L^1\text{-}S,O)]^+$ self-associates as well as hetero-associate with aromatic molecules such as fluoranthene. Moreover, it is reasonable to argue that these complexes will associate with haematin in solution and future studies are aimed at studying the association behaviour of these complexes with haematin derivatives like metal porpyrins. We are currently investigating these phenomena with various model systems in water/acetonitrile mixtures as a step towards understanding the mechanism of anti-malarial activity of the class of $[Pt^{II}(diimine)(L^n\text{-}S,O)]^+$ complexes.

References

References

1. J. Reedijk, *Macromolecular Symposia*, 2008, **270**, 193-201.
2. C. G. Hartinger, A. A. Nazarov, S. M. Ashraf, P. J. Dyson, B. K. Keppler, *Current Medicinal Chemistry*, 2008, **15**, 2574-2591.
3. L. Nagy, G. Csinatan, E. Kalman, E. Nagy, P. Sipos, *Acta Pharmaceutica Hungarica*, 2004, **74**, 213-222.
4. K. H. Thompson, C. Orvig, *Science*, 2003, **300**, 936–939.
5. S. J. Lippard, *Nature Chemical Biology*, 2006, **2**, 504–507.
6. B. Rosenberg, L. Van Camp, T. Krigas, *Nature*, 1965, **205**, 698-699.
7. D. Lebwohl, R. Canetta, *European Journal of Cancer*, 1998, **34**, 1522-1534.
8. T. W. Hambley, *Coordination Chemistry Reviews*, 1997, **166**, 181-223.
9. M. J. Cleare, J. D. Hoeschele, *Platinum Metals Review*, 1973, **17**, 2-13.
10. M. J. Cleare, J. D. Hoeschele, *Bioinorganic Chemistry*, 1973, **2**, 187-210.
11. N. J. Wheate, R. I. Taleb, A. M. Krause-Heuer, R. L. Cook, S. Wang, V. J. Higgins, J. R. Aldrich-Wright, *Dalton Transactions*, 2007, **43**, 5055–5064
12. S. Kemp, N. J. Wheate, M. J. Pisani, J. R. Aldrich-Wright, *Journal of Medicinal Chemistry*, 2008, **51**, 2787–2794
13. S. Kemp, N. J. Wheate, D. P. Buck, M. Nikac, J. G. Collins, J. R. Aldrich-Wright, *Journal of Inorganic Biochemistry*, 2007, **101**, 1049–1058
14. N. J. Wheate, P. G. Anil Kumar, A. M. Torres, J. R. Aldrich-Wright, W. S. Price, *Jornal of Physical Chemistry B*, 2008**, 112**, 2311-2314
15. A. M. Krause-Heuer, N. J. Wheate, M. J. Tilby, D. G. Pearson, C. J. Ottley, J. R. Aldrich-Wright, *Inorganic Chemistry*, 2008, **47**, 6880-6888
16. W Lu, D. A. Vicic, J. K. Barton, *Inorganic Chemistry*, 2005, **44**, 7970-7980.
17. M. Cusumano, M. L. Di Pietro, A. Giannetto, *Inorganic Chemistry*, 2006, **45**, 230-235.
18. T. J. Egan, K. R. Koch, P. L. Swan, C. Clarkson, D. A. Van Schalkwyk, P. J. Smith, *Journal of Medicinal Chemistry*, 2004, **47**, 2926–2934.
19. Y. S. Wu, K. R. Koch, V. R. Abratt, H. H. Klump, *Archives of Biochemistry and Biophysics*, 2005, **440**, 28–37.
20. D. A. Dougherty, *Science*, 1996, **271**, 163-168.

21. D. Cuc, D. Canet, J. P. Morel, N. Morel-Desrosiers, P. Mutzenhardt, *ChemPhysChem*, 2007, **8**, 643-645.
22. http://encarta.msn.com/media_461541582/life_cycle_of_the_malaria_parasite.html
23. T. J. Egan, T*rends in Parasitology*, 2006, **22**, 235-237.
24. T. J. Egan, *Drug Design Reviews Online*, 2004, **1**, 93-110.
25. D. J. Sullivan, I. Y. Gluzman, D. G. Russell, G. David, D. E. Goldberg, *Proceedings of the National Academy of Sciences of the U.S.A*, 1996, **93**, 11865-11870.
26. D. A. Fidock, T. Nomura, A. K. Talley, R. A. Cooper, S. M. Dzekunov, M. T. Ferdig, L. M. B. Ursos, A. B. S. Sidhu, B. Naude, K. W. Deitsch, Molecular Cell, 2000, **6**, 861-871.
27. R. A. Cooper, M. T. Ferdig, X. Su, L. M. B. Ursos, J. Mu, T. Nomura, H. Fujioka, D. A. Fidock, P. D. Roepe, T. E. Wellems, *Molecular Pharmacology*, 2002, **61**, 35-42.
28. K. Mueller-Dethlefs, P. Hobza, *Chemical Reviews*, 2000, **100**, 143-167.
29. R. J. Warr, A. N. Westra, K. J. Bell, J. Chartres, R. Ellis, C. Tong, T. G. Simmance, A. Gadzhieva, A. J. Blake, P. A. Tasker, *Chemistry A European Journal*, 2009, **15**, 4836-4850
30. T. Steiner, *Angewandte Chemie International Edition*, 2002, **41**, 48-76.
31. http://www.chemicool.com/definition/ion_pair.html
32. http://goldbook.iupac.org/I03231.html
33. A. Bakker, S. Gejji, J. Lindgren, K. Hermansson, M. M. Probst, *Polymer*, 1995, **36**, 4371-4378.
34. K. Miyoshi, *Bullitin.of the Chemical Society of Japan,* 1973, **46**, 426-430.
35. Sari Kiviniemi, PhD Thesis, *University of Oulu*, 2001.
36. K. R. Koch, C. Sacht, C. Lawrence, *Dalton Transactions*, **4**, 1998, 689-695.
37. P. J. Gallivan, D. A. Dougherty, *Proceedings of the National Academy of Sciences U.S.A.* 1999, **96**, 9459-9464
38. G. Gil-Ramirez, E. C. Escudero-Adan, J. Benet-Buchholz, P. Ballester, *Angewandte Chemie International Edition*, 2008, **47**, 4114-4118.
39. P. Ballester, *Structure and Bonding*, 2008, **129**, 127-174.

40. C. A. Hunter and J. K. M. Sanders, *Journal of the American Chemical Society*, 1990, **112**, 5525-5534.
41. S. K. Burley, G. A. Petsko, *Science*, 1985, **229**, 23-28.
42. C. A. Hunter, J. Singh, J. M. Thornton, *Journal of Molecular Biology*, 1991, **218**, 837.
43. L. S. Lerman, *Journal of Molecular Biology*, 1961, **3**, 18.
44. G. T. Morgan, F. H. Burstall, *Journal of the Chemical Society*, 1934, 965.
45. I. B. Douglass, F. B. Dains, *Journal of the American Chemical Society*, 1934, **56**, 719-21.
46. W. Hernandez, E. Spodine, R. Richter, K-H Hallmeier, U. Schröder, L. Beyer, *Zeitschrift für anorganische und allgemeine Chemie*, 2003, **629**, 2559-2565.
47. T. Brand, E. J. Cabrita, S. Berger, *Progress in Nuclear Magnetic Resonance Spectroscopy*, 2005, **46**, 159–196.
48. J. E. Huheey, E. A. Keiter, R. L. Keiter, *Inorganic Chemistry-Principals of Structure and Reactivity 4th Edition*, HarperCollins, New York, 2003, **4**, 344-348.
49. J. Y. Lallemand, J. Soulie, J. C. Chottard, *Chemical Communication*, 1980, **10**, 436-438.
50. S. J. Wilkens, W. M. Westler, J. L. Markley, F. Weinhold, *Journal of the American Chemical Society*, 2001, **123**, 12026-36.
51. M. S. Kaucher, Y-F Lam, S Pieraccini, G. Gottarelli, J. T. Davis, *Chemistry a European Journal*, 2005, **11**, 164 – 173.
52. P. Agrawal, S. K. Barthwal, R. Barthwal, *European Journal of Medicinal Chemistry*, 2009, **44**, 1437–1451.
53. T. D. W. Claridge, *High-Resolution NMR Techniques in Organic Chemistry - Tetrahedron Organic Chemistry Series*, Pergamon, Oxford, **19**, 1999.
54. M. Meloun, J. Havel, E. Högfeldt, *Computation of Solution Equilibria - A Guide to Methods in Potentiometry, Extraction, and Spectrophotometry*, Ellis Horwood, Chichester, 1987.
55. I. Horman, B. Dreux, *Helvetica Chimica Acta*, 1984, **67**, 754-764.
56. P. Kuzmic, *Analytical Biochemistry*, 1996, **237**, 260-273.

57. C. R. Brodie, J. G. Collins and J. R. Aldrich-Wright, *Dalton Transactions*, 2004, **8**, 1145-1152.
58. T. Brand, E. J. Cabrita and S. Berger, *Progress in Nuclear Magnetic Resonance Spectroscopy*, 2005, **46**, 159-196.
59. A. S. Reddy, H. Zipse and G. N. Sastry, *Journal of Physical Chemistry B*, 2007, **111**, 11546-11553.
60. J. C. Ma, D. A. Dougherty, *Chemical Reviews*, 1997, **97**, 1303-1324.
61. J. Sunner, K. Nishizawa and P. Kebarle, *Journal of Physical Chemistry*, 1981, **85**, 1814-1820.
62. H. J. Schneider, *Angewandte Chemie*, 1991, **103**, 1419-1439
63. N. Zacharias and D. A. Dougherty, *Trends in Pharmacological Sciences*, 2002, **23**, 281-287.
64. H. H. Klump, K. Koch and C. T. Lin, *South African Journal of Science*, 2006, **102**, 264-266.
65. J. J. Rebek, *Angewandte Chemie*, 1990, **29**, 245-255.
66. A. Macchioni, A. Romani, C. Zuccaccia, G. Guglielmetti and C. Querci, *Organometallics*, 2003, **22**, 1526-1533.
67. L. Fielding, *Tetrahedron*, 2000, **56**, 6151-6170.
68. P. S. Pregosin, *Progress in Nuclear Magnetic Resonance Spectroscopy*, 2006, **49**, 261-288.
69. F. Song, S. J. Lancaster, R. D. Cannon, M. Schormann, S. M. Humphrey, C. Zuccaccia, A. Macchioni, M. Bochmann, *Organometallics*, 2005, **24**, 1315-1328.
70. Ch. Wohlfarth, *Landolt-Börnstein - Group IV Physical Chemistry*, Springer, Berlin Heidelberg, **17**, 2008, 117-121.
71. X.-M. Lu, W.-G. Xu, X.-H. Chang, D.-Z. Lu and J.-Z. Yang, *Journal of Chemical Thermodynamics*, 2006, **38**, 5-9.
72. C. S. Johnson, *Progress in Nuclear Magnetic Resonance Spectroscopy*, 1999, **34**, 203-256.
73. H. Kato, T. Saito, M. Nabeshima, K. Shimada, S. Kinugasa, *Journal of Magnetic Resonance*, 2006, **180**, 266-273.
74. http://www.silver-colloids.com/Papers/hydrodynamic-radius.pdf

75. www.eng.uc.edu/~gbeaucag/Classes/properties/HydrodyamicRadius.pdf
76. A. N. Mautjana, J. D. S. Miller, A. Gie, S. A. Bourne and K. R. Koch, *Dalton Transactions*, **10**, 2003, 1952-1960.
77. M. Kato and J. Takahashi, *Acta Crystallographica, Section C: Crystal Structure Communications*, 1999, **C55**, 1809-1812.
78. O. Schramel, B. Michalke, A. Kettrup, *Fresenius Journal of Analytical Chemistry*, 1999, **363**, 452–455
79. M. Chou, C. Creutz, D. Mahajan, N. Sutin, A. P. Zipp, *Inorganic Chemistry*, 1982, **21**, 3989.
80. K. R. Mann, N. S. Lewis, R. M. Williams, H. B. Gray, J. G. Gordon, *Inorganic Chemistry*, 1978, **17**, 828.
81. Yu-Shan Wu, PhD Thesis, *University of Cape Town*, 2002.
82. www.chemistry-dictionary.com/definition/hydrophobicity.php
83. S. Enomoto, K. Kumagai, T. Tamura, M. Hasegawa, K. Nakada, T. Hoshi, M. Kobayashi, *Monatshefte fuer Chemie*, 2004, **135**, 471-481.
84. C. Elschenbroich, R. Moeckel, A. Vasil'kov, B. Metz, K. Harms, *European*
85. K. K. Laali, T. Okazaki, S. E. Galembeck, *Journal of the Chemical Society, Perkin Transactions*, 2002, **2**, 621-629.

Appendix A

^{1}H NMR data and calculated dimerization constants

Appendix B

Infrared Spectra

Appendix C

Publication (From this work)

Appendix A

^{1}H NMR data and calculated dimerization constants

Table A1: *Chemical shift data of the aromatic protons of* $[Pt^{II}(phen)(L^{1}\text{-}S,O)]^{+}$ *in acetonitrile at various temperatures from 267-299K.*

Temp. / K	Conc. / M	H^{2}	H^{9}	H^{4}	H^{7}	H^{3}	H^{5+6}	H^{8}
299.2	0.010255	9.005	8.661	8.848	8.774	8.147	8.122	7.838
286.3		8.919	8.549	8.813	8.738	8.113	8.087	7.788
279.9		8.872	8.487	8.802	8.725	8.097	8.076	7.763
273.5		8.830	8.426	8.782	8.703	8.077	8.057	7.735
267.1		8.783	8.360	8.765	8.684	8.059	8.040	7.704
299.2	0.008546	9.040	8.704	8.858	8.784	8.162	8.132	7.854
286.3		8.961	8.602	8.826	8.751	8.129	8.101	7.810
279.9		8.914	8.540	8.810	8.734	8.110	8.085	7.783
273.5		8.866	8.474	8.793	8.716	8.090	8.069	7.755
267.1		8.817	8.406	8.776	8.697	8.072	8.053	7.724
299.2	0.006837	9.081	8.754	8.871	8.797	8.176	8.146	7.873
286.3		9.000	8.651	8.839	8.764	8.144	8.116	7.829
279.9		8.959	8.598	8.825	8.750	8.128	8.103	7.807
273.5		8.914	8.539	8.810	8.734	8.111	8.088	7.782
267.1		8.867	8.476	8.794	8.717	8.093	8.073	7.755
299.2	0.005128	9.127	8.809	8.885	8.810	8.193	8.161	7.884
286.3		9.061	8.728	8.860	8.786	8.168	8.138	7.860
279.9		9.020	8.678	8.846	8.773	8.153	8.125	7.840
273.5		8.978	8.625	8.829	8.759	8.137	8.113	7.818
267.1		8.936	8.568	8.818	8.744	8.120	8.100	7.795
299.2	0.003077	9.191	8.885	8.904	8.829	8.216	8.182	7.921
286.3		9.137	8.822	8.885	8.810	8.197	8.164	7.896
279.9		9.103	8.780	8.874	8.800	8.185	8.154	8.880
273.5		9.068	8.737	8.862	8.789	8.172	8.143	7.863
267.1		9.029	8.689	8.849	8.776	8.158	8.132	7.843
299.2	0.002051	9.228	8.927	8.915	8.840	8.230	8.193	7.937
286.3		9.184	8.900	8.877	8.826	8.214	8.179	7.917
279.9		9.155	8.843	8.891	8.817	8.204	8.171	7.904
273.5		9.124	8.805	8.881	8.807	8.193	8.162	7.889
267.1		9.087	8.761	8.870	8.796	8.185	8.152	7.872
299.2	0.001043	9.267	8.972	8.928	8.851	8.244	8.205	7.953
286.3		9.239	8.940	8.919	8.843	8.235	8.197	7.941
279.9		9.217	8.915	8.912	8.838	8.228	8.192	7.932
273.5		9.199	8.895	8.906	8.832	8.222	8.186	7.924
267.1		9.175	8.866	8.899	8.825	8.213	8.180	7.913

299.2	0.000342	9.294	9.003	8.936	8.859	8.254	8.213	7.964
286.3		9.279	8.987	8.933	8.856	8.250	8.210	7.959
279.9		9.270	8.976	8.930	8.854	8.248	8.208	7.955
273.5		9.259	8.964	8.928	8.852	8.244	8.206	7.950
267.1		9.246	8.950	8.924	8.849	8.240	8.203	7.945

Table A2: *Chemical shift data of the aliphatic protons of $[Pt^{II}(phen)(L\text{-}S,O)]^+$ in acetonitrile at varied temperatures from 267-299K.*

Temp. / K	**Conc. / M**	**H^a**	**$H^{a'}$**	**H^b**	**$H^{b'}$**	**H^1**
299.2	0.010255	3.779	3.679	2.158	2.052	1.335
286.3		3.761	3.625	2.155	2.048	1.315
279.9		3.752	3.597	2.154	2.048	1.305
273.5		3.741	3.567	2.151	2.045	1.295
267.1		3.730	3.534	2.149	2.045	1.285
299.2	0.008546	3.783	3.693	2.156	2.049	1.339
286.3		3.766	3.645	2.153	2.046	1.321
279.9		3.756	3.615	2.152	2.045	1.311
273.5		3.745	3.584	2.150	2.043	1.300
267.1		3.735	3.550	2.148	2.042	1.289
299.2	0.006837	3.787	3.710	2.153	2.047	1.345
286.3		3.769	3.661	2.150	2.043	1.326
279.9		3.761	3.636	2.150	2.043	1.317
273.5		3.752	3.608	2.149	2.041	1.308
267.1		3.742	3.577	2.147	2.040	1.298
299.2	0.005128	3.791	3.728	2.149	2.043	1.351
286.3		3.777	3.689	2.147	2.040	1.336
279.9		3.769	3.665	2.146	2.039	1.327
273.5		3.761	3.640	2.146	2.038	1.077
267.1		3.752	3.613	2.145	2.038	1.309
299.2	0.003077	3.796	3.752	2.143	2.037	1.360
286.3		3.784	3.721	2.140	2.034	1.346
279.9		3.777	3.701	2.140	2.033	1.338
273.5		3.770	3.680	2.139	2.032	1.330
267.1		3.763	3.657	2.139	2.031	1.322
299.2	0.002051	3.798	3.766	2.139	2.034	1.364
286.3		3.787	3.739	2.135	2.029	1.352
279.9		3.780	3.722	2.134	2.027	1.345
273.5		3.774	3.703	2.133	2.026	1.337

267.1		3.767	3.682	2.133	2.025	1.329
299.2	0.001043	3.800	3.780	2.135	2.030	1.369
286.3		3.791	3.760	2.130	2.024	1.359
279.9		3.785	3.747	2.128	2.021	1.353
273.5		3.781	3.735	2.126	2.019	1.347
267.1		3.775	3.721	2.125	2.018	1.341
299.2	0.000342	3.802	3.790	2.132	2.027	1.373
286.3		3.793	3.775	2.125	2.019	1.364
279.9		3.788	3.767	2.122	2.016	1.359
273.5		3.784	3.758	2.119	2.013	1.355
267.1		3.779	3.748	2.116	2.009	1.350

Table A3: *Calculated dimerization constants, K_D from H^2 and H^9 for $[Pt^{II}(phen)(L\text{-}O,S)]^+$ in CD_3CN and thermodynamic data.*

Temp / K	K_D / M^{-1}	Δ_rH^o / $Jmol^{-1}$	Δ_rS^o / $Jmol^{-1}$	Δ_rG^o / $Jmol^{-1}$
Proton H^2				
299.2	17 (± 2)	-25129 (± 3112)	-61 (± 11)	-6998
286.3	27 (± 5)			-7777
279.9	29 (± 3)			-8167
273.5	46 (± 7)			-8556
267.1	56 (± 8)			-8946
Proton H^9				
299.2	13 (± 1)	24983 (± 3056)	-62 (± 11)	-6479
286.3	23 (± 4)			-7274
279.9	25 (± 3)			-7672
273.5	37 (± 5)			-8069
267.1	44 (± 7)			-8467

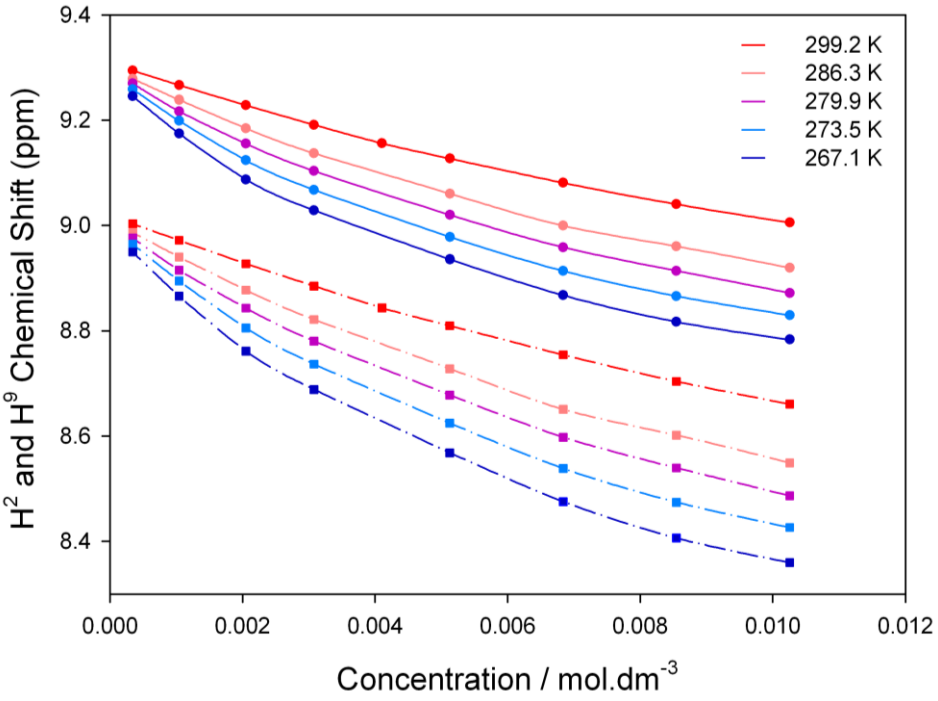

Figure A1: *Concentration dependence of H^2 (solid line) and H^9 (dashed line) of $[Pt^{II}(phen)(L^1\text{-}S,O)]^+$ in acetonitrile at varied temperatures from 267-299K.*

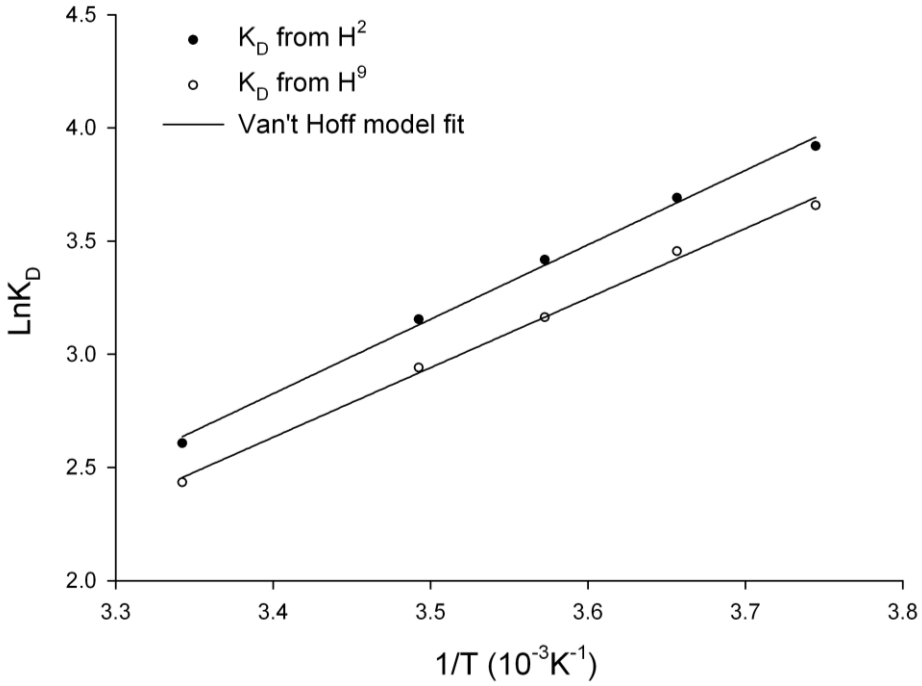

Figure A2: *Van't Hoff plot of H^2 and H^9 of $[Pt^{II}(phen)(L\text{-}S,O)]^+$ in acetonitrile.*

Table A4: *Calculated dimerization constants, K_D from all $[Pt^{II}(phen)(L^1\text{-}O,S)]^+$ protons in CD_3CN at 299K.*

Assignment	K_D / M^{-1}	error	Assignment	K_D / M^{-1}	error
H2	17	2	Ha	0.00	-
H9	13	1	Ha'	0.01	-
H4	19	3	Hb	0.03	-
H7	16	2	Hb'	0.03	-
H3	16	2	H1	0.01	-
H5+6	15	1	Average	0	-
H8	18	3			
Average	16	2			

Table A5: *Chemical shift data of the aromatic protons of $[Pt^{II}(phen)(L^1\text{-}S,O)]^+$ in acetonitrile at 299K with increasing fluoranthene concentration.*

Conc. / M	**H^2**	**H^9**	**H^4**	**H^7**	**H^3**	**H^{5+6}**	**H^8**
0.00000	9.042	8.858	8.783	8.705	8.161	8.132	7.854
0.00429	8.986	8.819	8.742	8.637	8.125	8.092	7.813
0.00773	8.935	8.785	8.706	8.576	8.094	8.055	7.777
0.01148	8.886	8.751	8.671	8.518	8.063	8.020	7.743
0.01523	8.854	8.728	8.647	8.480	8.042	7.996	7.720
0.02296	8.787	8.680	8.597	8.400	7.998	7.946	7.672
0.03046	8.722	8.630	8.545	8.324	7.953	7.912	7.623
0.04547	8.663	8.587	8.501	8.255	7.914	7.849	7.581
0.06099	8.599	8.536	8.449	8.180	7.868	7.796	7.532
0.08399	8.520	8.470	8.382	8.090	7.810	7.727	7.470
0.10700	8.460	8.415	8.328	8.021	7.763	7.670	7.421

Table A6: *Chemical shift data of the aliphatic protons of $[Pt^{II}(phen)(L\text{-}S,O)]^+$ in acetonitrile at 299K with increasing fluoranthene concentration.*

Conc. / M	**H^a**	**$H^{a'}$**	**H^b**	**$H^{b'}$**	**H^1**
0.00000	3.782	3.692	2.156	2.048	1.339
0.00429	3.782	3.687	2.158	2.051	1.341
0.00773	3.782	3.682	2.160	2.053	1.342
0.01148	3.782	3.678	2.162	2.055	1.344
0.01523	3.781	3.674	2.163	2.056	1.345
0.02296	3.781	3.669	2.166	2.059	1.348

0.03046	3.780	3.666	2.168	2.060	1.352
0.04547	3.778	3.658	2.170	2.061	1.353
0.06099	3.776	3.653	2.170	2.062	1.355
0.08399	3.773	3.645	2.170	2.061	1.358
0.10700	3.768	3.639	2.168	2.058	1.359

Table A7: *Chemical shift data of the fluoranthene protons in 0.00762M $[Pt^{II}(phen)(L\text{-}S,O)]^+$ acetonitrile at 299K with increasing fluoranthene concentration.*

Conc. / M	H^{3+17}	H^{3+16}	H^{9+11}	H^{3+17}	H^{8+12}
0.00429	7.927	7.882	7.818	7.604	7.346
0.00773	7.931	7.886	7.822	7.607	7.349
0.01148	7.938	7.892	7.827	7.611	7.353
0.01523	7.940	7.896	7.830	7.614	7.355
0.02296	7.948	7.902	7.836	7.619	7.359
0.03046	7.958	7.913	7.845	7.627	7.366
0.04547	7.959	7.914	7.846	7.627	7.367
0.06099	7.963	7.918	7.840	7.631	7.370
0.08399	7.967	7.923	7.854	7.634	7.373
0.10700	7.969	7.925	7.856	7.635	7.374
0.01071	8.058	8.009	7.929	7.703	7.430

Table A8: *Chemical shift data of protons H^2 and H^9 of $[Pt^{II}(phen)(L\text{-}S,O)]^+$ in acetonitrile at varied temperatures from 267-299K.*

10%D_2O			**20%D_2O**			**30%D_2O**		
Conc. / M	**H^2**	**H^9**	**Conc. / M**	**H^2**	**H^9**	**Conc. / M**	**H^2**	**H^9**
309.6K								
0.02636	8.841	8.467	0.02222	8.818	8.445	0.02051	8.757	8.375
0.01582	8.947	8.602	0.01333	8.910	8.560	0.01231	8.850	8.492
0.01054	9.019	8.691	0.00829	9.002	8.675	0.00821	8.917	8.576
0.00844	9.058	8.737	0.00746	9.018	8.695	0.00656	8.955	8.621
0.00633	9.100	8.787	0.00580	9.054	8.738	0.00492	9.000	8.677
0.00422	9.150	8.848	0.00497	9.075	8.763	0.00328	9.052	8.740
0.00316	9.179	8.881	0.00387	9.104	8.798	0.00246	9.089	8.784
0.00211	9.213	8.922	0.00223	9.163	8.868	0.00164	9.124	8.826
0.00105	9.256	8.971	0.00084	9.232	8.949	0.00082	9.191	8.905
0.00031	9.290	9.010	0.00022	9.271	8.994	0.00024	9.247	8.970

299.3K								
0.02636	8.773	8.379	0.02222	8.758	8.365	0.02051	8.702	8.301
0.01582	8.885	8.523	0.01333	8.856	8.490	0.01231	8.796	8.421
0.01054	8.962	8.619	0.00829	8.949	8.609	0.00821	8.865	8.508
0.00844	9.002	8.669	0.00746	8.966	8.630	0.00656	8.902	8.556
0.00633	9.048	8.725	0.00580	9.004	8.676	0.00492	8.949	8.614
0.00422	9.104	8.792	0.00497	9.026	8.704	0.00328	9.006	8.683
0.00316	9.139	8.835	0.00387	9.061	8.746	0.00246	9.046	8.731
0.00211	9.179	8.882	0.00223	9.128	8.825	0.00164	9.088	8.783
0.00105	9.233	8.945	0.00084	9.210	8.923	0.00082	9.165	8.826
0.00031	9.279	8.998	0.00022	9.262	8.984	0.00024	9.235	8.957
291.6K								
0.02636	8.716	8.303	0.02222	8.703	8.291	0.02051	8.653	8.236
0.01582	8.831	8.453	0.01333	8.759	8.362	0.01231	8.749	8.360
0.01054	8.912	8.557	0.00829	8.902	8.549	0.00821	8.820	8.450
0.00844	8.955	8.610	0.00746	8.920	8.572	0.00656	8.858	8.499
0.00633	9.003	8.671	0.00580	8.960	8.622	0.00492	8.907	8.560
0.00422	9.064	8.745	0.00497	8.984	8.652	0.00328	8.965	8.633
0.00316	9.102	8.790	0.00387	9.018	8.694	0.00246	9.007	8.684
0.00211	9.147	8.844	0.00223	9.098	8.790	0.00164	9.050	8.736
0.00105	9.212	8.921	0.00084	9.188	8.897	0.00082	9.138	8.842
0.00031	9.270	8.988	0.00022	9.253	8.975	0.00024	9.223	8.942
282.6K								
0.02636	8.651	8.215	0.02222	8.658	8.217	0.02051	8.610	8.174
0.01582	8.775	8.379	0.01333	8.759	8.362	0.01231	8.706	8.299
0.01054	8.857	8.486	0.00829	8.851	8.482	0.00821	8.776	8.391
0.00844	8.901	8.542	0.00746	8.870	8.507	0.00656	8.816	8.442
0.00633	8.951	8.605	0.00580	8.910	8.558	0.00492	8.863	8.503
0.00422	9.014	8.684	0.00497	8.935	8.589	0.00328	8.923	8.578
0.00316	9.055	8.734	0.00387	8.971	8.635	0.00246	8.965	8.631
0.00211	9.105	8.795	0.00223	9.053	8.736	0.00164	9.012	8.688
0.00105	9.182	8.886	0.00084	9.159	8.863	0.00082	9.108	8.805
0.00031	9.256	8.972	0.00022	9.241	8.960	0.00024	9.209	8.924

Table A9: *Calculated dimerization constants, K_D and thermodynamic data for $[Pt^{II}(phen)(L\text{-}O,S)]^+$ in D_2O/CD_3CN mixtures (calculated using the chemical shift of H^2).*

Temp / K	K_D / M^{-1}	Δ_rH^o / $Jmol^{-1}$	Δ_rS^o / $Jmol^{-1}$	Δ_rG^o / $Jmol^{-1}$
10% D_2O/CD_3CN (v/v)				
309.6	20 (± 2)	-19685 (± 2438)	-40 (± 7)	-7485
299.3	27 (± 3)			-7981
291.6	33 (± 5)			-8290
282.6	41 (± 7)			-8547
20% D_2O/CD_3CN (v/v)				
309.6	29 (± 4)	-20089 (± 2489)	-38 (± 7)	-8205
299.3	39 (± 5)			-8571
291.6	43 (± 8)			-8598
282.6	64 (± 10)			-9037
30% D_2O/CD_3CN (v/v)				
309.6	54 (± 8)	-18854 (± 2335)	-27 (± 5)	-10041
299.3	71 (± 10)			-10389
291.6	87 (± 12)			-10591
282.6	108 (± 15)			-10777

Appendix B

Infrared Spectra

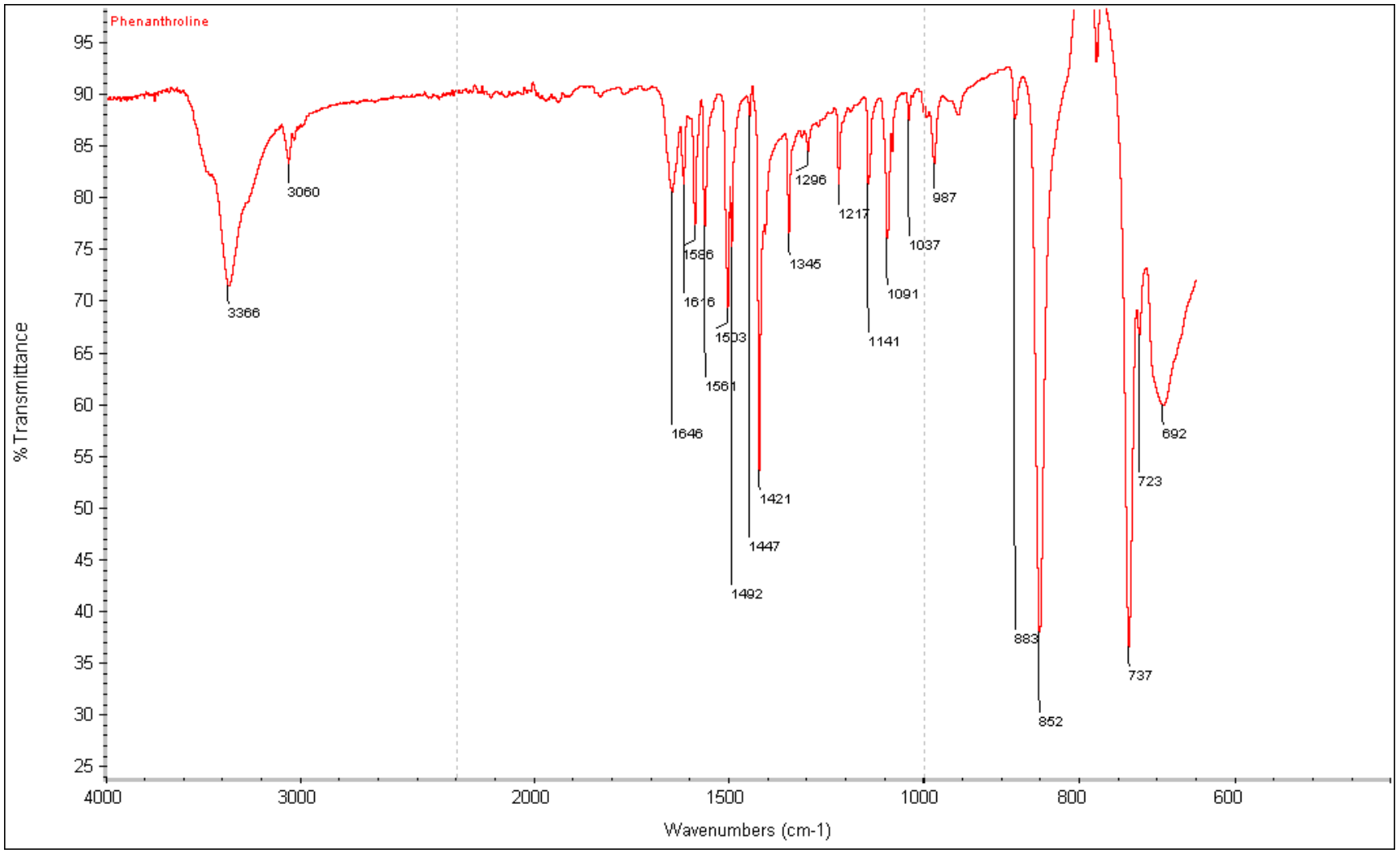

Figure B1: *Infrared spectrum of 1,10-phenanthroline*

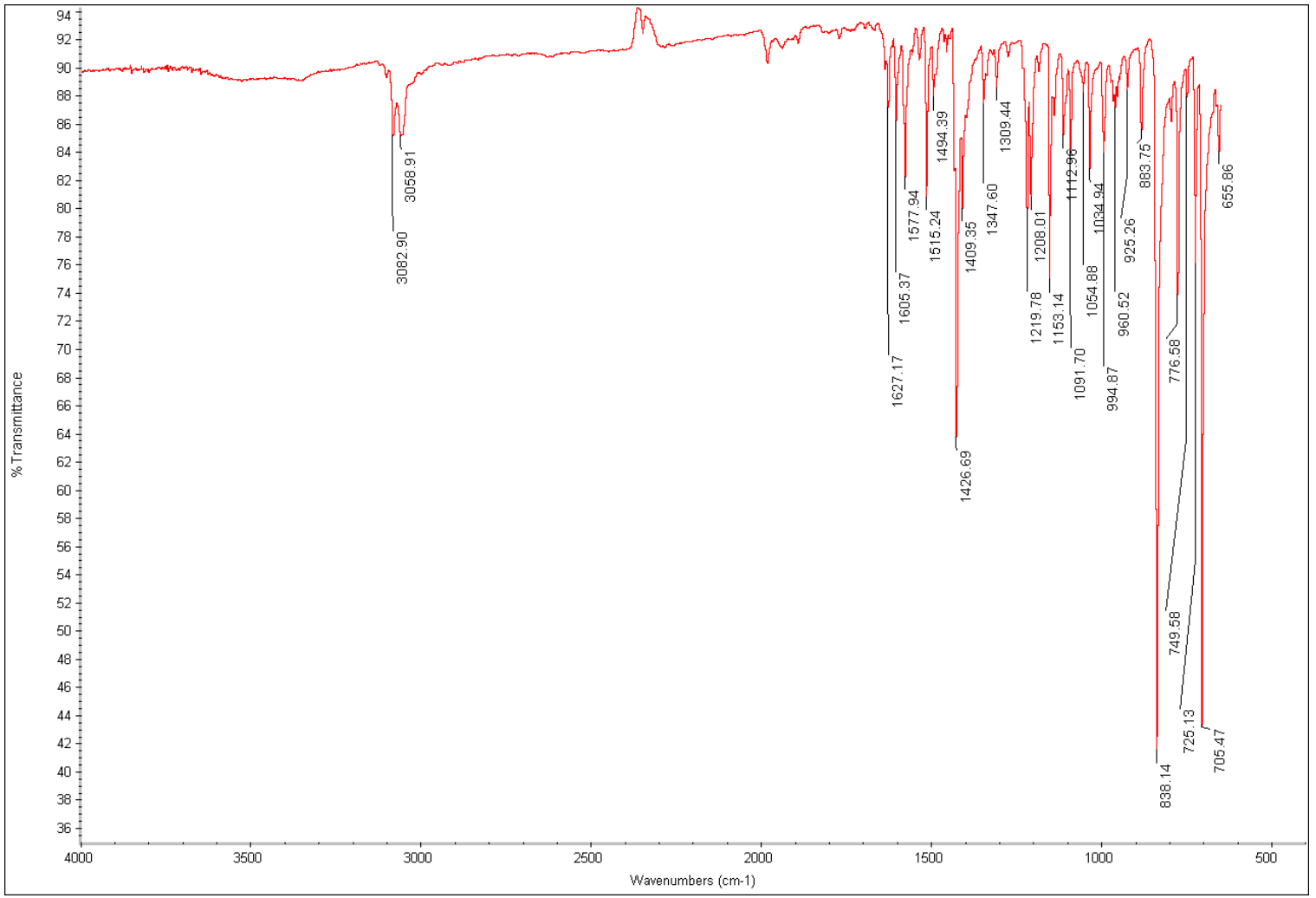

Figure B1: *Infrared spectrum of HL*[1]

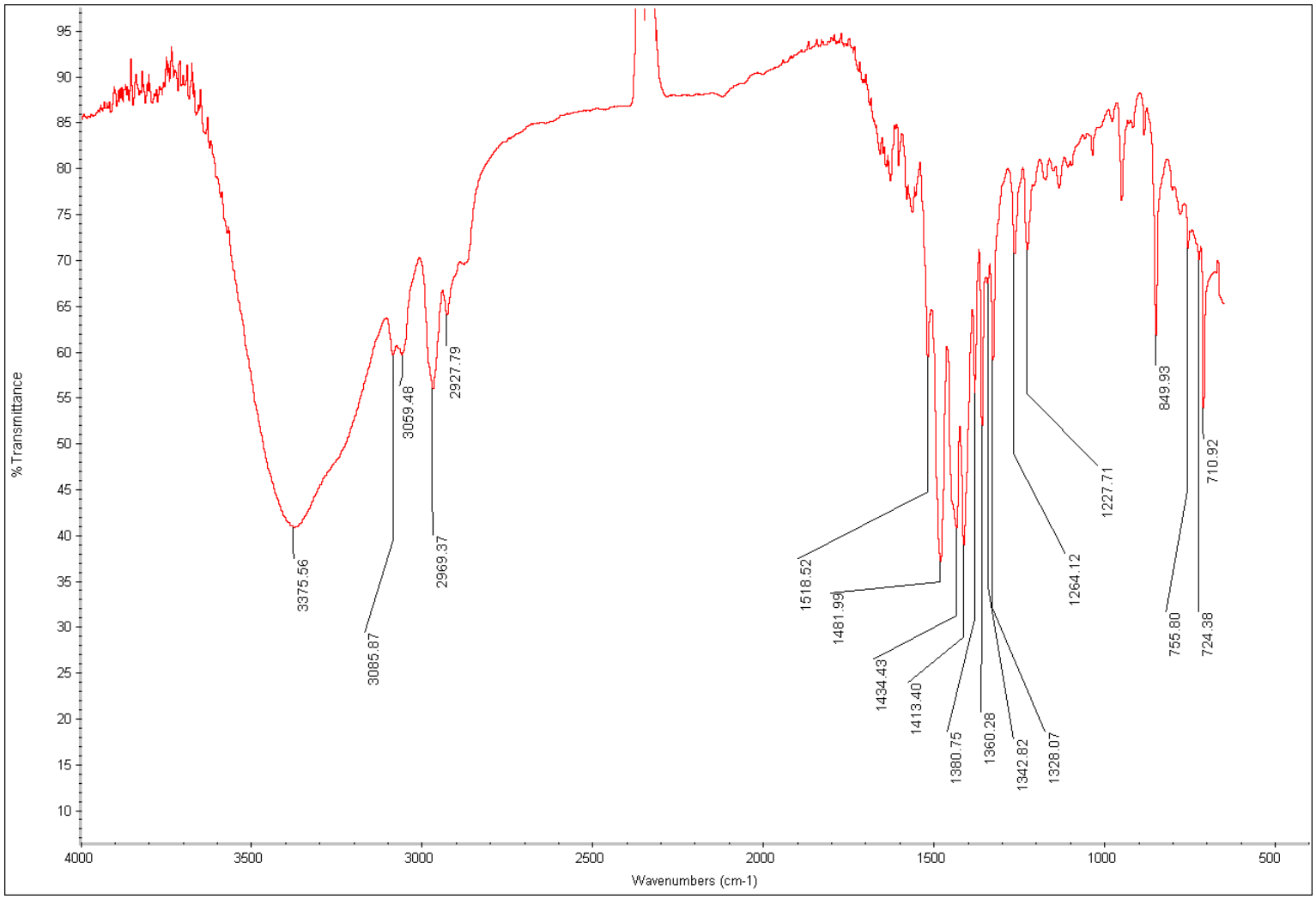

Figure B1: *Infrared spectrum of $Pt^{II}(phen)(L^1\text{-}S,O)]Cl$*

Appendix C

Publication (From this work)

DOI: 10.1002/ejic.200900059

Self-Association of [Pt^{II}(1,10-Phenanthroline)(*N*-pyrrolidyl-*N*-(2,2-dimethylpropanoyl)thiourea)]$^+$ and Non-Covalent Outer-Sphere Complex Formation with Fluoranthene through π–Cation Interactions: A High-Resolution ^{1}H and DOSY NMR Study

Izak A. Kotzé,[a] Wilhelmus J. Gerber,[a] Jean M. Mckenzie,[a] and Klaus R. Koch*[a]

Keywords: Noncovalent interactions / Pi interactions / NMR spectroscopy / Diffusion coefficients / Association constants

Competing outer-sphere self-association of [Pt^{II}(1,10-phenanthroline)(*N*-pyrrolidyl-*N*-(2,2-dimethylpropanoyl)thiourea)]$^+$ Cl^- (M) and the hetero-association of M with fluoranthene (F) have been investigated by means of the significant concentration dependence of ^{1}H NMR chemical shifts as well as by diffusion coefficients obtained from DOSY NMR spectroscopy. The NMR spectroscopic data is only consistent with the formation of a "dimer" M···M aggregate according to $2M \rightleftharpoons M_2$ in acetonitrile at several temperatures, with a calculated K_D of ca. 46 ± 7 M^{-1} at 273.5 K. In the presence of the aromatic molecule fluoranthene, relatively strong, presumably π–cation-type interactions between M and F according to $M + F \rightleftharpoons MF$ ($K_B \approx 67 \pm 7$ M^{-1} at 273.5 K) occur in acetonitrile. The calculated $\Delta_r H°$ and $\Delta_r S°$ for M···M (-25129 ± 3112 and -61 ± 11 J mol^{-1}) and M···F (-13560 ± 3180 and -17 ± 11 J mol^{-1}, respectively) is indicative of π–cation interactions. Interestingly any potential F···F aggregation interactions are negligible for the fluoranthene concentration range up to 0.1 M, indicating that non-covalent π–π interactions between fluoranthene molecules $2F \rightleftharpoons F_2$ are, in contrast to π–cation interactions, negligible under these conditions in solution.

Introduction

Non-covalent π–cation interactions have been the subject of extensive interest in the last decade in view of their well established role and importance in biological systems[1–5] as well as in supra-molecular chemistry and molecular recognition phenomena.[3,6–8] There are several manifestations of this type of non-covalent bonding interaction, the simplest and most extensively studied system involves group I and II metal cations or protonated amine with benzene and other aromatic molecules in the gas and solution phase.[2,9] The detailed nature of π–cation interactions have been reviewed and in the *gas phase* for example, the K^+···benzene interaction energies can exceed K^+···H_2O interaction,[10,11] and it has been convincingly shown that "organic" cations, such as ammonium ions, can strongly interact with suitably designed synthetic arene-based receptors as well as in numerous biological structures.[12,13] In aqueous solution, cations are obviously solvated resulting in the attenuation of the π–cation interaction leading to elongation of the interaction distance between the cation and arene centre as compared to such interactions in the gas phase.[9] In the case of "stacking" and/or aggregation of metalloporphyrins, Hunter and Sanders[14] derived an elegant simple electrostatic model which demonstrate that so-called "π–π" interactions in planar metalloporphyrins actually arise from favourable π–σ attractions which overcome π–π repulsions in such molecules. This model has resulted in a set of rules with which to predict the nature and relative interaction geometry of such aggregation phenomena, at least in the case of planar metalloporphyrins.

We have become interested in the chemistry of planar, formally cationic mixed-ligand Pt^{II} complexes of the general structure [Pt(diimine)(L-*S*,*O*)]$^+$ (where diimine is 2,2′-bipyridine or 1,10-phenanthroline and HL-*S*,*O* represents various chelating *N*-acyl-*N*,*N*′-dialkylthioureas) which have been shown to display interesting biological activity ranging from significant potential anti-malarial activity,[15a] to interesting DNA intercalation with demonstrable in vivo activity toward bacterial *E. coli* AB1886 (*uvr A*) cultures;[15b] moreover preliminary work shows that such complexes undergo some interesting DNA-mediated biomineralization.[16] We have previously studied a series of [Pt^{II}(diimine)(L-*S*,*O*)]PF_6 salts which were found to display well defined aggregation behaviour in acetonitrile solutions, which we ascribed to π–cation interactions leading to the formation of non-covalent "dimer aggregates" in solution.[17] For this system we found that the Gibbs free energy associated with the "dimer aggre-

[a] Department of Chemistry and Polymer Science, University of Stellenbosch,
Private Bag X1, Matieland, 7602 Stellenbosch, South Africa
Fax: +27-21-808-3342
E-mail: krk@sun.ac.za

Supporting information for this article is available on the WWW under http://www.eurjic.org or from the author.

gates" formation increases by approximately 2.4 kJ mol^{-1} per aromatic ring of the diimine bound to Pt^{II}; these Gibbs free energies are slightly higher than energies reported by Rebeck et al. for only "π–π stacking" interactions of 1.8 kJ mol^{-1}.[18]

By contrast to the well known group I and II metal cations and protonated amine systems which show significant π–cation interactions[2,9] outer-sphere complexes with uncharged aromatic molecules by means of π–cation or combinations of π–cation and π–π stacking interactions with planar complex cations such as $[Pt^{II}(diimine)(L\text{-}S,O)]^+$ and even $[Pt^{II}(diimine)_2]^{2+}$ have received comparatively little attention in the literature.[6,17,19] The in vitro anti-malarial activity of $[Pt^{II}(diimine)(L\text{-}S,O)]^+$ is postulated to arise by inhibition of β-hematin (synthetic hemozoin or malaria pigment) formation in view of the cationic Pt^{II} complexes forming moderately strong outer-sphere complexes with ferriprotoporphyrin IX in 40% aqueous dimethyl sulfoxide (DMSO) solution.[15]

In this context, we examined potential π–cation interactions between the $[Pt^{II}(phen)(L\text{-}S,O)]^+Cl^-$ complex (Scheme 1) and fluoranthene ($C_{16}H_{10}$) in acetonitrile as a model system, by means of ^{1}H NMR concentration-dependence studies as well as Diffusion Ordered Spectroscopy (DOSY) to probe these phenomena. ^{1}H NMR is particularly well suited for this type of investigation because the relevant thermodynamic parameters can be estimated from the concentration dependence of ^{1}H chemical shifts,[19–21] while the relative spatial orientation of the complex cation within an aggregate in solution can be inferred.[17] DOSY experiments[3] have been used as an independent method to estimate the thermodynamic properties of this system[3,20] and to obtain estimated hydrodynamic volumes of aggregates, which gives a measure of the number of molecules present in an "aggregate".[22,23] This model system is representative of competing non-covalent π–cation interactions leading to self-association of the complex $[Pt^{II}(phen)(L\text{-}S,O)]^+$ cation on the one hand, and π–cation interactions between fluoranthene and the complex in solution, on the other.

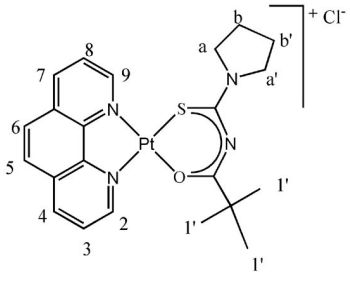

Scheme 1. Structure and numbering scheme for $[Pt^{II}(phen)(L\text{-}O,S)]^+Cl^-$.

Computational Methods

In the model system examined in this work, several simultaneous chemical equilibria may be present. From the average observed signal response, $X_{obsd.}$, equation (1) (where X_i = ^{1}H chemical shift, δ_i, or diffusion coefficient, D_i, and a_i = mole fraction of species i) and the total concentration of reagents, we want to calculate for the reactions defined in a chemical model the equilibrium constant(s), K_i, and chemical shifts, δ_i, or diffusion coefficients, D_i, of individual species (dimer aggregates, trimer aggregates, ion-pairs, etc).

$$X_{obsd.} = \sum_{i=n} a_i X_i \quad (1)$$

This particular type of mathematical problem can be solved in several ways.[24] We opted to use a program called, DIMER-K_D, written by us several years ago to fit data with a dimerization model[17] (the program utilizes the algorithm by Horman and co-workers[21]). When dealing with multiple equilibria we used a program called Dynafit version 3[25] that is freely available for academic purposes. The signal response that Dynafit version 3 can handle is however slightly different from equation (1); instead of using mole fraction in equation (1), Dynafit uses the concentration of the species, c_i. This problem was circumvented by multiplying equation (1) with the total concentration, C_T, of the reagent of interest and after grouping terms, equation (2) is obtained.

$$C_T X_{obsd.} = \sum_{i=n} c_i X_i \quad (2)$$

Results and Discussion

Self-Association of $[Pt^{II}(phen)(L\text{-}S,O)]^+$ in Acetonitrile

Figure 1 illustrates ^{1}H NMR spectra obtained as a function of $[Pt^{II}(phen)(L\text{-}S,O)]^+$ concentration at 267.1 K in CD_3CN. The marked concentration dependence of the chemical shift of particularly the H^2 and H^9 signals of the coordinated 1,10-phenanthroline moiety suggests that self-association/aggregation processes are occurring with increasing concentration, as we have previously demonstrated for related complexes.[17] Moreover, the spectra reveal that whatever aggregated species exist in solution are in fast-exchange (in chemical shift) on the NMR time-scale, because only sharp ^{1}H resonances for all protons on the complex are observed over the concentration and temperature ranges studied. Significantly, *all* the ^{1}H resonances of the 1,10-phenanthroline group show differing degrees of $\delta_{obsd.}$ concentration dependence, depending on their relative positions in the 1.10-phenanthroline ring system (Supporting Information, Figure S1), while the chemical shifts of the protons of the coordinated *N*-pyrrolidyl-*N*-(2,2-dimethylpropanoyl)thiourea ligands show a much smaller concentration dependence. Possible dissociation reactions of the $[Pt^{II}(Phen)(L\text{-}S,O)]^+$ complex over time, such as Cl^- coordination to the Pt^{II} metal centre following chelate ring-opening reactions, may be excluded because no spectral changes consistent with dissociation are observed over a 5 d period at any fixed concentration for the temperature range 278–301 K.

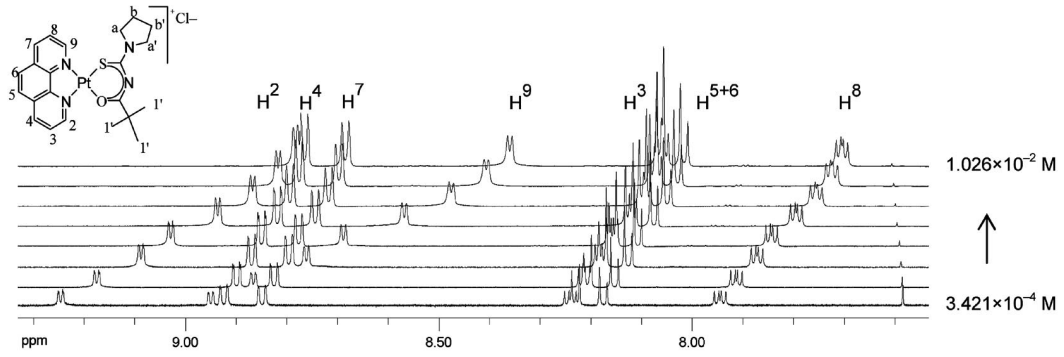

Figure 1. ^{1}H NMR spectra (599.99 MHz) of $[Pt^{II}(phen)(L\text{-}S,O)]^+$ in CD_3CN at 273.4 K with increasing complex concentration. Only a partial spectrum is shown as several nuclei (*N*-pyrrolidyl-*N*-(2,2-dimethylpropanoyl)thiourea protons) exhibit no or little chemical-shift concentration dependence.

Several intermolecular processes in solution may be invoked to account for the concentration dependence of the $\delta_{obsd.}$, notably self-association or aggregation of $[Pt^{II}(phen)(L\text{-}S,O)]^+$ cations and/or ion-pairing between the complex cation and Cl^- ion (due to the relatively low dielectric constant of acetonitrile, $k \approx 36$, at 298 K). We postulate that the concentration dependence of the $\delta_{obsd.}$ for the $[Pt^{II}(phen)(L\text{-}S,O)]^+Cl^-$ salt in acetonitrile solution is due essentially to "dimer aggregate" (D) formation consisting of two planar complex $[Pt^{II}(phen)(L\text{-}S,O)]^+$ cations participating in π–cation stacking interaction in solution (vide infra). Self-association of $[Pt^{II}(phen)(L\text{-}S,O)]^+$ leading to higher order aggregates such as a "trimer" or even "tetramer" aggregates would result in more highly charged species which are unlikely in acetonitrile. Nonetheless, to critically examine our postulate of the formation of only dimer aggregates, as well as to exclude the possibility of ion-pairing and/or higher order aggregates being present in solution, we attempted to fit various models including dimer, trimer, and tetramers, as well as a model in which $[Pt^{II}(phen)(L\text{-}S,O)]^+\cdots Cl^-$ ion-pairing occurs, to the data shown in Figure 2 using non-linear least-squares regression methods. With the exception of the simple dimer (D) model, relation (3), all other models however resulted in absurdly large relative percentage error for calculated equilibrium constants associated with possible ion-pairing and/or higher than dimer self-association processes, disqualifying such more complicated models.

The excellent fit between the $\delta_{obsd.}$ and calculated values obtained with only the dimer (D) model shown in Figure 2 [see also equation (4)] and further, the plausible calculated chemical shifts of the monomer and dimer of the H^2 protons (9.316 ± 0.029 and 7.851 ± 0.089 ppm, respectively, at 299.2 K) provide a compelling argument for only the dimer model postulated here. Using this model, where M = $[Pt^{II}(phen)(L\text{-}S,O)]^+$ monomer and M_2 = $[Pt^{II}(phen)(L\text{-}S,O)]^+$ dimer, "dimerization" constants (K_D) and chemical shifts (δ_i) for the relevant protons were estimated to within a 95% confidence limit for each temperature, while the relative percentage error for all parameters are below 13% at worst (Table 1).

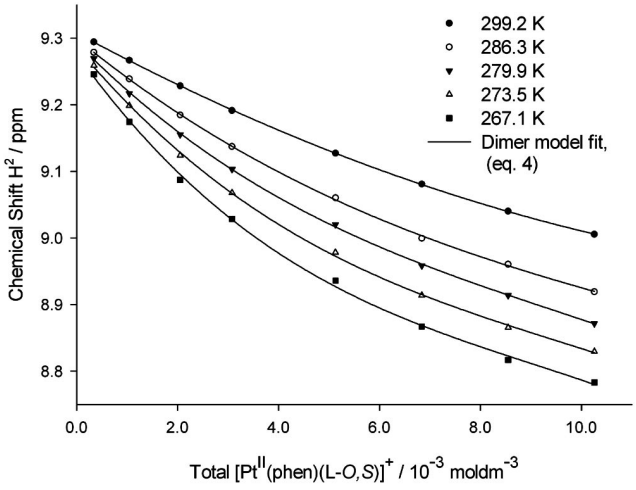

Figure 2. Excellent agreement was obtained between the dimer model least-squares fits and the experimental (symbols) chemical-shift dependence of the 1,10-phenanthroline H^2 proton on the concentration of $[Pt^{II}(phen)(L\text{-}S,O)]^+$.

$$2M \overset{K_D}{\rightleftharpoons} M_2 \quad (3)$$

$$C_{T(Pt)}\delta_{obsd.} = c_M\delta_M + 2c_{M2}\delta_{M2} \quad (4)$$

Table 1. Calculated dimerization constants, K_D for $[Pt^{II}(phen)(L\text{-}O,S)]^+$ in CD_3CN and thermodynamic data.

Temp [K]	K_D [M^{-1}]	$\Delta_rH°$ [J mol^{-1}]	$\Delta_rS°$ [J mol^{-1}]	$\Delta_rG°$ [J mol^{-1}]
299.2	17 (± 2)	–25129 (± 3112)	–61 (± 11)	–6998
286.3	27 (± 5)			–7777
279.9	29 (± 3)			–8167
273.5	46 (± 7)			–8556
267.1	56 (± 8)			–8946

As the temperature is raised from 267.1 to 299.2 K, the $K_D = 56 \pm 7$ M^{-1} decreases to 17 ± 2 M^{-1}, indicating as expected that dimer formation is exothermic. The standard reaction enthalpy, $\Delta_rH°$, and entropy, $\Delta_rS°$, can be estimated by fitting the Van't Hoff equation (5) to the temperature-dependent K_D data. Over the relatively small tempera-

ture range used here (Δ 32.1 K), it is expected that the $\Delta_r H°$ and $\Delta_r S°$ are temperature independent yielding a linear plot of $\ln(K_D)$ vs. T^{-1}. This is confirmed by the good linear trend obtained using the Van't Hoff equation (Figure 3), which further validates the dimer aggregate model; the standard reaction enthalpy (slope) and entropy (intercept) of reaction 3 are listed in Table 1. The relatively large, negative $\Delta_r S°$ is indicative of an association reaction consistent with the inference that only dimer aggregates are formed. By comparison, ion-pair processes are typically associated with a positive $\Delta_r S°$ changes, as solvated molecules are "released" upon ion-pair formation.[3,26] Furthermore, it is clear from the thermodynamic data (Table 1) ($\Delta_r H° < 0$, $T\Delta_r S° < 0$) that the dimer-formation reaction is enthalpy driven and that this thermodynamic behaviour is indicative of π–cation binding.[3]

$$\ln(K_D) = -\frac{\Delta_r H°}{RT} + \frac{\Delta_r S°}{R} \quad (5)$$

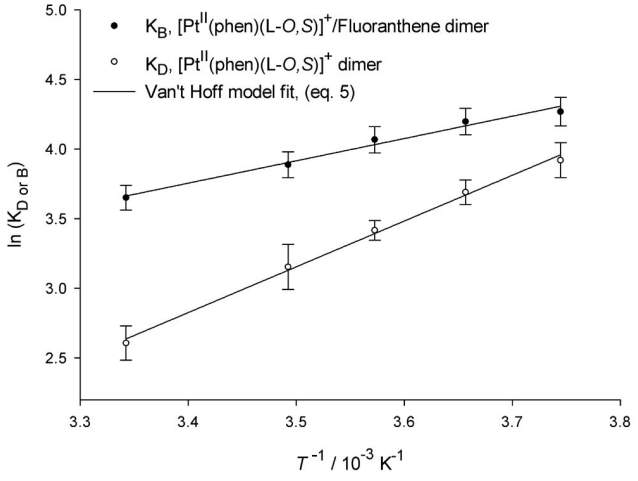

Figure 3. The good linear fits obtained with the Van't Hoff equation is further validation for the self- and hetero-association (vide infra) of $[Pt^{II}(phen)(L\text{-}O,S)]^+$ and fluoranthene in CD_3CN. The 95% confidence interval of the slopes and intercepts for the $[Pt^{II}(phen)(L\text{-}O,S)]^+$ and $[Pt^{II}(phen)(L\text{-}O,S)]^+$/fluoranthene dimers equal 3287.8 (± 374.2)x –8.4 (±1.3) and 1602.9 (± 383.0)x –1.7 (±1.4), respectively.

Given the relatively simple dimer model, it is reasonable to expect that molecular diffusion processes might be affected by increased dimer formation, as a function of increasing complex concentration. This expectation is confirmed by diffusion-ordered ^{1}H NMR spectroscopy (DOSY) which we show here to be an independent method with which to verify conclusions drawn from the concentration and temperature ^{1}H NMR chemical-shift dependence studies. Experiments with diffusion-delay times varying from 30 to 200 ms resulted in no significant differences in DOSY spectra nor in calculated diffusion coefficients (DOSY spectrum Supporting Information Figure S3); it is therefore reasonable to conclude that only an averaged diffusion coefficient, $D_{obsd.}$, is observed.[27] Unlike the ^{1}H-chemical-shift experiments discussed above, all protons of the complex $[Pt^{II}(phen)(L\text{-}S,O)]^+$ in equilibrium with the dimer yield the "same" diffusion coefficient and this method is therefore not dependent on the individual proton chemical shifts. The D_{CD_3CN} obtained here (39.5×10^{-10} m^2 s^{-1}) differs by less than 7% from the value obtained by Kato and coworkers[28] (4.3×10^{-9} m^2 s^{-1}), and consequently we used the D_{CD_3CN} as an internal "standard". The $D_{obsd.}$ for the complex is proportional to the sum of the product of the individual diffusion coefficients, D_i, and the concentration of the species (i) present [equation (6)]. Estimation of the K_D from diffusion data are based on the same mathematical algorithm[21] as for the ^{1}H-chemical-shift dependence described above.

$$C_{T(Pt)}D_{obsd.} = c_M D_M + 2c_{M2}D_{M2} \quad (6)$$

As the concentration of $[Pt^{II}(phen)(L\text{-}S,O)]^+$ increases experimental diffusion coefficients decrease (Figure 4), consistent with a dimer model. The least-squares fit with the dimerization model (relation 6) is in good agreement with the diffusion data (Figure 4) and the calculated K_D from diffusion data at 299.2 K is 15 ± 8 M^{-1} (ΔG = –6737 J mol^{-1}). This compares well with the K_D calculated from the chemical shift data 17 ± 2 M^{-1} (ΔG = –7048 J mol^{-1}) and supports the simple dimer model. The agreement is reasonably acceptable given that the relative percent error of measured diffusion coefficients is at best 4%, albeit much larger than the relative percentage error in the measurement of a ^{1}H NMR chemical shift (0.2%), arguably leading to a less precise value of K_D from DOSY NMR spectroscopic data (Figure 4). The satisfactory agreement between the two differing ways of estimating K_D indicates that this model is internally consistent.

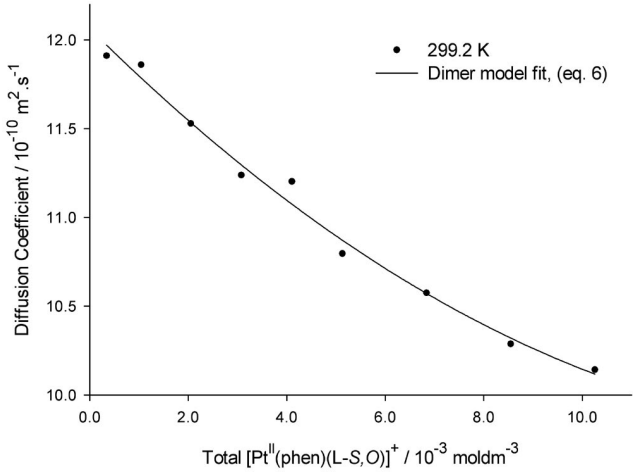

Figure 4. Good agreement was obtained between the dimer model least-squares fit and the experimental (symbols) diffusion-coefficient dependence on the concentration of $[Pt^{II}(phen)(L\text{-}S,O)]^+$ at 299.2 K.

In principle the hydrodynamic radius and volume of a complex may be estimated from DOSY data at a given concentration, because the diffusion coefficient is related to molecular size by the well known Stokes–Einstein equation

(7), from which the hydrodynamic radius, r_H, and volume, V_H, of the molecules/aggregates in question can be estimated,

$$D = \frac{kT}{6\pi\eta r_H} \quad (7)$$

where k is the Boltzmann constant, T is the absolute temperature and η the solvent viscosity.[22] This equation assumes a spherical molecule and is obviously a rather crude approximation of our square-planar complexes. We assumed that the solvent viscosity does not change significantly with solute concentration, which is justified for the relatively low solute concentrations used and by the negligible change in D_{CD_3CN} values ($39.53 \pm 0.72 \times 10^{-10}$ m^{2}s^{-1}) obtained for all solutions of differing solute concentration examined at 299.2 K. The hydrodynamic radii estimated (Table 2) from the $D_{obsd.}$ represents an "average" of the monomer and dimer. From the least-squares fit of the data in Figure 4, the [Pt^{II}(phen)(L-*S*,*O*)]$^+$ monomer and dimer individual diffusion coefficients were estimated at ca. $12.1 \pm 0.6 \times 10^{-10}$ and $5.9 \pm 0.8 \times 10^{-10}$ m^{2}s^{-1}, respectively from which the hydrodynamic radii for the monomer and dimer could be estimated to be 4.8 (± 2.3) and 10.1 (± 3.5) Å, respectively. The r_H value for the [Pt^{II}(phen)(L-*S*,*O*)]$^+$ complex is reasonable when compared to the $r_{H,X\text{-ray}}$ estimated from single-crystal X-ray data of two crystal structures,[29,30] which is 5.8 Å (Supporting Information Diagram S1), whereas the calculated r_H of the dimer is reasonable when considering two [Pt^{II}(phen)(L-*S*,*O*)]$^+$ species in close contact.

Table 2. Diffusion coefficients D ($\times 10^{-10}$ m^{2}s^{-1}), hydrodynamic radii r_H [Å] and hydrodynamic volumes V_H (Å^3) for [Pt^{II}(phen)(L-*O*,*S*)]$^+$ in CD_3CN at different complex concentrations [mM].

Concentration [mM]	D [10^{-10} m^{2}s^{-1}]	r_H [Å]	V_H [Å^3]
10.26	10.14 (± 0.07)	5.82	824.1
8.55	10.29 (± 0.09)	5.73	789.6
6.84	10.58 (± 0.08)	5.58	726.8
5.13	10.80 (± 0.11)	5.46	683.2
4.10	11.20 (± 0.11)	5.27	611.5
3.08	11.24 (± 0.13)	5.25	605.6
2.05	11.53 (± 0.17)	5.12	561.0
1.04	11.86 (± 0.12)	4.97	515.2
0.34	11.91 (± 0.18)	4.95	508.7

The consistency of the DOSY data with that obtained from the concentration dependence of the $\delta_{obsd.}$(^{1}H) of the [Pt^{II}(phen)(L-*S*,*O*)]$^+$ complex is convincing support of dimer formation through π–cation association of these planar Pt^{II} complexes. Unfortunately, numerous attempts to obtain crystals suitable for single crystal X-ray diffraction failed to date, so that direct structural support for the geometrical nature of the dimer aggregate is lacking at present. Nevertheless, from the ^{1}H-chemical-shift trends observed (Figure 1) it is possible to infer a most likely structure of the dimer aggregate. The relatively small concentration dependence of the $\delta_{obsd.}$ for the butyl and *N*-pyrrolidyl protons compared to the relatively large concentration dependence of the chemical shift of the 1,10-phenanthroline protons (H^2 and H^9), suggests that these complexes stack *regiospecifically* in a face-to-face manner involving the phenanthroline sides of the complex. An unlikely "T-shaped" edge-on geometry[14] for the dimer can be ruled out given the chemical shift trends observed (Supporting Information, Figure S1). Such a coplanar stacking arrangement will maximize the π–cation attractions and minimize π–π repulsion to result in an offset π–cation stacking geometry between adjacent complexes consistent with related metalloporphyrins suggested by the Sanders[14] model as in Scheme 2. Depicted in the scheme are the most reasonable dimer aggregate structures postulated in solution; because the system is in fast exchange in chemical shift, only an average structure can be proposed from NMR spectroscopic data in view of several possible geometric stacking interactions conceivable.

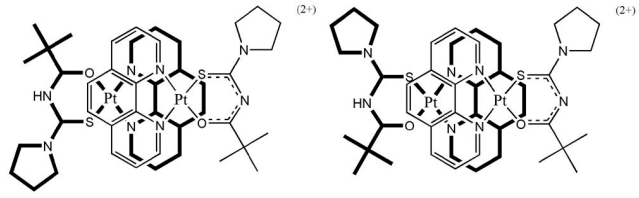

Scheme 2. Proposed average [Pt^{II}(phen)(L-*S*,*O*)]$^+$ dimer aggregate structures in solution.

Non-Covalent Association of [Pt^{II}(phen)(L-*S*,*O*)]$^+$ and Fluoranthene

Addition of small quantities of aromatic molecules such as fluoranthene ($C_{16}H_{10}$) to a solution of [Pt^{II}(phen)(L-*S*,*O*)]$^+$ in acetonitrile, leads to changes in the ^{1}H NMR spectrum of the complex (Figure S2), resulting in significant shielding of H^2 and H^9 protons of the [Pt^{II}(phen)(L-*S*,*O*)]$^+$ cation in proportion to the relative mole ratio of [Pt^{II}-(phen)(L-*S*,*O*)]$^+$ to fluoranthene. Such behaviour suggests substantial non-covalent association between fluoranthene and the [Pt^{II}(phen)(L-*S*,*O*)]$^+$ complex, through π–cation interactions. Because only single resonances for all ^{1}H of the [Pt^{II}(phen)(L-*S*,*O*)]$^+$ complex are observed at these temperatures in solution, the system is in fast exchange in chemical shift as observed for the self-association of the [Pt^{II}(phen)(L-*S*,*O*)]$^+$ described above. We have investigated this phenomenon quantitatively by means of the concentration dependence of the ^{1}H resonances ($\delta_{obsd.}$) of the platinum complex as a function of added fluoranthene, with the view of estimating the association constants between the π-electron-rich fluoranthene and the planar complex cation in acetonitrile. With the addition of fluoranthene (F) to a solution of [Pt^{II}(phen)(L-*S*,*O*)]$^+$ in acetonitrile, the simplest additional reactions to aggregation of the complex cation (M), are the aggregation of fluoranthene itself to form at least a fluoranthene dimer (F_2) – see equation (8) – and outer-sphere complex formation between M and F, through π–cation interactions, see equation (9).

$$2F \overset{K_A}{\rightleftharpoons} F_2 \quad (8)$$

$$M + F \overset{K_B}{\rightleftharpoons} MF \quad (9)$$

To test if fluoranthene undergoes aggregation in acetonitrile (equation 8), the concentration dependence of the ^1H chemical shift was studied in the temperature range 266 to 298 K. Changes in ^1H chemical shifts of fluoranthene were found to be very small (relative to the data in Figure 2) resulting in a total Δ 0.015 ppm over the range of 1.05 mM to 0.1 M fluoranthene. The relatively poor solubility of fluoranthene in acetonitrile prevented examination of higher concentrations, and hence precluded a reliable estimate of an aggregation (of at least dimer formation) constant from this data, so that we reasonably estimate a $K_A < 0.1\ M^{-1}$ at 266 K. Such a K_A value implies that the mole fraction of un-associated fluoranthene (α_F) is > 0.98 at the highest practical fluoranthene concentration of 0.1 M. Clearly any π–π stacking of fluoranthene in acetonitrile can be taken to be essentially negligible in a total concentration range up to 0.1 M fluoranthene achievable in [D_3]acetonitrile.

Addition of increasing amounts of fluoranthene to an acetonitrile solution containing a constant amount of [Pt^{II}-(phen)(L-*S*,*O*)]$^+$ (7.62 mM) caused a considerable change in the chemical shift of the H^2 and H^9 protons of 1,10-phenanthroline (Figure 5a). To initially simplify matters, we assumed that only self- and hetero-noncovalent dimer formation (relations 3 and 9) occur. Therefore, the $\delta_{obsd.}$ change of the H^2 and H^9 protons of 1,10-phenanthroline in the Pt^{II} complex as a function of increasing fluoranthene concentration can be expressed by equation (10), where M = [Pt^{II}-(phen)(L-*S*,*O*)]$^+$ monomer, M_2 = [Pt^{II}(phen)(L-*S*,*O*)]$^+$ dimer and MF = [Pt^{II}(phen)(L-*S*,*O*)]$^+$/fluoranthene dimer.

$$C_{T(Pt)}\delta_{obsd.} = c_M\delta_M + 2c_{M2}\delta_{M2} + c_{MF}\delta_{MF} \quad (10)$$

If the addition of fluoranthene only caused the dissociation of the [Pt^{II}(phen)(L-*S*,*O*)]$^+$ dimer in some manner and hence increased the [Pt^{II}(phen)(L-*S*,*O*)]$^+$ monomer concentration, c_M, the $\delta_{obsd.}$ change of the H^2 proton (Figure 5a) should undergo de-shielding. The data in Figure 5a clearly show the converse, indicating significant [Pt^{II}-(phen)(L-*S*,*O*)]$^+$/fluoranthene non-covalent aggregate formation (relation 9). Confirmation of [Pt^{II}(phen)(L-*S*,*O*)]$^+$ and fluoranthene non-covalent association can be obtained by analyzing the fluoranthene H^{2*} proton chemical-shift data (Figure 5b). The change in the $\delta_{obsd.}$ of the H^{2*} proton of fluoranthene as a function of increasing fluoranthene concentration may be expressed by equation (11), where F = fluoranthene and MF = [Pt^{II}(phen)(L-*S*,*O*)]$^+$/fluoranthene complex.

$$C_{T(F)}\delta_{obsd.} = c_F\delta_F + c_{MF}\delta_{MF} \quad (11)$$

Increasing concentration of fluoranthene leads to de-shielding of H^{2*} of fluoranthene after which the extent of de-shielding levels off (Figure 5b), in contrast to when no [Pt^{II}(phen)(L-*S*,*O*)]$^+$ is present in solution. The relative concentration ratio of MF to F determines whether the $\delta_{obsd.}$ [equation (11)] is relatively more shielded or de-shielded. The concentration ratio of MF to F is largest when the total fluoranthene concentration is lowest, so that as the total fluoranthene concentration increases, the concentration ratio decreases, resulting in the monomer term ($c_F\delta_F$) contributing relatively more to the $\delta_{obsd.}$ with each addition of fluoranthene so resulting in progressive de-shielding of the H^{2*} proton (Figure 5b). The concentration dependence of the fluoranthene chemical shift data is thus consistent with [Pt^{II}(phen)(L-*S*,*O*)]$^+$/fluoranthene aggregation.

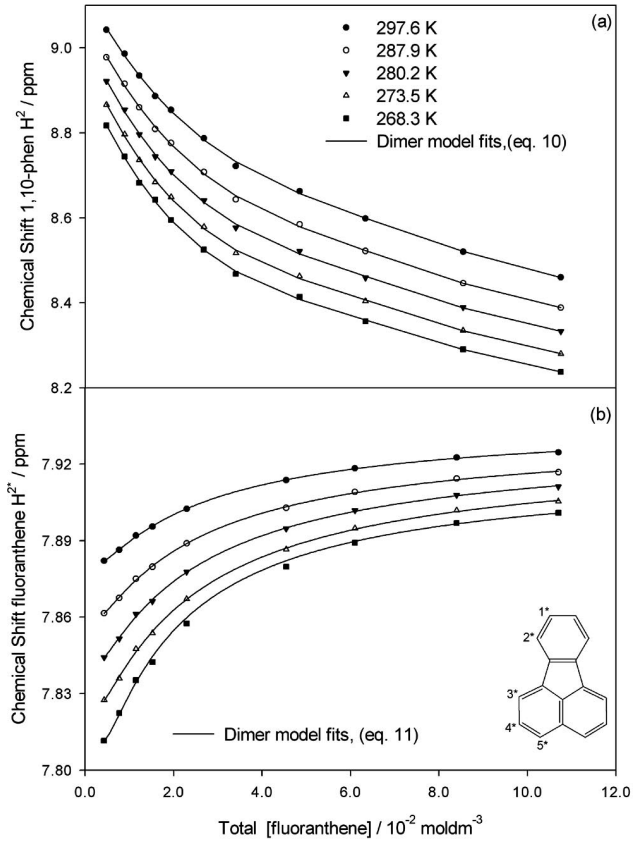

Figure 5. Excellent agreement was obtained between the experimental (symbols) chemical shift dependence of (a) the 1,10-phenanthroline H^2 proton and (b) the fluoranthene H^{2*} proton as a function of fluoranthene concentration and the self- and hetero-association dimer model least-squares fits.

The least-squares fit of the self- and hetero-association model (relations 3 and 9) to the proton chemical-shift data (see parts a and b in Figure 5) at several temperatures are in excellent agreement with the experimental data. When fluoranthene self-association (relation 8) is included in the least-squares model fit the program Dynafit only converged with K_A values very close to zero confirming that the extent of possible fluoranthene dimerization is *negligible* compared to reactions 3 and 9 (Figure 6).

Thermodynamic data for the self- and hetero-association model (relations 3 and 9) are obtained by the good fit with the Van't Hoff equation (5) (Figure 3), from which the standard reaction enthalpy and entropy of the [Pt^{II}-(phen)(L-*S*,*O*)]$^+$/fluoranthene π–cation interaction was estimated (Table 2). The $\Delta_rS°$ of relation M + F⇌MF (9) is

negative, suggesting association between reactants. It is clear from the thermodynamic data (Table 3) that this hetero-association reaction is also enthalpy driven, indicative of π–cation binding.[3] Comparing the thermodynamic parameters (Table 1 and Table 3) of the self- and hetero-association reactions 3 and 9, reveal that the $[Pt^{II}(phen)(L\text{-}S,O)]^+$/fluoranthene non-covalent complex has a more favourable standard reaction Gibbs energy ($\Delta_rG°$). This may be qualitatively attributed to the absence of charge repulsion present in the self-association interaction of $[Pt^{II}(phen)(L\text{-}S,O)]^+$ cations. The π–cation interaction is however crucial for these non-covalent complexes to form as it is demonstrated here that fluoranthene self-association is negligible under these reaction conditions.

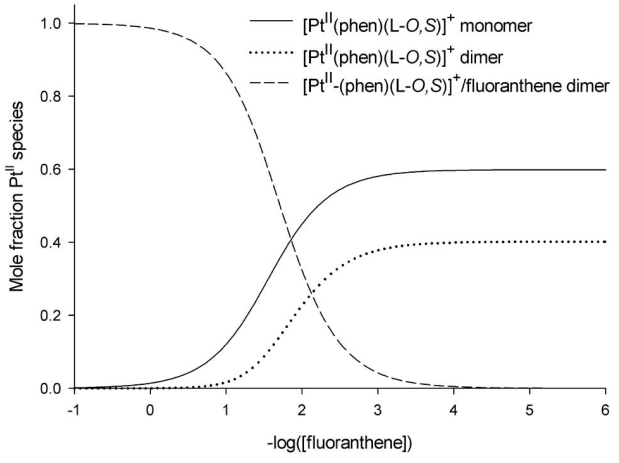

Figure 6. Species distribution diagram when increasing amounts of fluoranthene is added to a Pt^{II} solution, with determined constants K_D and K_B of 56 (±13) M^{-1} and 72 (±7) M^{-1}**, respectively at 267.1 K. Fluoranthene π–π stacking is negligible in the concentration range below 0.1 M.

Table 3. Calculated dimerization constants, K_B for $[Pt^{II}(phen)(L\text{-}O,S)]^+$/fluoranthene in CD_3CN and thermodynamic data.

Temp. [K]	K_B [M^{-1}]	$\Delta_rH°$ [J mol^{-1}]	$\Delta_rS°$ [J mol^{-1}]	$\Delta_rG°$ [J mol^{-1}]
297.6	39 (±4)	–13560 (±3180)	–17 (±11)	–9111
287.9	49 (±5)			–9265
280.2	58 (±6)			–9388
273.4	67 (±7)			–9496
267.6	71 (±7)			–9588

To sum up, our data is indicative of the fact that only a 1:1 $[Pt^{II}(phen)(L\text{-}S,O)]^+$/fluoranthene π–cation complex is present in our solutions in the concentration range studied. The chemical-shift trends observed as a result of the concentration dependence suggest that the 1:1 π–cation complex has an average structure shown in Scheme 3 in which a fluoranthene stacks *regiospecifically* in a coplanar manner to maximize π–σ attraction and minimize π–π repulsions in an offset stacking geometry, similar to that postulated for $[Pt^{II}(phen)(L\text{-}S,O)]^+$ dimer aggregate as shown in Scheme 1.

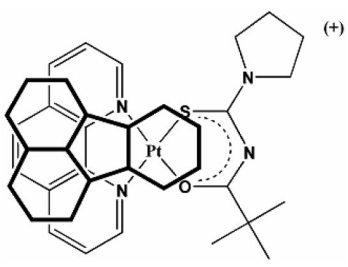

Scheme 3. Proposed average $[Pt^{II}(phen)(L\text{-}S,O)]^+$/fluoranthene dimer aggregate structure in solution.

Conclusions

In conclusion, the ^{1}H-NMR chemical shift and DOSY diffusion-coefficient dependence data of $[Pt^{II}(phen)(L\text{-}S,O)]^+$ validates its self-association into a $[Pt^{II}(phen)(L\text{-}S,O)]^+$ dimer in acetonitrile solutions with K_D (56 ± 8 M^{-1}). Moreover, $[Pt^{II}(phen)(L\text{-}S,O)]^+$ and fluoranthene form a 1:1 π–cation complex with an association constant, K_B (71 ± 8 M^{-1}) larger than the K_D obtained for the self-association of $[Pt^{II}(phen)(L\text{-}S,O)]^+$ into a dimer at 267 K. Higher order aggregates and ion-pairing were found to be negligible on the basis of the excellent least-squares fit of the dimer model to the ^{1}H NMR spectroscopic data and resulting linear Van't Hoff plots. The thermodynamic parameters calculated in this work indicate that π–cation interactions between cationic $[Pt^{II}(phen)(L\text{-}S,O)]^+$ and uncharged aromatic molecules, such as fluoranthene studied here ($\Delta_rG° \approx 9.6$ kJ mol^{-1}), are more favourable than self-association of the $[Pt^{II}(phen)(L\text{-}S,O)]^+$ ($\Delta_rG° \approx 8.9$ kJ mol^{-1}), compared to negligible π–π stacking of fluoranthene in acetonitrile. The data are consistent with essentially coplanar 1:1 aggregate strucrures in solution, resulting from regiospecific stacking interactions. We are currently investigating these phenomena with other model systems in water/acetonitrile mixtures as a step towards understanding the mechanism of anti-malarial activity of $[Pt^{II}(phen)(L\text{-}S,O)]^+$ class of compounds.

Experimental Section

Analytical Instrumentation: ^{1}H NMR and DOSY experiments were done in 5-mm tubes using a Varian Unity Inova 400 MHz spectrometer operating at 399.95 MHz or a Varian Unity Inova 600 MHz spectrometer equipped with an inverse-detection pulsed field gradient (idpfg) probe operating at 599.99 MHz. Diffusion coefficients were extracted using the Varian vnmrj software (version 2.1b). Experimental parameters: Pulse sequence: Dbppste_cc (Bipolar Pulse Pair Stimulated Echo with Convection Compensation), ^{1}H spectral width: 10 ppm, number of acquisitions varied from sample, recycling delay: 2 s, diffusion delay 30 ms, Gradient-pulse duration 2 ms, 20 different values of *G*, the gradient magnitude, varying between 0.0107 and 0.449 G m^{-1}. Melting points were determined using an Electrothermal IA9300 Digital Melting Point Apparatus. UV/Vis spectra were recorded with a single beam Agilent 8253E UV/Vis spectrophotometer. The IR absorbance spectra were recorded with a Thermo Nicolet Nexus FT-IR spectrometer fitted with a Smart-ATR adaptor. C and N were done with an EA Euro 3000 Elemental Analyser. Electro-spray mass spectra were obtained using a Waters API Quattro Micro Mass Spectrometer.

Synthesis of Compounds: All reagents and solvents were commercially available, and were used without further purification. The general method described by Morgan and Burstall for the synthesis of [Pt(1,10-phenanthroline)Cl_2] was used from commercially available $K_2[PtCl_4]$ and 1,10-phenanthroline monohydrate.[31] *N*-(2,2-Dimethylpropanoyl),*N*-pyrrolidylthiourea was prepared as described in the literature.[29] Commercially available fluoranthene (Aldrich) was used without further purification.

[Pt(1,10-phenanthroline)Cl_2]: Yield 201 mg (87.4%), m.p. > 350 °C. ^{1}H NMR (399.95 MHz, [D_6]DMSO, 25 °C): δ = 9.70 [dd, ^4J(H,H) = 1.3, ^3J(H,H) = 5.5 Hz, 2 H, H^9, H^2], 9.04 [dd, ^4J(H,H) = 1.3, ^3J(H,H) = 8.2 Hz, 2 H, H^4, H^7], 8.29 (s, 2 H, H^5, H^6), 8.17 [dd, ^3J(H,H) = 5.5, ^3J(H,H) = 8.2 Hz, 2 H, H^3, H^8] ppm. IR (ATR): $\tilde{\nu}$ = , 3083 (arom. C–H stretch), 3059 (arom. C–H stretch), 1427 (arom. C–C stretch), 1220 (asym. C–N stretch) 1208 (sym. C–N stretch) cm^{-1}. $C_{22}H_{25}ClN_4OPtS$ (624.07): calcd. C 32.3, N 6.3; found C 32.6, N 6.0.

***N′*-(*2,2*-Dimethylpropanoyl),*N*-pyrrolidylthiourea (HL):** Yield 564 mg (90.1%), m.p. 136–137 °C. ^{1}H NMR (399.95 MHz, [D_6]-DMSO, 25 °C): δ = 9.74 (s, 1 H, NH), 3.63 (m, 2 H, H^{a}), 3.42 (m, 2 H, $H^{a'}$), 1.90 (m, 4 H, H^{b}, $H^{b'}$), 1.16 (s, 9 H, $H^{1''}$) ppm. ^{13}C NMR (50.31 MHz, $CDCl_3$, 25 °C): δ = 27.16 ($C^{3''}$), 39.62 ($C^{2''}$), 54.43 ($C^{3'}$), 52.52 (C^3), 26.16 ($C^{4'}$), 24.59 (C^4), 176.66 (C^S), 174.38 (C^O) ppm. UV/Vis: λ_{max} (ε) 216(13 399), 276 nm (14 792 dm^3 mol^{-1} cm^{-1}). $C_{10}H_{18}N_2OS$ (214.33): calcd. C 57.8, H 8.5, N 13.1, S 14.96; found C 57.0, H 8.8, N 13.3, S 14.8.

[*N*-(2,2-Dimethylpropanoyl),*N*-pyrrolidylthiourea](1,10-phenanthroline)platinum(II) Chloride: The general method for the synthesis of mixed-ligand [Pt(diimine)(L-*S*,*O*)]PF_6 described by Koch et al.,[17] was modified for the preparation of [Pt^{II}(phen)(L-*S*,*O*)]Cl. A suspension of [Pt(phen)Cl_2] (0.045 g, 0.1 mmol) in 10 mL of acetonitrile was heated under reflux for 10 min, after which *N*-(2,2-dimethylpropanoyl),*N*-pyrrolidylthiourea (0.022 g, 0.101 mmol) in 2 mL of acetonitrile was added dropwise and the mixture heated under reflux for 45 min. A suspension of sodium acetate (0.028 g, 0.15 mmol) in acetonitrile was added and the mixture was left to gently reflux overnight. The cooled mixture was filtered through Celite to remove any Na/KCl precipitate formed. The filtrate was concentrated by evaporation to volume of ca. 2 mL. Diethyl ether (100 mL) was added and the precipitate was collected by centrifugation, resuspended several times with cold diethyl ether and centrifuged again. The yellow product was dried overnight in a vacuum oven at 70 °C; yield 58 mg (93%), m.p. 134–135 °C ^{1}H NMR (599.99 MHz, CD_3CN): δ = 9.01 [dd, ^4J(H,H) = 0.9, ^3J(H,H) = 4.5 Hz, 1 H, H^2], 8.85 [dd, ^4J(H,H) = 0.9, ^3J(H,H) = 7.7 Hz, 1 H, H^4], 8.77 [dd, ^4J(H,H) = 0.6, ^3J = 7.8 Hz, 1 H, H^7], 8.66 [d, ^3J(H,H) = 5.3 Hz, 1 H, H^9], 8.15 [dd, ^3J(H,H) = 4.5, ^3J(H,H) = 7.7 Hz, 1 H, H^3], 8.12 (m, 2 H, H^5, H^6), 7.84 [dd, ^3J(H,H) = 5.3, ^3J(H,H) = 7.3 Hz, 1 H, H^8] ppm. IR (ATR): $\tilde{\nu}$ = 3086 (arom. C–H stretch), 3059 (arom. C–H stretch), 2969 (C–H stretch), 2927 (C–H stretch), 1482 (C–O stretch), 1380 (CH_3 umbrella deformation), 1434 (arom. C–C stretch) 1264 (asym. C–N stretch) 1228 (sym. C–N stretch) cm^{-1}. (+) ESI MS: *m*/*z* 588 (M^+, calcd. 588.6).

Supporting Information (see also the footnote on the first page of this article): Figure S1 depicts the concentration dependence of the 1,10-phenanthroline protons. Figure S2 illustrates the set of resonance signals for the 1,10-phenanthroline and fluoranthene protons. Figure S3 shows the DOSY plot and the average diffusion coefficient for the aggregating complex. Diagram S1 illustrates how the r_H of [Pt^{II}(phen)(L-*S*,*O*)]$^+$ was estimated from two closely related crystal structures.

Acknowledgments

Financial support from the Stellenbosch University, the National Research Foundation (GUN 2069294) and Angloplatinum Ltd., is gratefully acknowledged.

[1] C. R. Brodie, J. G. Collins, J. R. Aldrich-Wright, *Dalton Trans.* **2004**, *8*, 1145–1152.
[2] D. A. Dougherty, *Science* **1996**, *271*, 163–168.
[3] D. Cuc, D. Canet, J.-P. Morel, N. Morel-Desrosiers, P. Mutzenhardt, *ChemPhysChem* **2007**, *8*, 643–645.
[4] T. Brand, E. J. Cabrita, S. Berger, *Prog. Nucl. Magn. Reson. Spectrosc.* **2005**, *46*, 159–196.
[5] W. Lu, D. A. Vicic, J. K. Barton, *Inorg. Chem.* **2005**, *44*, 7970–7980.
[6] M. Cusumano, M. L. Di Pietro, A. Giannetto, *Inorg. Chem.* **2006**, *45*, 230–235.
[7] A. M. Krause-Heuer, N. J. Wheate, M. J. Tilby, D. G. Pearson, C. J. Ottley, J. R. Aldrich-Wright, *Inorg. Chem.* **2008**, *47*, 6880–6888.
[8] N. J. Wheate, P. G. A. Kumar, A. M. Torres, J. R. Aldrich-Wright, W. S. Price, *J. Phys. Chem. B* **2008**, *112*, 2311–2314.
[9] A. S. Reddy, H. Zipse, G. N. Sastry, *J. Phys. Chem. B* **2007**, *111*, 11546–11553.
[10] J. C. Ma, D. A. Dougherty, *Chem. Rev.* **1997**, *97*, 1303–1324.
[11] J. Sunner, K. Nishizawa, P. Kebarle, *J. Phys. Chem.* **1981**, *85*, 1814–1820.
[12] H. J. Schneider, *Angew. Chem.* **1991**, *103*, 1419–1439.
[13] N. Zacharias, D. A. Dougherty, *Trends Pharmacol. Sci.* **2002**, *23*, 281–287.
[14] C. A. Hunter, J. K. M. Sanders, *J. Am. Chem. Soc.* **1990**, *112*, 5525–5534.
[15] a) T. J. Egan, K. R. Koch, P. L. Swan, C. Clarkson, D. A. Van Schalkwyk, P. J. Smith, *J. Med. Chem.* **2004**, *47*, 2926–2934; b) Y.-S. Wu, K. R. Koch, V. R. Abratt, H. H. Klump, *Arch. Biochem. Biophys.* **2005**, *440*, 28–37.
[16] H. H. Klump, K. R. Koch, C. T. Lin, *S. Afr. J. Chem.* **2006**, *102*, 264–266 .
[17] K. R. Koch, C. Sacht, C. Lawrence, *J. Chem. Soc., Dalton Trans.* **1998**, *4*, 689–695.
[18] J. J. Rebek, *Angew. Chem.* **1990**, *29*, 245–255.
[19] A. Macchioni, A. Romani, C. Zuccaccia, G. Guglielmetti, C. Querci, *Organometallics* **2003**, *22*, 1526–1533.
[20] L. Fielding, *Tetrahedron* **2000**, *56*, 6151–6170.
[21] I. Horman, B. Dreux, *Helv. Chim. Acta* **1984**, *67*, 754–764.
[22] P. S. Pregosin, *Prog. Nucl. Magn. Reson. Spectrosc.* **2006**, *49*, 261–288.
[23] F. Song, S. J. Lancaster, R. D. Cannon, M. Schormann, S. M. Humphrey, C. Zuccaccia, A. Macchioni, M. Bochmann, *Organometallics* **2005**, *24*, 1315–1328.
[24] M. Meloun, J. Havel, E. Högfeldt, *Computation of Solution Equilibria – A Guide to Methods in Potentiometry, Extraction, and Spectrophotometry*, Ellis Horwood, Chichester, **1987**.
[25] P. Kuzmic, *Anal. Biochem.* **1996**, *237*, 260–273.
[26] X.-M. Lu, W.-G. Xu, X.-H. Chang, D.-Z. Lu, J.-Z. Yang, *J. Chem. Thermodyn.* **2006**, *38*, 5–9.
[27] C. S. Johnson, *Prog. Nucl. Magn. Reson. Spectrosc.* **1999**, *34*, 203–256.
[28] H. Kato, T. Saito, M. Nabeshima, K. Shimada, S. Kinugasa, *J. Magn. Reson.* **2006**, *180*, 266–273.
[29] A. N. Mautjana, J. D. S. Miller, A. Gie, S. A. Bourne, K. R. Koch, *Dalton Trans.* **2003**, *10*, 1952–1960.
[30] M. Kato, J. Takahashi, *Acta Crystallogr., Sect. C: Cryst. Struct. Commun.* **1999**, *55*, 1809–1812.
[31] G. T. Morgan, F. H. Burstall, *J. Chem. Soc.* **1934**, 965–971.

Received: January 16, 2009
Published Online: March 18, 2009

